



# Smarter Lignite Open Pit Engineering Solutions **(SLOPES)**

A large, abstract graphic in the background features swirling blue and white lines forming circular patterns, resembling stylized water or energy flow. It covers the lower half of the page.

EUR 30443 EN

**Smarter Lignite Open Pit Engineering Solutions (SLOPES)**

European Commission

Directorate-General for Research and Innovation

Directorate D – Clean Planet

Unit D.3 — Low Emission Future Industries

Contact Hervé Martin

E-mail [RTD-PUBLICATIONS@ec.europa.eu](mailto:RTD-PUBLICATIONS@ec.europa.eu)

European Commission

B-1049 Brussels

Manuscript completed in 2019.

This document has been prepared for the European Commission however it reflects the views only of the authors, and the Commission cannot be held responsible for any use which may be made of the information contained therein.

More information on the European Union is available on the internet (<http://europa.eu>).

Luxembourg: Publications Office of the European Union, 2020

PDF ISBN 978-92-76-25276-4 ISSN 1831-9424 doi: 10.2777/87470 KI-NA-30-443-EN-N

© European Union, 2020.

Reuse is authorised provided the source is acknowledged. The reuse policy of European Commission documents is regulated by Decision 2011/833/EU (OJ L 330, 14.12.2011, p. 39).

For any use or reproduction of photos or other material that is not under the EU copyright, permission must be sought directly from the copyright holders.

All pictures, figures and graphs © University of Nottingham (UoN), RFSR-CT-2015-00001 SLOPES

# Research Fund for Coal and Steel

## ***Smarter Lignite Open Pit Engineering Solutions*** **(SLOPES)**

Alec MARSHALL (project coordinator)

Mohammad REZANIA, Charles HERON, Stuart MARSH, Martin SMITH, Hossein ZANGANEH, Mohsen MASOUDIAN, Amid HASHEMI, April BOWMAN

**University of Nottingham (UoN)**

University Park, NG7 2RD, Nottingham, UK

Alejandro Fernández, Alonso Gullón

**GEOCONTROL SA (GEOCONTROL)**

Calle Cristobal Bordiu 19, 28003, Madrid, Spain

Carlos RODRIGO, Manuel DE CABO, Vanesa POZO, David de PAZ, José Miguel GALERA

**SUBTERRA INGENIERIA, S.L. (SUBTERRA)**

Vallehermoso 30, 28015, Madrid, Spain

Zbigniew BEDNARCZYK

**POLTEGOR Institute of opencast mining (POLTEGOR)**

Ul. Parkowa 25, 51 616, Wroclaw, Poland

Petr SVODOBA, Jan BURDA

**Výzkumný ústav pro hnědé uhlí a.s. (VUHU)**

Budovatelů 2830, 434 37, Most, Czech Republic

Nikolaos KOUKOZAS, Alexandros DELIVERIS, Ioannis ZEVGOLIS

**Centre for Research and Technology-Hellas (CERTH)**

Charilaou Thermi road 6 km, 57001, Thermi Thessaloniki, Greece

John COGGAN, Matthew EYRE, Claudio VANNESCHI

**The University of Exeter (UNEXE)**

Northcote House, The Queen's Drive, EX4 4QJ, Exeter, UK

Stella COCCIA, Laurent CAUVIN, Marwan AL HEIB, Thomas RICHARD

**Institut national de l'environnement et des risques (INERIS)**

Parc Technologique Alata, 60550, Verneuil en Halatte, France

Grant Agreement RFSR-CT-2015-00001

1/07/2013 to 31/12/2015

**Final Report**

## Table of Contents

<b>1 FINAL SUMMARY .....</b>	<b>5</b>
1.1 WP1 - Development and application of modern monitoring techniques for slope stability in open pit lignite mines .....	5
1.2 WP2 - Advanced modelling and risk analysis of open pit rock-face slopes.....	6
1.3 WP3 - Stability and long-term behaviour of lignite mine spoil heaps and reclaimed ground.....	8
1.4 WP4 – Reporting and coordination .....	11
<b>2 SCIENTIFIC AND TECHNICAL DESCRIPTION OF RESULTS .....</b>	<b>13</b>
2.1 Objectives of the project.....	13
2.2 Description of activities and discussion .....	13
WP1 - <i>Development and application of modern monitoring techniques for slope stability in open pit lignite mines</i> .....	13
WP2 - <i>Advanced modelling and risk analysis of open pit rock-face slopes</i> .....	35
WP3 - <i>Stability and long-term behaviour of lignite mine spoil heaps and reclaimed ground</i> .....	56
<b>3 CONCLUSIONS.....</b>	<b>87</b>
WP1 - <i>Development and application of modern monitoring techniques for slope stability in open pit lignite mines</i> .....	87
WP2 - <i>Advanced modelling and risk analysis of open pit rock-face slopes</i> .....	87
WP3 - <i>Stability and long-term behaviour of lignite mine spoil heaps and reclaimed ground</i> .....	88
<b>4 EXPLOITATION AND IMPACT OF THE RESEARCH RESULTS.....</b>	<b>91</b>
WP1 - <i>Development and application of modern monitoring techniques for slope stability in open pit lignite mines</i> .....	91
WP2 - <i>Advanced modelling and risk analysis of open pit rock-face slopes</i> .....	91
WP3 - <i>Stability and long-term behaviour of lignite mine spoil heaps and reclaimed ground</i> .....	91
<b>5 LIST OF FIGURES.....</b>	<b>93</b>
<b>6 LIST OF TABLES .....</b>	<b>97</b>
<b>7 LIST OF ACRONYMS.....</b>	<b>99</b>
<b>8 REFERENCES.....</b>	<b>101</b>



## **1 Final Summary**

### **1.1 WP1 - Development and application of modern monitoring techniques for slope stability in open pit lignite mines**

WP leader: INERIS      Partners: UoN, Geocontrol, SUBTERRA, POLTEGOR, VUHU, UNEXE

Objectives of WP1: The objective of this work package (WP) was the development and deployment of technology and methodologies for effective monitoring of slopes within open pit lignite mines. The WP aimed to apply modern systems for the challenging demands of monitoring within open pit mines. The main challenges related to the large areas that require detailed and continuous measurements in order to fully appreciate the risks associated with the geotechnical systems involved. The objectives were achieved in three tasks which focused on (1) aerial monitoring systems, (2) automated and continuous monitoring for challenging large-displacement applications, including the use of Interferometric Synthetic Aperture Radar (InSAR) technology, and (3) laser scanning.

#### **TASK 1.1: Aerial monitoring systems – advancement and deployment of technology and application methods (INERIS, VUHU, POLTEGOR, UNEXE, GEOCONTROL, UoN)**

In order to monitor a slope of an open pit coalmine, a number of surveying methodologies can be applied, including terrestrial laser scan, aerial laser scan, conventional surveying methodologies, terrestrial photogrammetric solutions, Unmanned Aerial Vehicle (UAV) based solutions. The choice of one or more of these methods depends on site conditions, accessibility, and cost. UAV based solutions were applied to two trial open pit mines as part of the SLOPES project: the Belchatow mine in Poland, and the CSA mine in the Czech Republic. The potential of the drone monitoring system was considered as a support of specific tools for large ground movement monitoring in the open pit mine context. Aerial photogrammetry was also tested at the Belchatow mine in Poland (conducted by INERIS with support of POLTEGOR) and the CSA mine in the Czech Republic (conducted by VUHU). InSAR methods were also tested but only in Poland. The coupling of drone, InSAR, in-situ observations and advanced 3D numerical modelling present a useful tool for slope stability analysis of active and abandoned open pit mines. It allows assessment and identification of the global and local stability of a slope after sliding. Point cloud data from drone Light Interferometry Detection and Ranging (LiDAR) or photogrammetry can also be incorporated into automated monitoring systems that can provide early warning of potential slope failure. Areas of displacement can then be identified and assessed in order to illustrate areas of higher magnitude.

VUHU conducted 11 UAV imaging flights from April 2016 to December 2017 at the CSA open pit mine; 10 flight campaigns used a DJI Phantom 3 UAV, and one campaign used a DJI s900 UAV. Comparing the Phantom and S900 results gave an interesting result: the difference in resolution of the cameras was not so critical in the open-pit mine environment, where the goal is to achieve an accuracy of less than 30 mm, ideally below 20 mm, which was achieved by both cameras. Even the "low-cost" DJI Phantom 3 UAV equipped with a 4k camera can be used to create full-fledged Digital Elevation Models (DEMs). It was found that the distribution of ground control points had a considerable effect on the obtained accuracy, with random placement of ground control points achieving considerably better accuracy than having the control points in regular grids.

GEOCONTROL focused on the identification of critical unstable zones of slopes using a software application that they developed which processed the obtained UAV point cloud data. They applied a numerical indicator of the degree of local folding of the terrain surface; the value and change of the indicator allows identification of landslide scarp features and the analysis of registered displacements in the context of landslide geomorphology. A methodology defined as Analytical Scarp Detection Model (ASDM) was developed and implemented through the software application. GEOCONTROL applied the methodology to UAV data from the CSA mine to conduct a landslide analysis which allowed the identification of the main active regions in the surveyed area and the segmentation of areas prone to vegetation interference.

#### **TASK 1.2: Advanced systems for automated and continuous monitoring of mass ground movements (INERIS, POLTEGOR, SUBTERRA)**

Geotechnical investigations were conducted by POLTEGOR on the west slope of the Belchatow mine to obtain new geotechnical data for use within stability analyses. Site investigations included drillings and in-situ instrumentation. On-line inclinometer and pore pressure monitoring devices were installed and supplemented by high resolution satellite Persistent Scatterer Interferometry (PSI) conducted by POLTEGOR in cooperation with GAP-Technical University Bari (Italy). The monitoring data was made available for near real-time monitoring using the E-cenaris cloud-monitoring platform provided by INERIS, which has a module to implement simple and complex alarms. INERIS created and activated for Belchatow open mine, as a case study, only a warning level, because of the short time monitoring period. The monitoring system and E-cenaris worked well during the project period and permitted a near real time monitoring and warning system for the open pit mine context.

SUBTERRA undertook a survey comparing the effectiveness of different monitoring systems, especially for large displacements and pore pressure evolution at rock faces and spoil heaps.

Dynamic inclinometers, total pressure cells and piezometers were employed to acquire data and to calibrate the modelling process and threshold definition, aiming to assist the geotechnical control of an open pit mine and its spoil dumps. Data from the Belchatow mine, as well as from other sites such as CLC mine in Spain, were considered. The CLC mine, despite being a copper mine, was suitable as it provided monitoring data both for open pit slopes and spoil dumps, thereby providing an example for the explanation of the modelling, monitoring and warning system establishment. In addition, the nature of the materials involved (clayey blue marls) was also suitable for the study of the geomechanical properties of spoil dumps, an issue tackled in WP3. The work conducted as part of the SLOPES project provided geomechanical characterization by means of in situ and lab tests and enabled an understanding of the problem and the triggering mechanisms. The CLC mine study included accurate numerical models (implementing detailed geometry of the slope and the boundaries of materials) and represented the first step to predict displacements, shear surfaces and pore pressure evolution depending on dumping or excavation phases. A proper modelling process and thorough analysis lead to a quantitative range of values for every targeted parameter. Field data require to be analysed often (daily, and when is steady, weekly) to provide displacements, pore pressure and rate of movement data to establish thresholds for warning systems in open pit mines. For every warning level for the CLC mine, a corrective action (or an increasing of measures) was suggested.

#### **TASK 1.3: Application of laser scanning (INERIS, UNEXE, UoN, VUHU, POLTEGOR)**

UNEXE produced a comprehensive document entitled "Feedback and recommendations of the use of laser scanning technology for open pit mine stability diagnostics". The report covered in detail the development and application of technology, with focused discussion on deliverable outputs that can be generated from its deployment in open pit mining. Following a scoping study, a laser scanning campaign was undertaken at the Belchatow site in Poland with the support of POLTEGOR. A Riegl VZ-4000 for long range terrestrial laser scanning (TLS) was used to scan the East slope. The laser scanning surveys were carried out in conjunction with 3D Laser Mapping (3DLM), who provided the Riegl VZ-4000, and a comprehensive point cloud was established. Following the work at Belchatow, UNEXE conducted a scan at the CSA mine in the Czech Republic, supported by VUHU. The scoping exercise highlighted that access on site was not restricted and allowed for personnel to operate in the landslide area. Therefore, a shorter range scanner was selected: the Leica ScanStation C10, with a maximum range of 300m. All generated point clouds were referenced to the WGS84 system for ongoing comparison of data.

INERIS applied laser scanning to characterise the stability of abandoned open pit mines and dumps. INERIS used a short-range laser scan (FARO Focus3D X330, 0.6-330 m range with ranging error is  $\pm 2$  mm) to scan instabilities in a small abandoned French coal mine. The objective of the application was the evaluation of the capacity of terrestrial laser scan (TLS) for slope stability analysis within a lignite mine. The INERIS laser scan results were also integrated into a 3D numerical modelling process. Results of the numerical modelling and laser scan were compared to existing displacement measurements. Terrestrial laser scanner technology proved to be a very useful tool to characterize and analyse the stability of the inaccessible slopes with very reasonable costs comparing to classical displacement surveys. 3D datasets were also used to carry out a slope assessment and generate a numerical model. This innovative methodology, based on crossing and combination of 3D datasets, numerical modelling and in-situ observation, was successfully used for a real case study.

### **1.2 WP2 - Advanced modelling and risk analysis of open pit rock-face slopes**

WP leader: CERTH      Partners: Geocontrol, SUBTERRA, POLTEGOR, UNEXE, INERIS

Objectives of WP2: The focus of this work package was the stability analysis of open pit slopes for the evaluation of potential risks to the mine and surrounding area. This work package aimed to achieve the following objectives: (1) to apply probabilistic analysis to open-pit mining scenarios for the reliability-based assessment of risks; (2) to apply advanced numerical modelling methods to open pit mining scenarios, including the integration of probabilistic analysis results and the detailed effects of pore pressure dissipation and bedding planes, and consideration of how monitoring data (e.g. from WP1) is best incorporated into numerical analyses for the continued improvement of predictive models and evaluation of risks; and (3) consideration of the vulnerability of structures and infrastructure systems within nearby urban areas to the effects of open pit mining activities.

#### **TASK 2.1: Probabilistic analysis for reliability-based evaluation of risks (CERTH, UNEXE)**

CERTH developed a slope reliability model, coupling the Monte Carlo simulation probabilistic method with the limit equilibrium method. Through this work, it was demonstrated that primarily cross-correlation between shear strength components, and secondarily, the statistical distribution type that random variables follow, both play a very important role in the probabilistic outcome. Ignoring the dependency between shear strength frictional and cohesive components leads to conservative probabilistic results. Lognormal distributions gave the lower calculated probability of failure values, whereas Normal truncated and Beta distribution yielded very similar probabilistic

results. In addition, the non-linear relation of the failure probability with the mean safety factor was demonstrated for the most sensitive random variable of the slope examined. It was also shown that there is a non-linear relation of probability of failure and the deterministic safety factor with the overall pit slope angle using a series of parametric probabilistic analyses.

UNEXE made a review of probabilistic approaches to plane failure analysis and slope stability acceptance criteria, and application of Eurocode 7 requirements in a mining context. The report entitled "Probabilistic approaches to plane failure analysis" was supplied to complement the deliverables of the SLOPES project. The review was based on example plane failure analyses typically of a limited size (e.g. benches) using a probabilistic approach and different methods of solution. The review considered the geotechnical aspects of the probability of failure and consequences were considered mainly for the scale of the slope. The cases studied did not include consideration of singular features such as major faults.

#### **TASK 2.2: Application of advanced numerical methods (SUBTERRA, UNEXE, GEOCONTROL, CERTH, POLTEGOR, INERIS)**

For the effective integration of WP1 data into numerical modelling processes, GEOCONTROL developed a methodology whereby point-type data is processed separately to surface and 3D data. Both UAV-campaign point clouds (as outputs from WP1) and water table data were treated as point-type data and converted into geometrical surfaces to be imported to numerical models. For this objective, the free software *CloudCompare* was used, considering its ability to process point clouds and its use in other parts of the SLOPES project. This scheme offers several benefits. First, UAV clouds can be filtered and converted into subsampled surfaces. Coupling of high resolution topography (UAV clouds), piezometer and other water-related data, allows the definition of interpolated water tables for numerical modelling. Finally, mesh generation is achieved through a FISH code in FLAC3D, avoiding the use of additional (expensive) commercial software. This is applicable for cases of relatively simple geometry (defined by surface layers), the CSA slope being a good representative example.

SUBTERRA conducted an analysis of a particular case of slope stability in an active open pit lignite mine. For the material characterization it was necessary to perform a geotechnical field campaign, as well as complete laboratory testing. Once the main geotechnical parameters were obtained, a 2D reconfiguration of the former slope (where the slide occurred) was carried out and implemented in the code FLAC2D. After a back-analysis process employing different software solutions, calibration of rock and soil properties were possible. Finally, water table conditions were taken into account and stability results were obtained. Several conclusions and recommendations for mine operators to foresee the mining plan have been obtained, and the pros and cons of the modelling processes have been established for further applications.

UNEXE produced a report on the "Application of advanced numerical methods", which investigated the development of a methodology for effectively integrating data captured as part of WP1 into numerical modelling packages. UNEXE integrated data obtained from the work undertaken at a UK validation site, exploring the application of aerial and terrestrial laser scanning in an open pit mining environment. A modelling approach for the different case studies highlighted within the SLOPES project was suggested, i.e. a framework for incorporation of remotely captured digital data in slope stability analysis. With the aim of testing the illustrated methodology to a real case study, UNEXE applied a three-dimensional discrete element method approach to an example case study, identifying the critical parameters that influence direct toppling instability in an open pit environment.

INERIS tested and applied a distinct element method analysis to assess the stability of open pit coal mines in Europe. The use of the distinct element method allows one to take into account the natural fractures and faults and the induced discontinuities. The coupling between large scale and local scale numerical modelling with the observations helped to explain the causes and the consequences of slope instabilities in active coal mines.

POLTEGOR conducted field investigations and laboratory testing to provide inputs for numerical modelling of the Belchatow Mine. The obtained results were used in numerical modelling using shear strength reduction (SSR) and limit equilibrium method (LEM) approaches. For numerical modelling, POLTEGOR analysed two cross-sections with the highest slope inclination. The analyses indicated that the west slope is a high risk landslide area. These results were confirmed by the monitoring field observations which detected activation of mass movements in these areas. The movements were caused by multiple factors such as mining, strength parameters, slope height and salt dome influence.

CERTH developed a slope reliability methodology, coupling the point estimate probabilistic method with the finite element numerical method. Taking advantage of finite element models to directly consider the construction sequence of slope formation, the operating stress states within the slope were determined. In this manner, both local and global slope safety levels along critical slip surfaces were evaluated. Via the probabilistic treatment of the above stability indicators by the point estimate method, local and global safety factors were matched with local and global probabilities of failure along certain critical slip surfaces. It was found that the probability of failure

decreases from a slope's toe to the slope's crest. Thereby, areas within a slope presenting significant potential for local overstress and progressive failure occurrence were manifested. The probabilistic simulation of progressive failure was attempted, and the updated global slope probability of failure during its development was computed. A detailed presentation of this work was published in Deliveris et al. (2018a) and Deliveris et al. (2018b).

### **TASK 2.3: Vulnerability issues (CERTH, INERIS)**

The vulnerability of structures and infrastructure to open pit mining activities was studied and analysed. Different damage classes were described and presented from slight damage to partial or full destruction of the structure or infrastructure component. A global damage index (GDI) was proposed as part of the SLOPES project which can consider the mining and environmental parameters. The GDI can be used to compare different scenarios of mine operation, open pit mining projects, or mining design options to minimize the damage on structures and infrastructure. The developed methodology was applied to case studies from Greece open pit lignite mines. CERTH recorded the type of damages in Mavropigi village, which is located near an active open pit lignite mine operated by the Public Power Corporation (PPC). The establishment of a preliminary relation between the severity of structural building damage and their distances from the advancing pit walls was attempted. Two site visits were organized in 2011 and 2016 to identify damaged buildings in relation to mine activities. The main aim of this site inspection was to detect and record as many building damages as possible, and to identify their location in relation to the position direction of advance of the pit mine. The results of the vulnerability analysis highlighted the main role of the faults to increase the influence of the mine excavations on surrounding buildings and infrastructure. Numerical modelling was used to evaluate the critical distance between the mine and the existing villages and infrastructure. The critical distance may be considered equal to 500 m when faults are identified.

### **1.3 WP3 - Stability and long-term behaviour of lignite mine spoil heaps and reclaimed ground**

WP leader: UoN      Partners: VUHU, POLTEGOR, CERTH, UNEXE, SUBTERRA, GEOCONTROL

Objectives of WP3: There are significant issues related to the stability of lignite mine spoil materials, including the safety of mine operatives and equipment as well as the economic success of open pit mines, and the successful use of reclaimed land for redevelopment (e.g. factories, commercial or recreational space). This work package investigated the long-term behaviour and stability of open pit lignite mine spoil heaps and reclaimed ground, through:

- collection of existing and new data of the characteristics and behaviour of lignite mine spoil heap materials,
- development of physical models of spoil heaps in order to obtain new data to better understand the relationships between material characteristics and spoil heap behaviour under different loading conditions,
- development of advanced constitutive relationships and numerical models which can simulate the complex and time-dependant behaviour of spoil heap materials, and
- application of probabilistic analyses for a reliability-based evaluation of risks, associated with mine spoil heaps.

#### **TASK 3.1: Collection of detailed data sets and material testing of lignite mine spoil heap materials (VUHU, POLTEGOR, UoN, CERTH)**

This task focused on collecting valuable new data sets related to the characteristics of lignite spoil heap materials and putting these data within the context of existing data for spoil materials as well as natural soils. The physical properties of spoil soils of lignite mines from the Belchatów mine in Poland and the Vrsany mine in the Czech Republic were evaluated in relation to those from around the world. It was shown that there is significant variability in the reported physical characteristics of spoil soils. This is true even for samples obtained from a single spoil heap (see Masoudian et al., 2018; Masoudian et al., 2019b). As part of the SLOPES project, the variability of spoil properties from a single spoil heap was characterised to a degree not previously achieved using data from the Soulou spoil heap. Data illustrated that spoil heap stratigraphy is greatly variable (or even nearly chaotic). Given the large variability of the spoil regarding its engineering properties, an adoption of probabilistic concepts for the direct incorporation and expression of geotechnical uncertainty in the design is considered essential. The collected data from Task 3.1 was interrogated using probabilistic methods to attain statistical distributions of the geotechnical parameters, which were integrated and used within work carried out in Tasks 2.1, 2.2, and 3.4. The outcomes of this task are extremely valuable as they provide a unique quantitative assessment of the variability of spoil heap characteristics. The outputs from this task have already been integrated into stochastic stability analyses from researchers within this project (e.g. Masoudian et al. 2019a), and ultimately the outcomes should be adopted more widely within the international mining community.

#### **TASK 3.2: Physical modelling of spoil heaps and reclaimed ground (UoN, VUHU, POLTEGOR)**

This task set out to develop and test two physical models which could be used to replicate stability and deformation issues related to spoil dump slopes. The first was a meso-scale physical model, measuring 5m long by 1.5m wide and 2m high. The second model was a small-scale model measuring approximately 700mm length by 200mm width by 400mm height (inner box dimensions) which was tested under elevated gravity conditions within the UoN geotechnical centrifuge.

The meso-scale experiments were designed to provide a better understanding of the effects of water level variations and wetting-drying cycles on the stability and movement of spoil material slopes. Transparent acrylic windows enabled digital images to be taken of the subsurface soil, which were subsequently analysed to evaluate soil displacements. Water was fed into the box through a standpipe which was also used to regulate the water level. The soil used in the experiments was sandy silt prepared at a slope angle of 60° (from horizontal). LVDTs and tensiometers were also installed to monitor the crest displacements and internal pore water pressures, respectively. Experiments focused mainly on the performance of the slope model when the water level was raised and lowered and on the wetting and drying cycles. The tests consisted of four water level elevation steps with each elevation increment being 400mm. Each water level elevation was held for almost 72h, followed by four equivalent draining steps. Results demonstrated that settlement of the crest during these initial stages was most significant and was attributed to wetting-induced collapse of the unsaturated loose silt. Results from the pore water pressure measurements indicated that negative values (suctions) played a key role in maintaining the slope stability, and in fact throughout all water levels tested, a global instability phenomenon was not observed because pore suctions were maintained.

The centrifuge model tests simulated slope stability of spoil heap materials under specific rainfall and groundwater conditions. The climatic chamber used for centrifuge tests was a plane-strain rigid container with a transparent acrylic window that allows acquisition of digital images of the subsurface soil. Rainfall was simulated by the flow of water through misting spray nozzles. To monitor the subsurface pore water pressure during testing, miniature pore pressure transducers (PPTs) were installed within the soil. Three types of soils were used in the study: the first with 100% sand (Sa100), the second consisted of the same sand but with 10% silt added (Sa90Si10), and the third was the same silty sand used in the meso-scale models (Sa50Si45). Note that these soils do not completely represent the spoil materials, however this work focused on a more fundamental approach where the effect of sand, silt and clay contents were examined with the aim of eventually providing an understanding of how these affect slope stability in spoil heaps. All slopes were made at 50 degrees from horizontal. In order to study how different soil materials influence the results of centrifuge modelling, the soil types were tested under different rainfall intensities and at different compaction states. All tests were conducted at 60g (i.e. 60 times gravity). Introducing rainfall to the model led to development of displacements in all models, due to the infiltration of water within the soil. In tests with pure sand, no failure mechanism was observed, whereas the Sa90Si10 silty sand exhibited failures under both low and high rainfall intensities. Analysis of the time-dependent displacements showed that the failure was sudden for high intensity rainfall while a more progressive failure was observed for lower intensity rainfall. Prior to the onset of rainfall, suction (negative pore pressure) developed within the model at all locations, due to desaturation during the gravity increase to 60g. Upon rainfall initiation, pore pressure increased slowly at all points, with the first increase near the crest of the slope, indicating the rainfall infiltration and development of the wetting front. The advancement of the wetting front in the soil then lead to the increase in pore pressure at the other locations in order of their depth.

This work package included ambitious aims related to physical modelling of spoil heap embankments, which were generally well achieved, however a rigorous approach to centrifuge testing of unsaturated slopes remains a challenge. The elevated gravity experiments in the centrifuge involving unsaturated soils is still a significant challenge which has not been solved within the physical modelling community. The use of the representative spoil dump material within centrifuge tests brought unforeseen difficulties related to surface erosion and drainage system blockage. Many lessons were learned and future research will endeavour to continue to find ways in which unsaturated soil slopes can be effectively modelled within the centrifuge.

### **TASK 3.3: Numerical modelling of spoil heaps and reclaimed ground (UoN, UNEXE, SUBTERRA, GEOCONTROL)**

Each of the deterministic modelling exercises conducted as part of this task focused on the same case study from the Slatinice spoil dump located at Vrsany mine, Czech Republic. Geocontrol performed a stability analysis of an excavation profile by employing the software FLAC3D. UoN modelled the problem using an elasto-viscoplastic constitutive model. SUBTERRA developed a 3D model of the excavation (using the same sequence as Geocontrol) specifically analysing the variation of pore pressure distribution within the spoil material and the critical basement layer. UNEXE completed an analysis on the Slatinice spoil dump using two-dimensional Limit Equilibrium Method (LEM) and Finite Element Method (FEM) approaches. In addition to the above, and driven by the outcomes of the project in terms of the evaluation of the characteristics and spatial variation of dump materials, an additional numerical modelling exercise was conducted by UoN in which stability was assessed using multivariate random fields.

The Slatinice spoil dump represents a challenge considering that the spoil heap is currently registering movements, in spite of the fact that its surface is not steep. There is also potential for future re-exploitation of the dump and a previous historical event of significant instability make it an example worthy of study in terms of its long-term behaviour. GEOCONTROL first conducted an analysis of current movements of the spoil. Data indicated that there was a clear localised instability at the contact layer of the bottom part of the spoil. This layer, which according to the geology, is comprised of water-saturated clay, clearly represents a weak plane for the stability of the dump. Displacements in this layer were higher than those located at shallower locations within the spoil material. Results indicated that the existence of pore pressure concentrations within the contact layer at the base of the spoil heap, dependent in seasonal water content changes, plays a leading role in the development of large scale failures of the dump. Monitoring of these pressures, as well as the use of mitigation strategies, should be considered for cases similar to Vrsany spoil dump.

UNEXE produced a document detailing the integration of numerical modelling of spoil heaps and reclaimed ground. The document included numerous numerical modelling simulations of the Slatinice spoil dump using LEM and FEM. UNEXE concluded that a critical condition of the slope is related to the superficial instability involving local benches. According to the results of the analyses (both LEM and FEM), instability occurs even in dry conditions, but a higher number of unstable benches was detected if the slope was considered fully saturated (1 in dry condition, 5 in wet conditions). This is due to the fact that the presence of water decreases the strength properties of the material and in the case of abundant precipitation (rainfall) and snow melting during spring time, if the slope becomes saturated, the critical bench angle may significantly decrease and instability occur.

SUBTERRA conducted a FLAC3D model of the Slatinice spoil heap. Their results provided evidence of the advantages of advanced constitutive models and different approaches to simulate the behaviour of the ground structures. For the 3D model, the focus was on hydrogeological conditions as well as excavation sequence. Recommendations relating to the modelling and simulation of spoil heaps were provided, and the new findings helped to understand the geotechnical nature of spoil heaps composition, and its stability under changing conditions such as water variations and slope construction.

Advanced numerical models offer the benefit of the potential to match more complex soil behaviour than more conventional (i.e. Mohr-Coulomb or Cam-Clay) models. Their use, however, has the drawback of the requirement for additional soil parameters, some of which can be difficult to obtain using standard field or laboratory test methods. UoN adopted the use of an advanced elasto-viscoplastic model that uses an improved iteration of the EVP-SANICLAY model in this project. The model uses a novel rotational-hardening (RH) law that guarantees the uniqueness of the critical state line, prevents excessive rotation of the yield surface, and is sufficiently simple that it could be adopted for some practical applications. The elasto-viscoplastic anisotropic constitutive model was implemented in the commercial software PLAXIS. A comparative study using the EVP-SANICLAY, Mohr-Coulomb, and Modified Cam-Clay constitutive models was undertaken using Plaxis 2D based on the Slatinice spoil dump. The results demonstrated some important differences between the Mohr-Coulomb, Modified Cam-Clay, and EVP-SANICLAY models. The location of the predicted ground movements in the EVP-SANICLAY model was quite different than the Mohr-Coulomb model, but similar to the Modified Cam-Clay model (though magnitudes were considerably different).

In addition to the above work, due to the observed variability of the spoil material, an additional numerical modelling exercise was conducted by UoN in which stability was assessed using multivariate random fields (see Masoudian et al., 2019a). Spoils are variable over space and their variability must be considered for numerical models to realistically represent the actual conditions. Despite the relatively large number of studies on rainfall-induced slope instabilities in partially-saturated soils, only a few studies have considered the spatial variability of geotechnical properties. The study considered four dependent random variables of void ratio, dry unit weight, cohesion, and friction angle which were cross-correlated using a multivariate Gaussian copula. The spatial correlation of random variables was based on a Gaussian auto-correlation function. The numerical model used was a fully coupled transient hydro-elasto-plastic model constructed in Abaqus, where saturated permeability was related to the random field of void ratio through the Kozney equation. A multivariate cross-correlated random field was generated for the four variables of cohesion, friction angle, dry unit weight, and void ratio. The set of random fields were exported to Abaqus where the numerical simulation was carried out. 1,000 different random fields were generated and simulated using Abaqus. Using MATLAB, an analysis of the most likely failure surface and its safety factor was carried out. Results illustrated that a homogeneous spoil case gives a slip line smaller than most of the random field simulations, therefore showing the importance of considering heterogeneity. The outcomes of the analyses can be used to investigate the evolution of safety factor with rainfall duration. Results indicate that the factor of safety in a homogenous case is overestimated compared to the nonhomogeneous condition, while the sliding volume is underestimated. Moreover, the factor of safety decreases as the rainfall simulation continues and the probability of failure increases to nearly 100% after 10 days of rainfall.

#### **TASK 3.4: Probabilistic analysis of reliability-based evaluation of risks (CERTH, UNEXE)**

The reliability methodology developed by CERTH for the case of pit wall stability was applied for the case of spoil dumps. The primary benefits derived from this slope reliability methodology are related to: (1) the capability of disclosing both local and global slope reliability levels; and (2) the possibility for considering a slope's construction method in the stability analysis. The proposed methodology could be further extended in the future, for the establishment of a unified slope stability-performance reliability framework, considering jointly stresses and deformations within a slope, independent of the construction method followed.

Limit Equilibrium and Finite Element analyses (undertaken in Task 3.3 and 3.4) were used by UNEXE to assess the effects of data uncertainty on spoil heaps at a lignite operation in the Czech Republic. The case study provided valuable insight into the effects of geological parameters and model uncertainty. A sensitivity analysis was undertaken to understand the controlling influences of input parameters on model behaviour. The results highlight, as expected, that water table level and material input parameters have the greatest influence on stability of the slope. The potential for both deep-seated instability and superficial land sliding were investigated. More detailed probabilistic analysis suggests that possible instability is connected to local bench failure, while there is a minor possibility for deep-seated instability in case of a fully saturated slope. Nevertheless, if the presence of deep pore pressure affecting the contact layer at the base of the dump material is considered, possible instability may occur even in case of dry slope. However, such a hypothesis has to be validated with field monitoring data. In particular, the real pore pressure value should be evaluated with specific in situ tests. The modelled results, using LEM and FEM, demonstrated good agreement. The investigation allowed improved understanding of the possible response of the dump material to a system disturbance caused by new excavation activity at the lignite open pit-mine site. The increased level of knowledge obtained through numerical modelling provides improved hazard assessment and data for mine planning purposes. The importance of performing sensitivity analyses with both Limit Equilibrium and Finite Elements approaches is highlighted within the analyses undertaken. Complementary use of both approaches is recommended for routine checks on model behaviour and associated results. The work highlighted that sensitivity analyses should include both deterministic and probabilistic analyses, but an in situ monitoring system and site-specific analyses for the highlighted critical areas, with sample collections, are always fundamental to verify the results of the analyses in case of strongly heterogeneous materials with a high degree of uncertainty.

#### **1.4 WP4 – Reporting and coordination**

WP leader: UoN; Partners: Geocontrol, SUBTERRA, POLTEGOR, VUHU, CERTH, UNEXE, INERIS

Objectives of WP4: Work Package 4 provided reports, deliverables and communications regarding the research results throughout the SLOPES project. In addition to the Annual, Mid-term and Final reports supplied to the Commission and TGC1, various other forms of dissemination were employed during the project. To date, 21 papers have been published as a result of the project, with several others under review or in preparation. In addition, a SLOPES project session was organised at the International Symposium on Slope Stability in Open Pit Mining and Civil Engineering, Seville, Spain, April 11-13, 2018.

All other coordination activities proceeded as scheduled in Technical Annex.



## **2 Scientific and technical description of results**

### **2.1 Objectives of the project**

The SLOPES project aimed to enable the development of effective reliability-based methods for the evaluation of risks based on monitoring and modelling results to provide significant benefits to design optimisation and decision support within open-pit lignite mines.

The SLOPES project objectives related to: (1) evaluating how modern monitoring techniques can be applied and integrated within automated systems that provide 'real-time' assessments of risk, with particular focus is the potential use of unmanned aerial vehicles because of their versatility and elimination of the need for people and equipment in hard to access and potentially dangerous areas. (2) Stability analysis of open-pit rock-face slopes incorporating advanced probabilistic analyses, providing improved methods for evaluating the performance and potential risks associated with open-pit slope faces. This work incorporated advanced numerical modelling techniques to gain an in-depth understanding of the behaviour of the slope faces, as well as an assessment of the potential vulnerability of mining and other nearby infrastructure. (3) The long-term behaviour of lignite mine spoil materials, with particular attention on stability and ground movements within spoil heaps and reclaimed ground. This work involved laboratory testing of soils, small-scale physical modelling (including elevated gravity modelling using a geotechnical centrifuge) and numerical/probabilistic modelling.

### **2.2 Description of activities and discussion**

#### **WP1 - Development and application of modern monitoring techniques for slope stability in open pit lignite mines**

WP leader: INERIS

WP Partners: UoN, Geocontrol, SUBTERRA, POLTEGOR, VUHU, UNEXE

TASK 1.1: Aerial monitoring systems – advancement and deployment of technology and application methods (INERIS, VUHU, POLTEGOR, UNEXE, GEOCONTROL, UoN)

Aerial monitoring systems allow acquisition of a variety of data with many potential benefits, including (i) large aerial coverage, (ii) rapid collection of information, (iii) access to hard-to-reach areas without exposing personnel to danger, and (iv) fully geo-referenced x, y, z point cloud data. The point cloud data can be used to determine key parameters relating to the discrete fracture network of the rock mass such as orientation, spacing and persistence of major discontinuities. The point cloud data, in the form of a terrain model, can also be incorporated into numerical models to assess the impact of slope geometry and rock mass parameters on the potential for slope instability.

This task explored the use of unmanned aerial vehicle (UAV or drone) technology for the cost-effective and frequent acquisition of high-quality aerial monitoring data. Investigation of the potential for use of drones to acquire high-quality aerial monitoring data has included: (a) digital images for photogrammetry analysis, and (b) Laser Interferometry Detection And Ranging (LiDAR). This investigation was done within the active CSA (Czech Rep.) open pit mine by VUHU with the support of UNEXE and within Polish open pit mines (Bełchatów) by INERIS in collaboration with UNEXE and UoN, and with the support of POLTEGOR.

The choice of Belchatow as a test site was related to the fact that long term production at the mine has influenced the development of horizontal displacements and slope instabilities. Landslides have occurred at Belchatow over the years and have forced the necessity of geotechnical monitoring. The current dimensions of the mine are 12.5 km in length and 3 km width, with a current mined depth of 310 m with two exploitative fields: Belchatow and Szczerbow. A vast monitoring program is in place over its western slope which is subject to the differential movement of multiple geological structures partly related to the Debina salt dome. Therefore, the UAV-borne LiDAR survey targeted an Area of Interest (AOI) of the western slope.

INERIS selected the YellowScan company to carry out the UAV-borne LiDAR survey at the Belchatow mine. The UAV platform selection was constrained on one hand by the mine policy and Polish Air Law, which gave priority to Polish contractors, and on the other hand by the characteristics of the LiDAR used during the mission, the YellowScan Surveyor. This left the YellowScan company to choose the candidate who could complete the survey: MSP. MSP is a Polish company specialized in designing UAVs from drawings to manufacture. The company has developed dozens of UAV platforms including fixed wings and multirotors. The Zawisak quad copter is one of them and was the fittest UAV for the Belchatow LiDAR acquisition. The LiDAR survey was completed with the Surveyor LiDAR developed by YellowScan. It is an ultra-light-weight 1.6 kg standalone sensor, self-powered which integrates easily to multiple platform types. In addition to the LiDAR, an RGB camera was setup on the LiDAR frame. The mounting bracket was developed by MSP and enables the camera to be directed towards the ground and capture a frame size virtually identical to the LiDAR swath length.

The LiDAR mission was scheduled for the 21st of October 2016 but re-scheduled because of the weather conditions to the 26th of October. Again, the mission had to be re-scheduled and finally the acquisition took place on the 23rd of November. That day, 6 flights were completed successfully with the LiDAR. However, the triggering of the camera failed over 1.5 flights. The generated orthophoto covered about 75% of the surface. To complete 100% of the photogrammetric coverage of the survey perimeter, a subsequent mission was planned. Again, bad weather and snow cover of the area delayed the survey. In order to speed up the acquisition it was suggested by MSP and agreed by INERIS to survey the area by airplane at a ground sample distance (GSD) of 25mm coherent with the LiDAR acquisition. The aerial acquisition took place on the 3<sup>rd</sup> of March 2017. In addition, during the field acquisition mission on the 23<sup>rd</sup> of November, a total of 11 ground control points (GCPs) were picked up in the field within the area of the survey. Control points were materialized with a table structure colorized at its centre. Control points were used for the LiDAR dataset as validation ground truth points, thus enabling a more accurate report. The control points were also used during the ortho-rectification process and therefore they were considered as control points rather than validation points.

Data processing of the Surveyor LIDAR dataset acquired at Belchatow mine site was conducted in three steps. Initially the data from the INS (Inertial Navigation System) and the scanner collected from a USB drive plugged to the LiDAR are copied to a ground station computer in the field. This step is typically completed directly after the flight in order to run QC (Quality Control) checks on the raw data. This enables visualization of the point cloud, identification of missing patches or weak overlap to determine if additional flights are needed. Then, further processes are compiled to run Post Processed Kinematic (PPK) to the trajectory. Point clouds corresponding to the flight lines can be re-generated based on the corrected trajectory. Finally, several additional LiDAR processes are achieved to improve the quality of the deliverables. These include noise filtering, flight line matching and classification. In parallel the geotagged photos are taken through a routine process (aero-triangulation, 3D mesh and orthophoto creation) generating the orthophoto of the project. Both LiDAR and photo processes can be merged together to provide a colorized point cloud giving an entirely immersive experience to the user. We identified several issues during the processing of the LiDAR and photo datasets. These include the following items:

- Reflectivity gaps – lignite related: multiple gaps of “no data” were found in the LiDAR dataset and in particular over the southern portion of the AOI. These gaps appear to correspond to dark soil material most probably related to their high lignite content. The alignment, location and size of the gaps occurring in the LiDAR dataset appear to depict the coal complex horizon. The point density over such material falls down to about 3 pts/m<sup>2</sup> – the LiDAR beam is completely absorbed.
- Reflectivity gaps – water related: in a similar fashion, water bodies are depicted by areas of “no data” in the LiDAR dataset. The water reflects the beam as a mirror and hence the sensor never collects the return.
- Reflectivity gaps – pipe related: just like coal material, black plastic pipe will not show on the LiDAR and will create “holes” in the dataset.

The produced point cloud from the LiDAR survey has a density of 250 to 300 pts/m<sup>2</sup> in most areas. Over dark soil cover (e.g. coal sands) the point density is affected and can be reduced to under 10 pts/m<sup>2</sup> - this has been noted on less than 3% of the overall AOI. The point cloud from the manned aircraft photogrammetry has an equivalent point density but does not show low point density issues in the dark soil cover. Only one patch of very homogenous colour was noticed to not generate correlation points and left the area as a gap of data.

Figure 2.1 displays point density per square metre as a 1 m resolution grid. The impact of dark soil on the LiDAR is clearly exposed and does not seem to be affecting the photogrammetric point density.

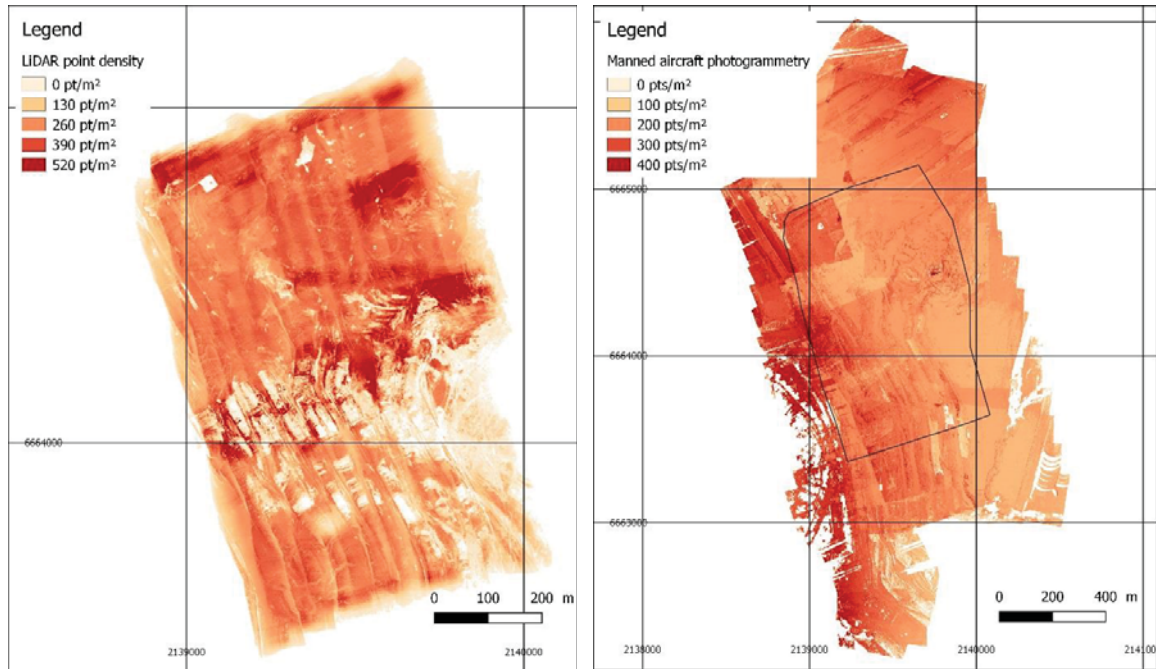


Figure 2.1: Point density for the LiDAR to the left and for the manned aircraft photogrammetry to the right (note that the outline of the LiDAR extent is displayed as black polygon over the photogrammetry density).

The following series of snapshots (Figure 2.2 and Figure 2.3) display different views of the product obtained from LiDAR and photogrammetry both from the UAV and from the manned aircraft.

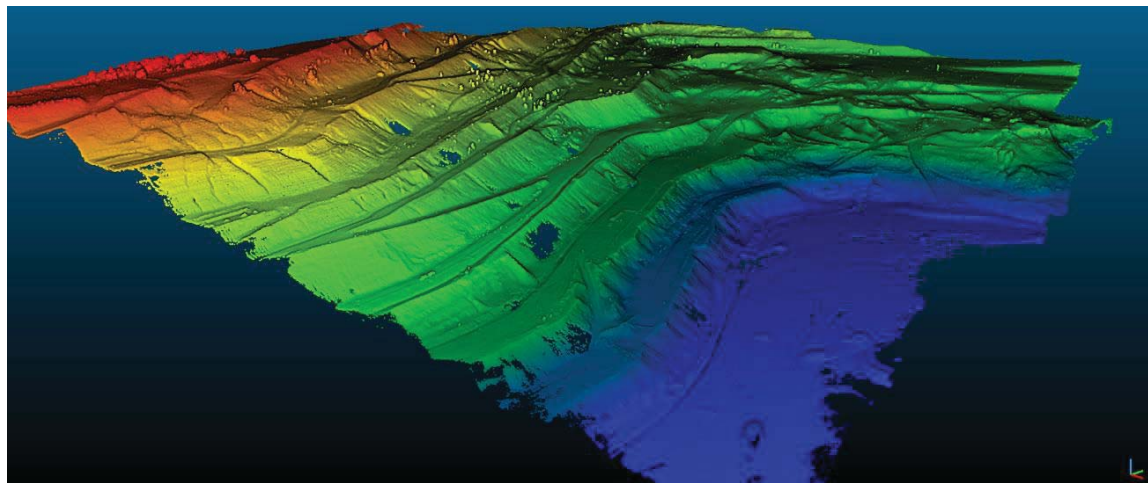


Figure 2.2: Eight-colorized point cloud from the LiDAR acquisition.

The image (Figure 2.3) below captures a specific area to the NE of the AOI that is suspected to have slipped significantly between November 2016 and March 2017. The hillshade rendering between the LiDAR and the UAV photogrammetry is very similar. It appears the fracture network and other lineament features can be detected the same way.

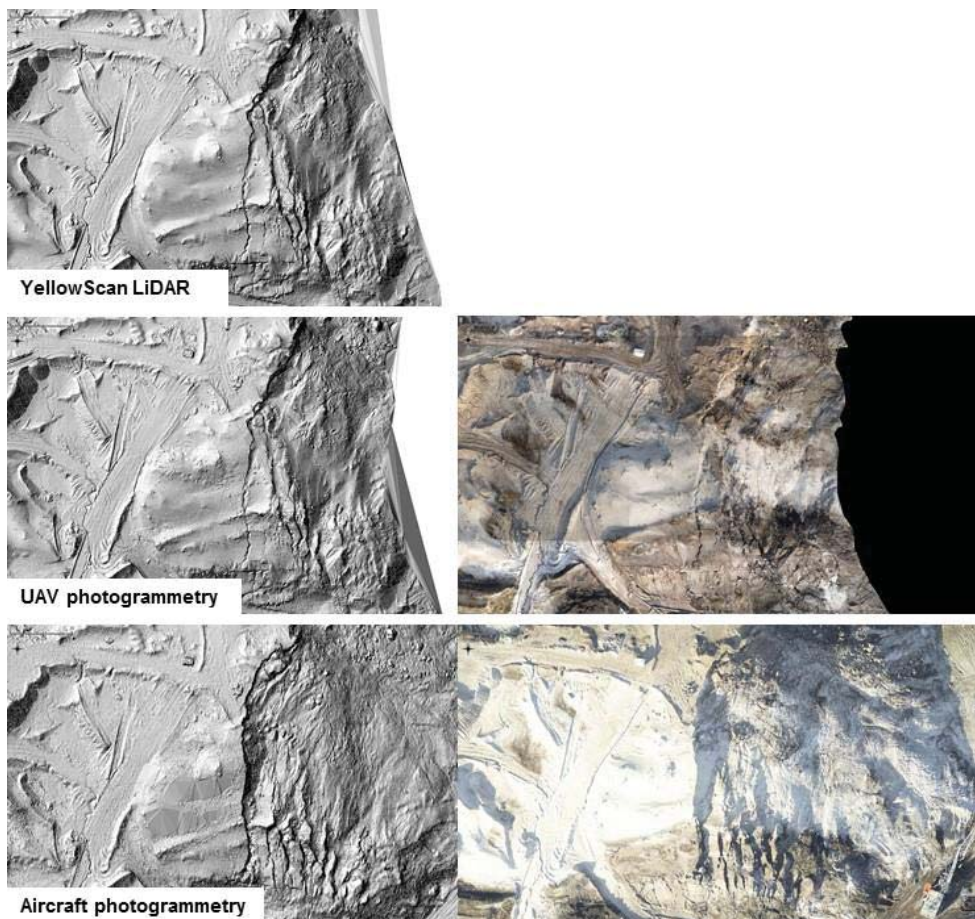


Figure 2.3: Hillshade terrain of the point clouds from all 3 different sensors with the RGB imagery on the right.

The aircraft photogrammetry at the bottom of the image shows a clear ground slippage (Figure 2.3). To confirm and assess the magnitude of ground displacement, the LiDAR point cloud and the March 2017 aerial photogrammetric point cloud were compared in CloudCompare. Figure 2.4 highlights the areas where ground has changed between the end of November 2016 and March 2017. A landslide is clearly identified, and displacement can be estimated from the comparison of the two point clouds.

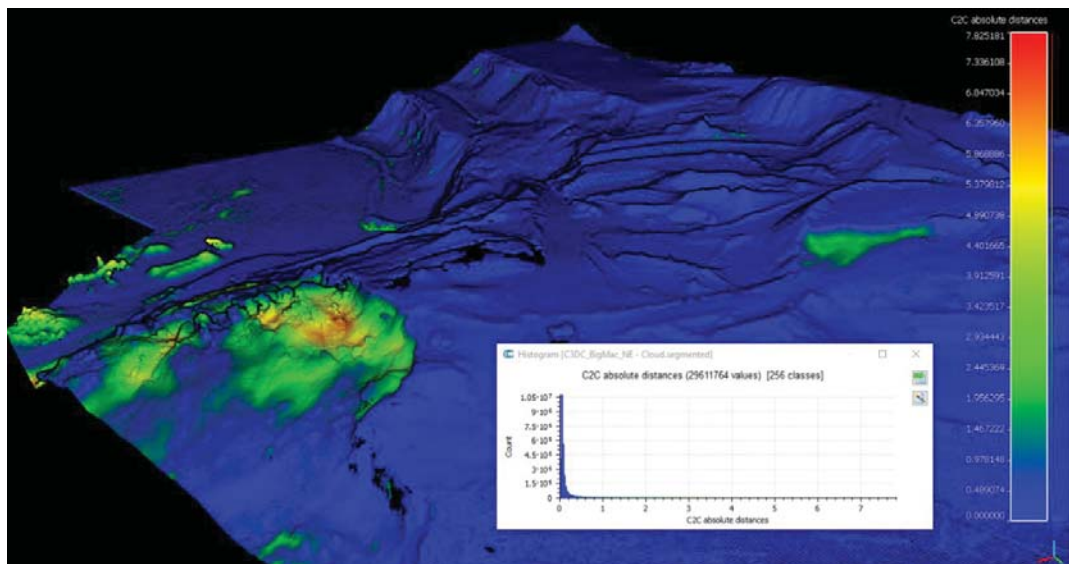


Figure 2.4: Cloud to cloud comparison – reference is the LiDAR point cloud and the image shows the March 2017 photogrammetric point cloud colour coded by ground movement that occurred over 3 months.

In addition, the terrestrial laser (TL) dataset produced by UNEXE in Task 1.3, 3 months before the UAV flight, was used as a reference of ‘quality’ for subsequent aerial Lidar and photogrammetric data to identify potential geometry changes at the Belchatow lignite test site. In this example the

TL data was considered as a standard baseline for all the subsequent data capture campaigns at Belchatow. In addition, as the TL data was undertaken first (July 2016) any deformation of the slope was identified relative to this model. Firstly, the TL data was compared to the first aerial photogrammetry campaign undertaken by INERIS, the result of the comparative analysis is shown in Figure 2.5.

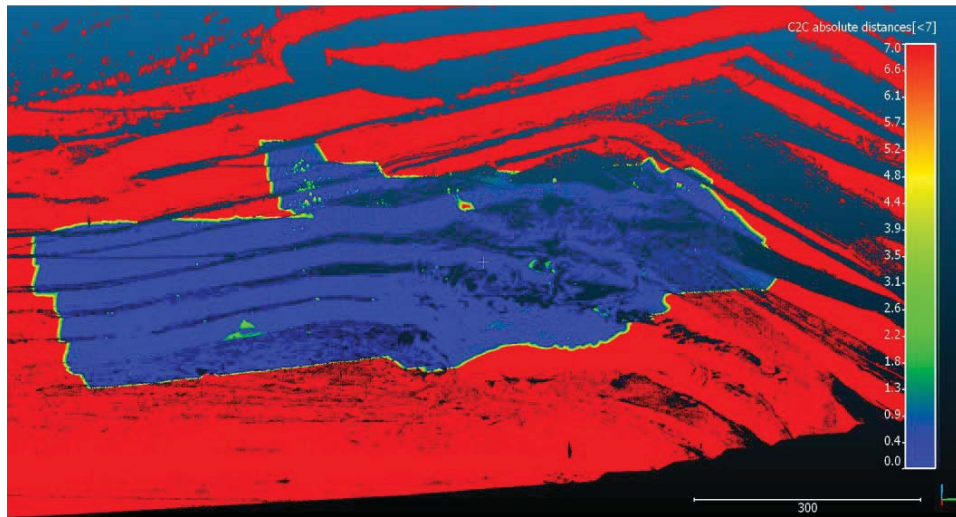


Figure 2.5: Cloudcompare analysis of TL in comparison of the first photogrammetric survey using a Sony camera (West Slope at Belchatow open pit mine).

In addition, during the flight of the aerial photogrammetry survey data was obtained using mobile aerial LiDAR with a YellowScan sensor illustrated in Figure 2.6.

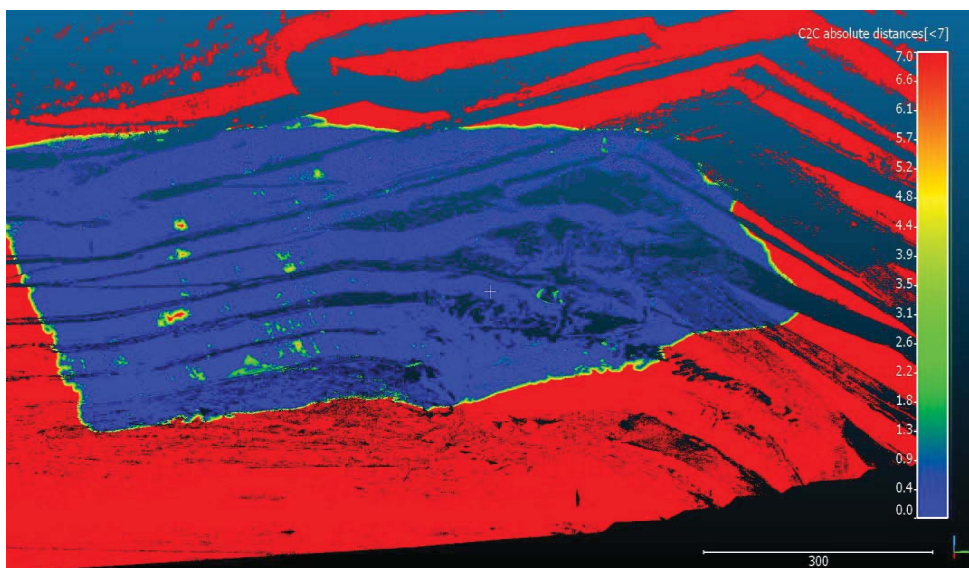


Figure 2.6: Cloudcompare analysis of TL in comparison to the YellowScan aerial LiDAR survey (West Slope at Belchatow open pit mine).

It can be seen from the analysis in Figure 2.5 and Figure 2.6 that there are a number of areas of potential deformation (yellow, red, green in the middle of the blue area), the magnitude of which is illustrated using the scale bar on the image. The TL data was also compared with the second aerial photogrammetric flight (data provided by INERIS) and the result is shown in Figure 2.7.

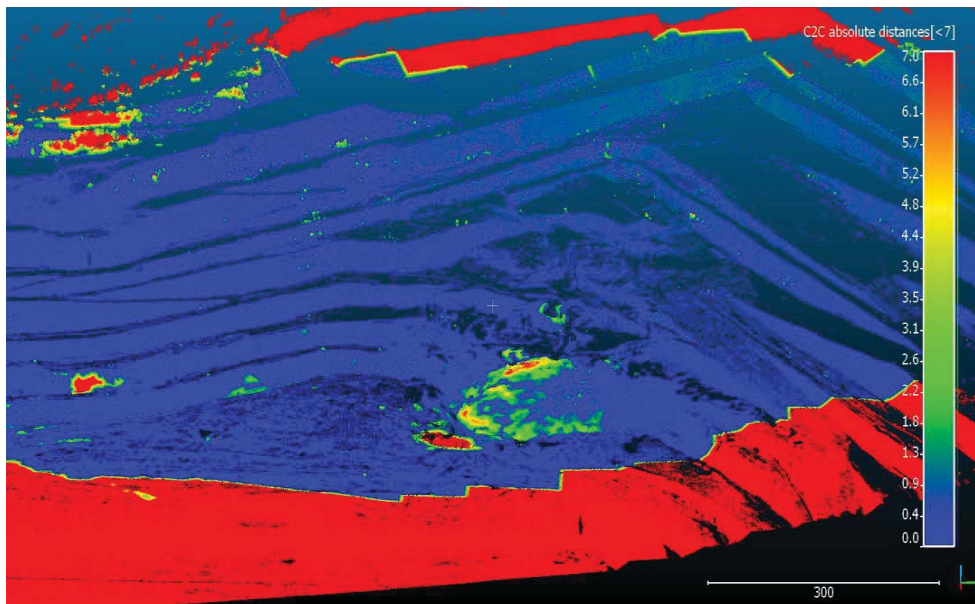


Figure 2.7: Cloudcompare analysis of TL in comparison to the MicMac aerial photogrammetric survey (West Slope at Belchatow open pit mine).

It can be seen using the various comparisons that there is a good synergy between the datasets of the West slope, confirming that areas of deformation have occurred after the initial laser scan undertaken in July 2016 and the last flight in March 2017.

For the ČSA open pit mine, 11 imaging flights from April 2016 to December 2017 were done by VUHU to create a digital terrain model of the ČSA landslide area. In total 10 flight campaigns were obtained using DJI Phantom 3, and one campaign with DJI s900 in cooperation with Czech Technical University (see Table 2.1). Imaging flights were done according to a computed flight plan, which was always determined based on required overlay images (usually 60% and 45%) of the desired image resolution (1.2 to 2.0 mega pixels / cm) and a cruising speed (at scanning velocity does not exceed 18 km/h). Pictures were taken in the calculated interval, and each point on the ground was always captured by several images, each at a different angle. Image correlation method stacks all images into a single image and creates a 3D image of study area. Images were processed in specialized Agisoft PhotoScan software which determines the position of the image in the absolute coordinate system with minimal need for ground control points (normally use 10 targets with dimensions of 500 x 500 mm).

Open-cast mine spaces are generally suitable for UAV use, particularly due to visual variation area and the absence of dense vegetation. Using ground control points, a Digital Elevation Model (DEM) from unmanned aerial surveying can achieve accuracies of  $\pm 10$  mm in places where the open-cast mine slopes are without vegetation (see Table 2.1).

Table 2.1: Details of the 11 flights at the ČSA mine.

Flight No.	Date	Machine	Resolution	Pixel size
1	13.4.2016	DJI Phantom3	4000 x 3000	1,56 x 1,56 µm
2	18.8.2016	DJI Phantom3	4000 x 3000	1,56 x 1,56 µm
3	11.10.2017	DJI Phantom3	4000 x 3000	1,56 x 1,56 µm
4	11.4.2017	DJI Phantom3	4000 x 3000	1,56 x 1,56 µm
5	17.5.2017	DJI Phantom3	4000 x 3000	1,56 x 1,56 µm
6	14.7.2017	DJI Phantom3	4000 x 3000	1,56 x 1,56 µm
7	14.7.2017	DJI s900	6000 x 4000	4,07 x 4,07 µm
8	31.8.2017	DJI Phantom3	4000 x 3000	1,56 x 1,56 µm
9	22.9.2017	DJI Phantom3	4000 x 3000	1,56 x 1,56 µm
10	13.10.2017	DJI Phantom3	4000 x 3000	1,56 x 1,56 µm
11	13.12.2017	DJI Phantom3	4000 x 3000	1,56 x 1,56 µm

Comparing the Phantom and S900 results gave an interesting result: the difference between the two DEMs is very low (Table 2.2). It shows that the difference in resolution of the camera is not so critical in the open-pit mine environment, where the goal is to achieve an accuracy of less than 30 mm, ideally below 20 mm, which is achieved by both DEMs. Even a "low-cost" UAV equipped with a 4k camera can be used to create a full-fledged DEM. From this point of view, an important factor is the distribution of ground control points which are inappropriate to be placed in the lines. Much more convenient is a random pattern of ground control points. It is clear from the table below that the precision of the DEMs has gradually faded. For flights no. 1 - 3, ground control points were always placed in three lines, the accuracy of the X and Y axes oscillated around 30-50 mm. In the

following flights no. 4 - 11, a random placement of ground control points across the entire area was used, and the precision of the models was on the order of several millimetres. With such achievements, accuracy of the method can be used as an inexpensive and operational complement conventional aerial photogrammetry, as well as a method for monitoring the side slopes of open-pit mines and for operational monitoring landslide movements in the ČSA open-cast mine.

Table 2.2: Comparison between the Phantom and S900 results.

Flight No.	UAV	X error (mm)	Y error (mm)	Z error (mm)
1	DJI Phantom3	42,6	44,2	19,7
2	DJI Phantom3	28,9	33,9	8,5
3	DJI Phantom3	42,0	57,4	31,9
4	DJI Phantom3	8,9	5,8	2,5
5	DJI Phantom3	13,6 15,4	20,4 13,9	23,3 6,9
6	DJI Phantom3	12,3	7,9	7,3
7	DJI s900	8,8	9,6	3,8
8	DJI Phantom3	4,5 1,3	8,1 1,9	8,6 3,4
9	DJI Phantom3	5,5	7,3	2,9
10	DJI Phantom3	2,7	2,2	0,7
11	DJI Phantom3	1,8	0,7	0,2

GEOCONTROL focused on the identification of critical unstable zones of slopes through the processing of aerial monitoring data. To accomplish that, a software application was developed that, through local dispersion analysis of UAV point clouds, helped in the efficient analysis of movements and displacements of landslides. More specifically, research was aimed to the development of a numerical indicator of the degree of local folding of the terrain surface, whose values and changes allow the identification of landslide scarp features and the analysis of registered displacements on the context of landslide geomorphology. To achieve this objective, a methodology defined as Analytical Scarp Detection Model (ASDM) was developed and implemented through a software application. Both the methodology and the application are described in detail within project Deliverable 1.1.2; a brief overview of the methodology is provided here.

Local dispersion analysis can be summarized as a process consisting in the observation of spatial distribution of a local set of points, for which a covariance matrix is obtained from point coordinates. It has been frequently used for obtaining normal vectors, roughness calculation, or features extraction (Gumhold et al., 2001; Mitra and Nguyen, 2003; Pauly et al., 2002). It has also been approached for landslide monitoring (Al-Rawabdeh et al., 2016; Kasai et al., 2009) and rock discontinuities analysis (Riquelme et al., 2016, 2015).

Within the developed algorithm, results are achieved by a massive iteration through all the points in the cloud (e.g. acquired by UAV survey), where a series of steps are repeated for every point "i". First, a sub-set of surrounding points is extracted by spherical search from the point "i" being analysed, thus defining a local neighbourhood of that point, as shown by Figure 2.8. Then a covariance matrix is built from the neighbourhood point's coordinates, therefore obtaining the principal components (eigenvalues and eigenvectors). These algebraic components provide a representation of the average principal directions of the local neighbours point cloud, as shown in a 2D example in Figure 2.8. Then, analytically obtained equations of these eigenvalues enable the determination of the angle " $\delta$ " as a measurement of the degree of "folding" of the surface surrounding point "i" and, based in that angle, the classification of regions in four classes.

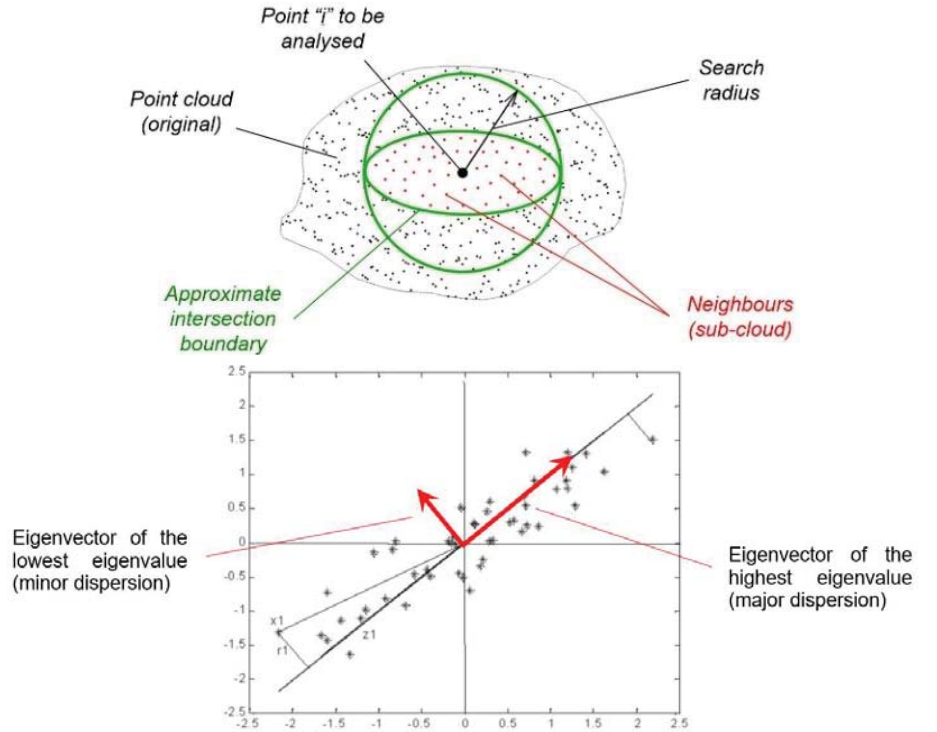


Figure 2.8: Neighbour search operation scheme (top) and example of 2D point cloud and main directions obtaining (right). Bottom figure modified after Peña (2002).

The complete work scheme of the methodology, up to the obtaining of the “ $\delta$ ” angle and prior to the classification of regions, is summarized in Figure 2.9.

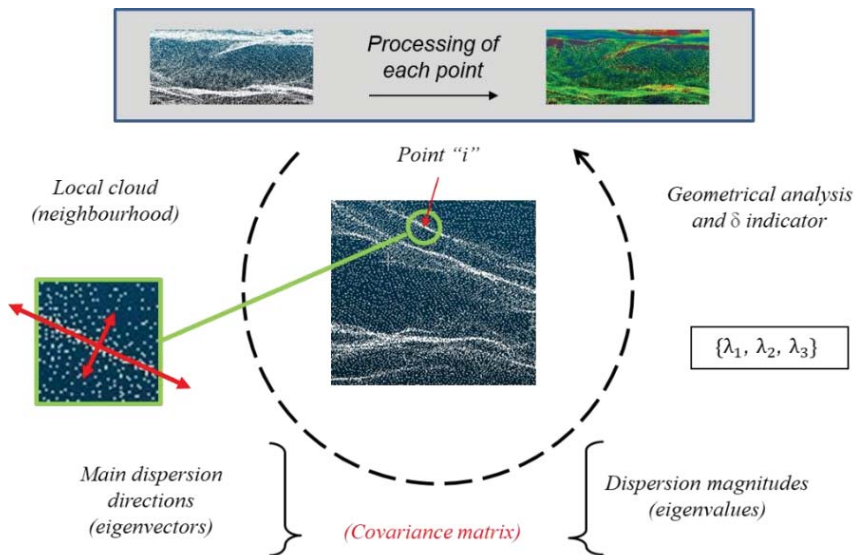


Figure 2.9: Structure of the obtaining of  $\delta$  through local dispersion analysis of a point cloud.

Within this process, the analytical formula that allows the calculation of  $\delta$  from the eigenvalues of a certain point was developed through the detailed analysis of idealised surfaces representing perfect scarps and flat regions. A first adopted hypothesis for the methodology was the assumption that every terrain surface (represented through a point cloud) can be approximated by a series of planes of different size and geometry (as, for example, typical triangular networks). Therefore, every local region can ideally be thought of as a perfect plane or the intersection of two planes forming a fold of angle  $\delta^*$ , equivalent to the angle between their normal vectors. This way, scarps within the perfect-planes-model would be simply one-axis folds of the surface (intersections between planes).

The next step in the development of the model, was the study of the type of neighbourhoods to be obtained during search operations if the local-dispersion approach would be applied over the continuum surfaces of the hypothetical surface. According to this, three geometries could be obtained: perfect circles (flat surface neighbourhoods), circles bent by a chord and circles bent by a

diameter, as a particular case obtained when point "i" being studied belongs to the edge of a scarp. Figure 2.10 shows an example of the third case, where two planes of the terrain surface intersect forming an angle  $\delta^*$ . These idealised local neighbourhoods were analysed considering them as point clouds of infinite density and the three analytical formulas for their expected eigenvalues of dispersion (Table 2.3) were obtained by surface integration, depending on two variables: the angle of folding of the geometry and the radius used for search operations.

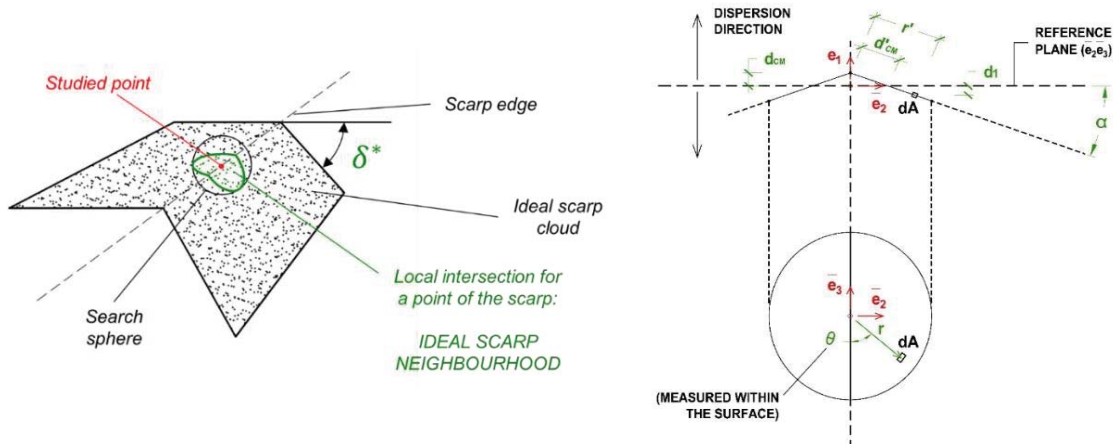


Figure 2.10: Local neighbourhood associated to points belonging to scarp edges (left) and example of the geometrical model used for the integration of  $\lambda_1$  formula.

While the complete development of analytical eigenvalue equations can be found in Deliverable 1.1.2, here Table 2.3 summarizes the three formulas, plus the resultant equation of eigenvalues ratio  $ER_2$ . This parameter is obtained as the ratio between the first and third eigenvalues, which removes the dependence on the search radius " $R$ ", thus representing a numerical value dependent exclusively on the local folding angle  $\delta$ .

Table 2.3: Analytical eigenvalue equations obtained according to ASDM model

Value	Analytical formula
$\lambda_1$	$\lambda_1 = \sin^2 \frac{\delta}{2} * \left[ \frac{1}{4} - \frac{16}{9\pi^2} \right] * R^2$
$\lambda_2$	$\lambda_2 = \frac{\cos^2 \frac{\delta}{2}}{4} * R^2$
$\lambda_3$	$\lambda_3 = \frac{1}{4} * R^2$
$ER_2$	$ER_2 = \frac{\lambda_1}{\lambda_3} = (\sin \frac{\delta}{2})^2 * \left[ 1 - \frac{64}{9\pi^2} \right]$

Finally, the analytical equation of  $ER_2$  can be modified to isolate angle  $\delta$ , leading to the final following equation which allows the calculation of local folding around a point in the cloud, based in the eigenvalues of its covariance matrix.

$$\delta = 2 * \arcsin \sqrt{ER_2 * \left[ 1 - \frac{64}{9\pi^2} \right]^{-1}}$$

This methodology was tested, prior to its application to real case point clouds, on a series of "artificial scarps" of perfect geometry, as the one shown by Figure 2.11. Conclusions were that the equations correctly represent the empirical values (error tends to zero for higher densities of the point cloud), as can be observed in Figure 2.11 as well.

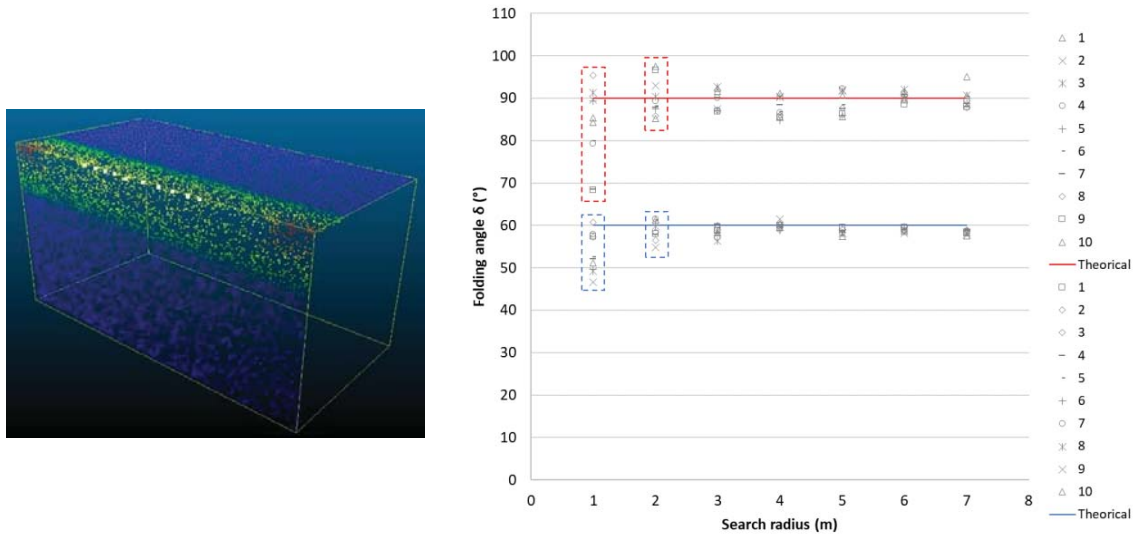


Figure 2.11: Example of obtained  $\lambda_1$  eigenvalues for the geometrical model representing a 90° scarp (left) and folding angle results for the models of 60° and 90° (right).

As commented before, values of  $\delta$  angle were used not only to help in surface analysis, but also to allow surface classification. Four classes of regions, as shown by Figure 2.12, were defined according to their physical meaning:

- *Flat regions*, for those areas whose equivalent degree of folding ( $\delta$ ) is lower than 15°
- *Lesser scarps*, for points with folding angle ranging between 15° and 25°
- *Main scarps and lower vegetation*, for angles between 25 and 90°
- *Interferences* (mainly dense vegetation), for those regions with angles above 90° or unable to be calculated.

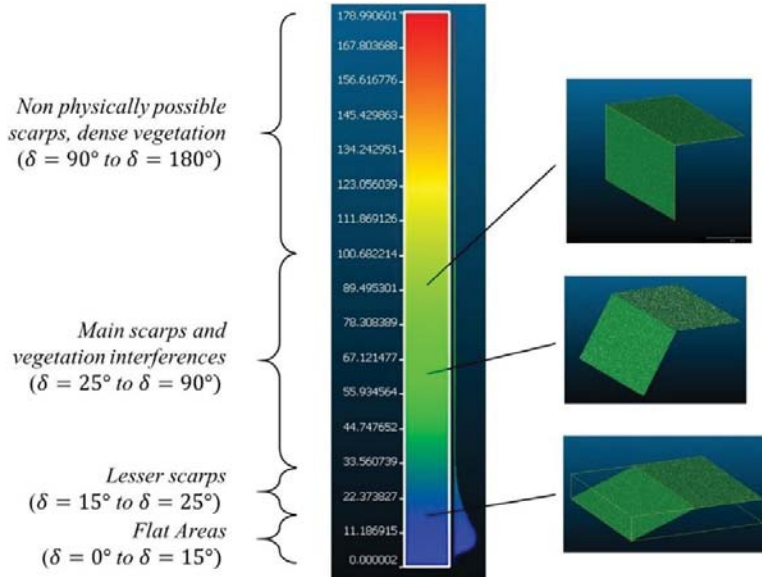


Figure 2.12: Proposed classification based on  $\delta$  scalar field (left) and artificial scarps used for testing of the algorithms (right).

Thus, the algorithm developed by GEOCONTROL allows the assignment to every point of the cloud of three principal values: “ $\delta$ ” angle, slope angle (of immediate calculation from eigenvectors analysis) and a classification index (to differentiate areas potentially belonging to scarps, vegetation, etc.).

The whole process of the methodology was implemented through a desktop application written in C# language and applied on CSA mine real-case data. A detailed analysis of the landslide geomorphological features through the application was coupled with the analysis of displacement trends for different periods of time within the project schedule. This kind of landslide analysis allowed the identification of the main active regions of the landslide and the segmentation of areas prone to vegetation interference. Figure 2.13 shows two of the graphical results obtained through the application to CSA mine of the developed algorithm and cloud displacement tools of CloudCompare software.

In these images, using the algorithm developed by GEOCONTROL, main scarp features have been extracted as sub-clouds (green colour), as well as the densest vegetation masses (blue colour points), allowing a better interpretation of the landslide morphology and activity during a certain period of time. Points belonging to "flat areas" and "lesser scarps" classes, are coloured in a red-white-black scale indicating the variations of Z coordinate between August and October 2016.

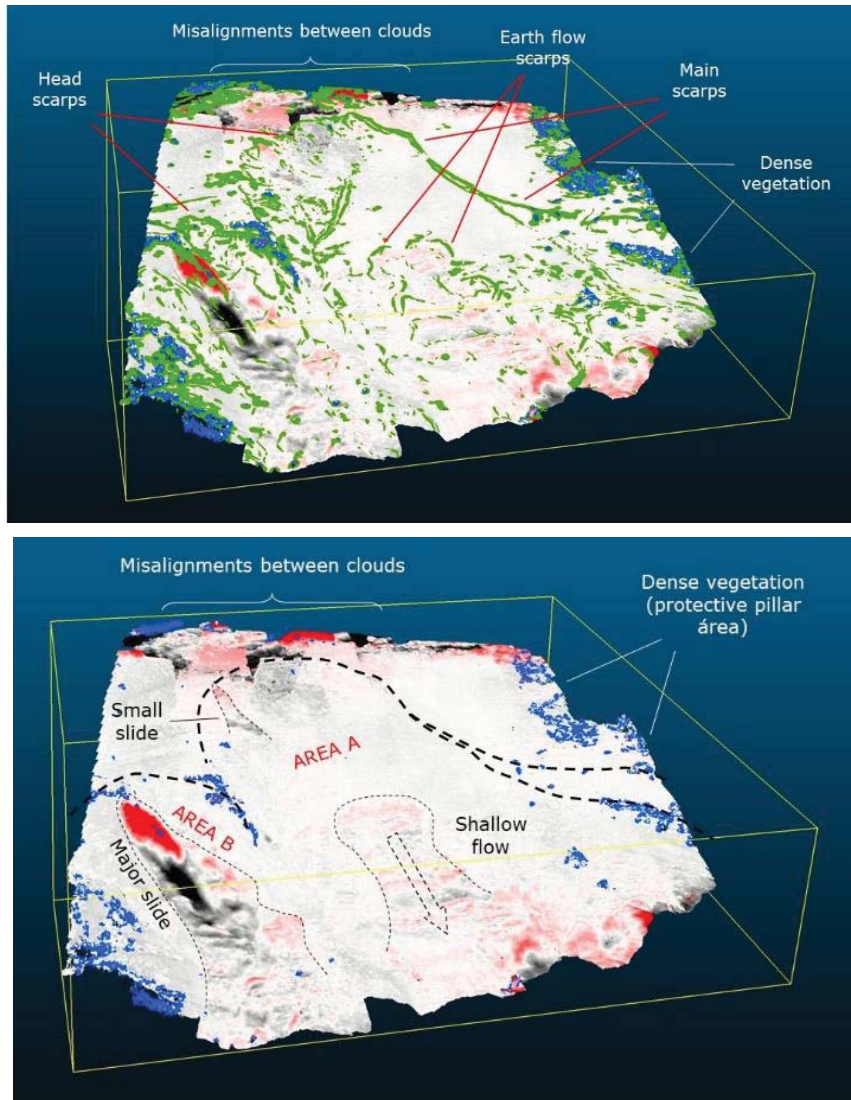


Figure 2.13: Combined analysis of ASDM classification and displacements calculation between August and October 2016, including scarps (green), dense vegetation (blue) and displacements (red-black coloured scale representing reduction-increase in Z coordinate respectively)

From these results, many conclusions of importance for the landslide monitoring could be extracted. First, two connected landslide areas can be identified, represented in Figure 2.13 as "Area A" and "Area B". Both these areas present curved head scarps and, during the studied period, a major landslide was developed within Area B, where it can be easily observed the sliding area (red) and its deposition downwards (black). Moreover, this ground movement is located just beneath the upper scarp of this area. On the other hand, a smaller landslide was developed in Area A, beneath its head scarp as well. Both these instabilities prove the headward erosive potential of the active landslide. A third identifiable ground movement was observed within the body of Area A, probably belonging to a shallow earth flow. This instability also shows clear head scarps coincident with the top part of the mobilised area and minor scarps at the sides of the flow path.

Another observation of importance was that few points belonging to "Interferences" class (blue) were located within displacement areas, thus validating the detected displacements as real ground movements. Exception to this fact were a few points located at the centre of the west landslide. However, since these points are few and cloud-to-cloud displacements were above 3 metres for this area, it is clear that vegetation could not be responsible for the movements.

It is also clearly seen that the only remaining vegetation of importance inside the cloud (not at the borders of the landslide) is located at the remaining peak between the two active areas. On the

other hand, the chaotic displacements above the head scarp of Area A are due to the different UAV flight cover within these upper parts.

To continue with the analysis, Figure 2.14 shows a different representation of the results, where displacements have been filtered just to show points of regions where Z coordinate was reduced from August to October flights. Remaining points are substituted with the original RGB coloured cloud.

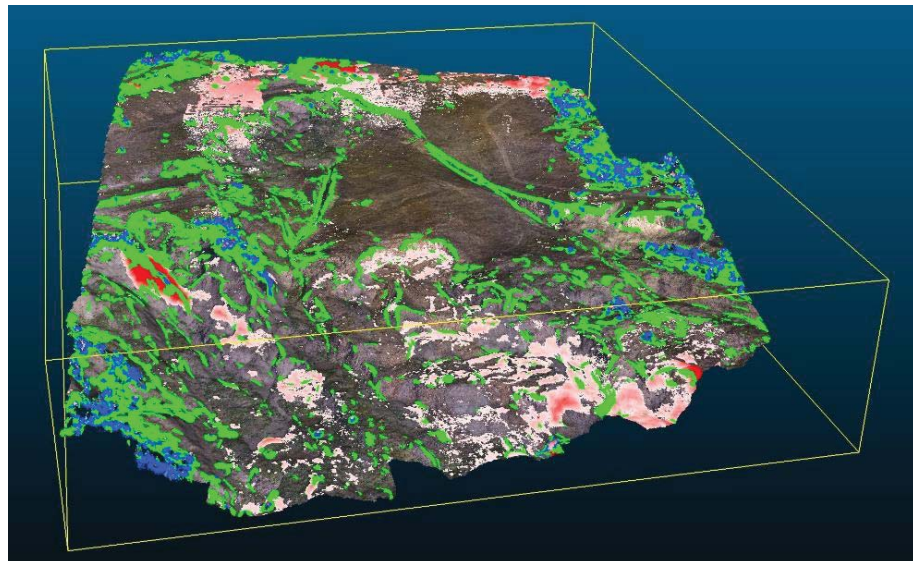


Figure 2.14: Representation of the identified scarps (green), vegetation (blue) and slided/eroded areas (red-white scale shows reductions in Z coordinate).

Through this representation, most unstable areas are better identified, which are most of all located in steeper parts beneath scarps. However, the main scarp which separates Area A from the protective pillar does not appear to be affected by local instabilities for the studied period.

Previous results show that coupling morphological classification of the point cloud with registered movements helps in the better understanding of the landslide evolution, as well as in preventing its behaviour. To complement point cloud results, the analysis of registered displacement trends against water-related and geomorphological parameters has been performed, where it was determined that the main factor triggering the instability reactivation in CSA case of study was the water content, as it is detailed in project Deliverable 2.2.1.

**TASK 1.2: Advanced systems for automated and continuous monitoring of mass ground movements (INERIS, POLTEGOR, SUBTERRA)**

Task 1.2 focused on the application of advanced automated monitoring systems that can provide continuous data for the identification of slope instability hazards in open pit mines. Project partners, INERIS and POLTEGOR worked together for the design and implementation of a monitoring system and the development of an intelligent data management and early warning system (EWS). INERIS and SUBTERRA focused on the definition of criteria for landslide activation (displacement, velocity, pore pressures, etc.) for helping the mine authority to manage the mine under safety conditions.

To achieve the objective, two pilot sites were chosen: the Polish mine Belchatow and the Spanish mine CLC. For the first site, an advanced 3D mass movement monitoring and early warning system was deployed using e.cenaris infrastructure (INERIS: <https://cenaris.neris.fr/SYTGEMweb/public/>). For the second site, different studies and numerical modelling were carried out to define appropriate criteria for EWS.

For this task INERIS created a web-monitoring page for the Belchatow mine in Poland during the summer of 2017. This cloud-monitoring solution permits: streamlined monitoring and database management, on-line data processing, advanced plotting, tailored web monitoring desk, data and metadata sharing and messaging for operational decision making. Access to the e.cenaris Belchatow page is secured; at the end of September 2017 each partner of the project and PGE (mine managers) received a personal login to the web-page. The web-monitoring page is characterized by two parts: Welcome and Monitoring (Figure 2.15). The "Welcome part" contains a short summary of the project description. The second part is dedicated to the Belchatow geotechnical monitoring data presented in the previous chapter. The monitoring data are integrated into the e.infrastructure via a secured FTP server. The raw data are then processed through advanced numerical routines to yield relevant variables with customized plots and catalogues, according to POLTEGOR and PGE's request. Each partner can view these time series and can download them in pdf format or Excel format. In the web-monitoring page, it was also

possible to store all SLOPES project reports, technical files, maps, etc available in the framework of the project.

Figure 2.15: Web-monitoring page of Belchatow web monitoring e.cenaris page overview.

The implementation of an early warning system was also executed via e.cenaris. For the Belchatow mine, it was decided to use and test the remote alarm management tool available in the e.cenaris web-monitoring platform as it permits to set up different types of alarm according to our needs:

- simple alarm: alarm from a direct sensor measure (e.g. pore pressure, temperature, displacement, etc.),
- simple alarm on complex variables: alarm from calculation results (e.g. average value, ratio value, etc.),
- complex alarm: operational alarm ("and", "or") binding together several simple alarms (e.g. pore pressure and displacement at the same time or temperature average values and displacements, etc.).

The system can create different types of complex alarms depending on our needs and data.

First of all, for Belchatow open pit mine, alarms for data absence for all geotechnical data were set up and activated. In this way if data were not put on the server an alarm was generated. Then, some simple alarms in agreement with POLTEGOR and according to the results of the first period of monitoring, were created for x and y displacement (between 10 and 30 mm a day after the last value) and pore pressure (the pore pressure drop and increase probably cause during the monitoring period the largest movements, according to POLTEGOR). These two measures were coupled with the creation of a complex alarm. Generally, the presence of more than one threshold is more efficient than only one parameter threshold. The geology and monitoring show that for Belchatow mine the displacements in deeper layers were caused by complex factors including above all uplift of the coal due to the salt dome. Concerning warning levels, for Belchatow mine only one warning level was established. Generally, the adopted strategy for risk management is based on three warning levels: "attention", with instrumental real-time monitoring and real time simulation model running; "alert", involving civil protection agencies and field direct control; "alarm", involving population to be evacuated. Because of the short period of monitoring it was not possible to establish different warning levels, such as attention level, warning level and alarm level.

Geotechnical investigations conducted by POLTEGOR carried on the west slope delivered new geotechnical data. Site investigations included drillings and in-situ instrumentation. On-line inclinometer and pore pressure monitoring devices were installed. These monitoring measurements were supplemented by high resolution satellite Persistent Scatterer Interferometry (PSI) conducted by POLTEGOR in cooperation with GAP-Technical University Bari (Italy). The in-situ monitoring installation was located in northern part of west slope of Belchatow field (Figure 2.16). Field works were performed from 12-19 December 2016. The installation of on-line monitoring system in 132 mm borehole included detailed geological description of the core. Sampling and in-situ instrumentation was designed and supervised by POLTEGOR. The borehole was located in a risk area in the NE contact zone of the salt dome. Instrumentation was designed to identify the risk posed in this area. The design instrumentation included innovative shape accelerated arrays system with automated measuring devices containing 200 ground displacement sensors. The continuous inclinometer system is 100 m in depth and built from rigid 0.5m long segments. The system includes 3 magnetometers for control of system rotation. One segment includes 3 tilt sensors measuring range  $\pm 45$  degrees, accuracy 0.02 mm/m, and admissible error of joints +/-

0.250 mm. Every octet (8 segments) is equipped with a ground temperature sensor for correction of temperature effects. The maximum measuring range of the equipment depends on the speed and depth of movements (usually not more than 500 mm). The system is waterproof up to 980 kPa. The system was additionally equipped with a pore pressure sensor located at a depth of 30 m. The field station is powered by a solar panel. The monitoring data are registered every 6 hours and were available on-line from 19 December 2016. Connection with the field station was realized every day and was interpreted in the SAA3D software for creation of plots of magnitude, cumulative, incremental displacements and pore pressure. Results were sent every week to the Belchatow Mine (PGE) along with a report describing observed trends, risks and conclusions. Monitoring data were registered from 20 December 2016 until the end of March 2018. However, data will be registered till end of 2018. If the mine will be interested in further measurements station will be working also after that time.



Figure 2.16: On-line monitoring station in Belchatow mine

Over 1700 series of data from 200 displacement, 50 ground temperature, three magnetometers, one pore pressure and temperature transducer at 30 m depth were collected until the end of March 2018. The online system registered parameters which allow correction of measurements for temperature and rotational effects (temperature sensors and magnetometers). The largest variations of temperature was registered up to 5 m depth and varied between 0-23C; below this depth temperature was nearly constant at 13C. The depth of observed ground displacements varied from 0-77m (Figure 2.17a). The magnitude of displacements reached 120 mm; displacement direction was initially NE then changed to E. On-line monitoring measurements detected that the largest cumulative displacements in slope inclination direction X (slope inclination) reached 120 mm; in the perpendicular Y direction it was 68 mm (Figure 2.17b). A pore pressure drop from 259 kPa in Dec 2016 to 105 kPa in March 2018 was measured. The relationship between ground movements and pore pressure changes is shown in Figure 2.18.

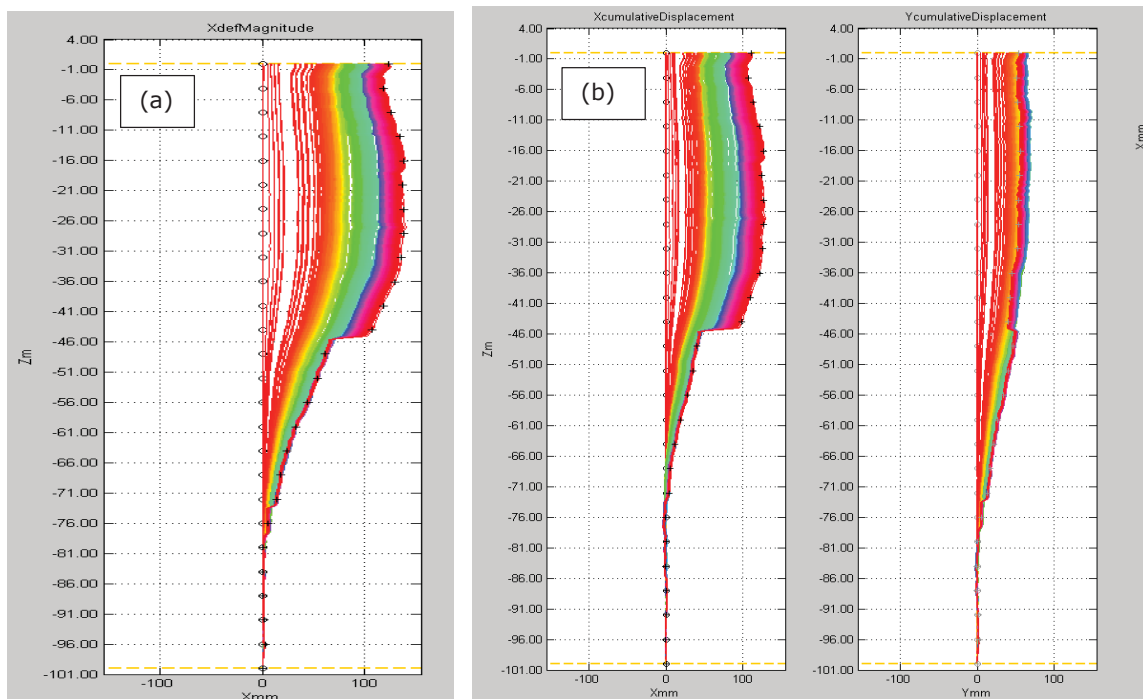


Figure 2.17: (a) Displacement magnitude; (b) cumulative X, Y displacement at Belchatow mine

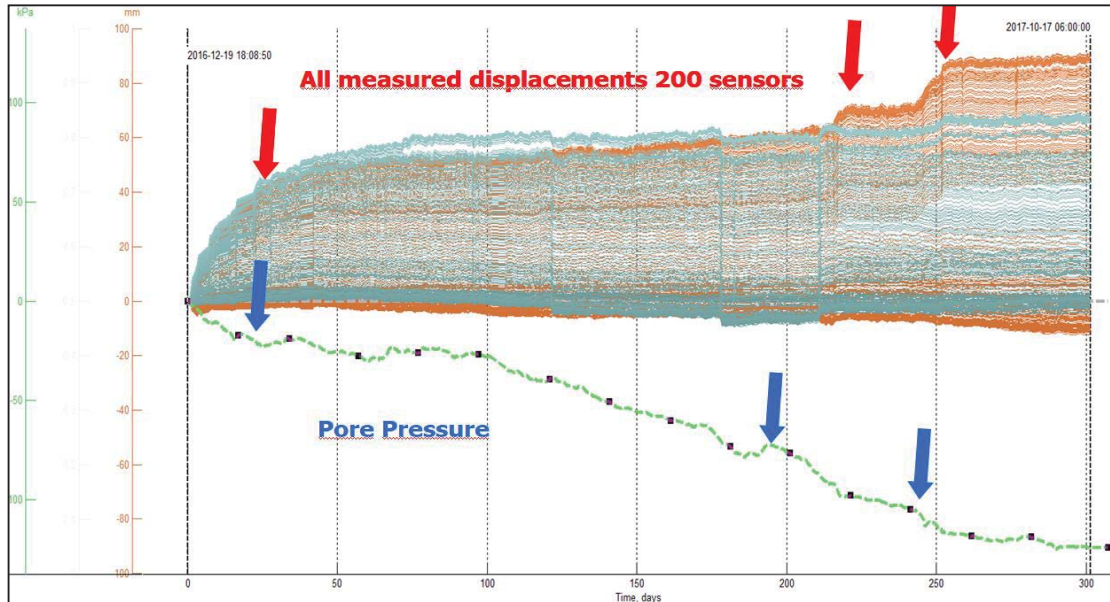


Figure 2.18: Comparison displacement and pore pressure values, Belchatow mine

The location of the largest observed ground movements were in a thin clay layer inside the lignite deposit at 45 m depth and at the top of the lowest 3.3 m thick lignite deposit. However, the monitoring system didn't reach the Mesozoic bedrock which is 50 m deeper therefore it is difficult to assess deeper layers (the mine exploitation is 300 m deep). The displacements in deeper layers were caused by complex factors including uplift of the coal seems by the salt dome.

In October-November 2017, there were some communication difficulties with the field station; an additional external directional antenna was installed to address this problem. Improvements to the power supply system was also implemented, including modification to the download protocols. After these changes, the field station worked continuously, however the GSM data transfer system did required periodic maintenance every few months.

Satellite PSI monitoring was conducted by POLTEGOR in cooperation with Geophysical Applications Processing s.r.l. (GAP), a spin-off company of Politecnico di Bari, Italy. The technique used for this monitoring is based on the multi-temporal SAR (Synthetic Aperture Radar) interferometry applied to COSMO-SkyMed X-Band SAR acquisitions, also known as PSI (Persistent Scatterer Interferometry). GAP was involved in the development of SPINUA (Stable Points Identification in Non Urbanized Area), a multi-temporal SAR interferometric processing chain for infrastructure and ground instability monitoring. SPINUA offers a systematic processing strategy, capable of utilizing all archived data of a certain area, by creating a stack of differential interferograms that have a common master image. Instead of analysing the phase only in the spatial domain, the phase of PS (persistent scatter) is analysed as a function of time and space. PS techniques bypass the problem of geometrical and temporal decorrelation by considering temporal coherent scatterers. Furthermore, by using a large amount of data, the atmospheric signal is estimated and corrected for. It offers a convenient processing framework that enables the use of all acquired images (irrespective of baseline), and a parameter estimation strategy for interferograms with low spatial coherence (Bovenga et al. 2004). Improvements of the SPINUA algorithmic steps have been carried out in collaboration with the University of Delft, with the Department of Physics of Bari and with the CNR-ISSIA of Bari.

The work related to the SLOPES project included the selection of the area of interest for the application of the SPINUA processing: the Belchatów mine. At the beginning of the project no images were available and, for that reason, GAP interacted with the Italian Space Agency (ASI) to prepare and agree an acquisition plan to cover the period and the area of interest. The acquisition plan was monitored by GAP for almost two years (from June 2016 to April 2018) by interacting with ASI when necessary, thus leading to a stack of 50 COSMO-SkyMed images acquired in STRIPMAP HIMAGE mode equally distributed in the period of interest. The images obtained in this step represent the data-set processed in the research activity illustrated in this document. The final coverage was determined by the overlapping area of the fullframe input SAR images. The candidate PS were used to (1) remove atmospheric artefacts, (2) identify the definitive PS locations, (3) measure accurately their height and position (4) and finally produce the displacement maps over the whole frame. The data-set processed by SPINUA is composed of 50 acquisitions.

In order to monitor with PS techniques an area around the Belchatow mine, the acquisition of COSMO-SkyMed SAR images was planned for the period June 2016 – April 2018. The area covered

by the tasked acquisitions has an extension of around  $40 \times 40 \text{ km}^2$ . The images are acquired in STRIPMAP mode, in ascending geometry, with a spatial resolution of 3 meters.

As illustrated in Figure 2.19a, SPINUA generated a displacement map covering an extension of about  $1600 \text{ km}^2$ . It is important to note that displacements estimated by the PSI techniques are projected along the line of sight (LOS) of the satellite. In other words, PS velocities are relative to the satellite position: positive values (blue points) correspond to points moving toward the satellite, whereas negative values (red points) correspond to points moving away from satellite. Points moving orthogonally to the line of sight are “seen” as motionless points by the satellite. Figure 2.19b shows a zoomed-in view of the mine and illustrates that it is possible to detect that the largest subsidence (red colour) occurred on the external spoil dump storage in Szczercow, on the internal spoil dump, and on the internal storage of ashes from the power plant. The largest uplift – probably due to changes of the slope morphology (blue colour) connected with landslide movements, occurred at the north and south slope of the Belchatow Field.

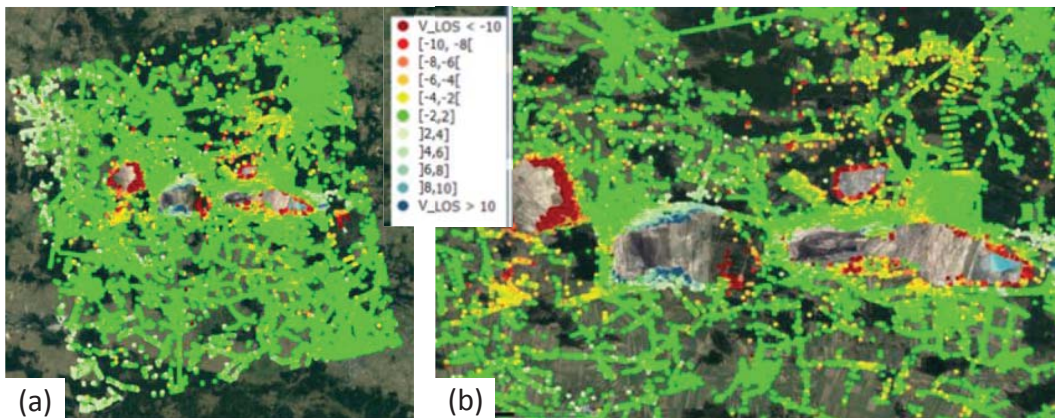


Figure 2.19: Average displacement velocities: (a) coverage of the area processed by SPINUA; (b) zoomed-in view of the mining area

Based on the obtained data, a selection of unstable areas was identified using PSI, as illustrated in Figure 2.20: A1 and A2 = the external Szczercow spoil dump; A7 = East slope of Szczercow Field (mine) + Debina salt Dome; A8, A10 and A11 = West, North and South slopes of the Belchatow field (mine), respectively; A9 = sedimentary collector for groundwater pumped out of the mine; A12 = Belchatow field internal spoil dump with storage of power plant ashes; A13 = area close the border of Belchatow Field (former part the of mine) and non-exploited Kamiensk field (partly covered by Kamiensk Mountain - external dump); A14 = Kamiensk Mountain – external remediated the oldest spoil dump, now recreational and ski area with chair lift.

The largest settlements and dislocations were identified on the eastern slopes of the external Szczerców spoil dump where displacements exceeded 60 mm per year. The western slope of this dump registered displacement (subsidence) of 30-40 mm per year. On the northern and southern slopes of the Szczerców Field, displacements were 30-40 mm per year. In the area of the southern slope of Belchatów open pit, displacements amounted to 19-24 mm per year, whereas in the investigated region the western slope varied from 9.5 to 19 mm

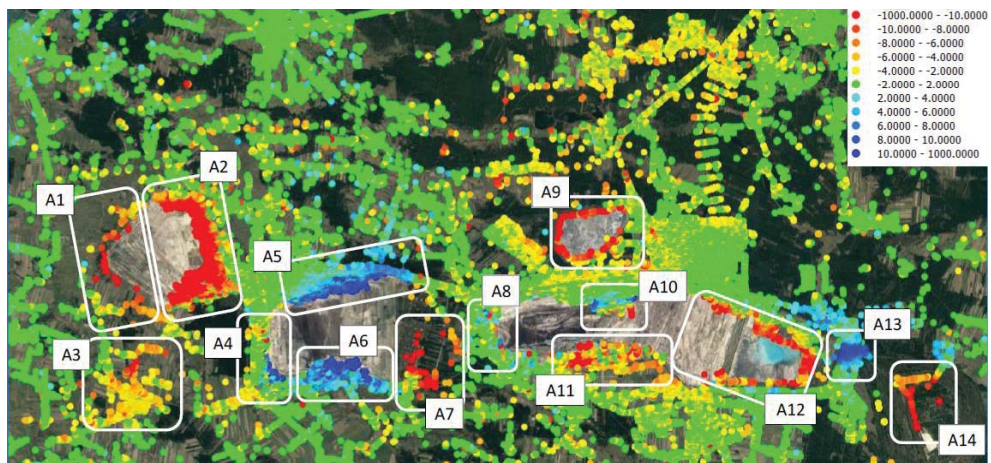


Figure 2.20: Labels of unstable areas identified through the analysis of the PS displacement maps.

In this task, SUBTERRA reviewed the input data, modelling process and threshold definitions aiming to assist the geotechnical control of an open pit mine and its spoil dumps. Data from Belchatow and other sites, such as CLC mine in Spain, was used. The CLC mine was ideal for this

project as it provided monitoring data both for open pit slopes and spoil dumps. Therefore, it was a suitable site for the explanation of the modelling, monitoring and warning system establishment. In addition, the nature of the materials involved (clayey blue marls) is also suitable for the study of the geomechanical properties of spoil dumps.

CLC is a copper mine sited in Gerena, Seville (Spain) and is one of the largest open pit mines in Spain. The pit measures are 1.600 m long x 900 m wide and 250 m of maximum depth. A pre-stripping of around 120 to 150 m of marls was required. These marls geotechnically behaves as a soil (over consolidated clay) but in which bedding planes and other vertical joints play a major role, acting as a jointed and brittle rock mass. As a result, their geotechnical behaviour can be considered as challenging and problematic (Ayala 1978 and Tsige et al. 1995).

For the CLC mine the first approach to the definition of thresholds for the warning system was a simulation of the geometry, geology, boundaries and contour conditions of the considered slope. By means of the software FLAC2D, numerical models were analysed, and the main values of total displacement, shear strain contours and pore pressure were obtained. Once reliable results have been obtained, it is possible to make a first hypothesis of the magnitude of those values. Once predictive models of the pit slopes and the spoils have been performed, special attention has been paid to the displacement forecast, velocity, and pore pressure evolution. Initially, both displacements and pore pressure are easy-to-measure parameters with relative accuracy employing the proposed devices. Displacements: it has been considered that the velocity of the deformation is more effective than the deformation itself, due to the possibility of predicting in a better manner the deformation in a given period; surface and deep displacements are registered by means of automatic topographic control points and inclinometers. Pore Pressure: related to the water pumping that is going on in the pit contour and the ground pressure release that take place during the process.

In order to obtain a range of horizontal displacements and pore pressure variations, results of several phases of numerical modelling have been analysed. SUBTERRA analysed the design of the pit excavation and, based on the numerical model results and limit equilibrium analyses, suggested the following three levels of a warning system:

#### WARNING SYSTEM (cm)

Phase	Attention	Warning	Alarm
1 to 4	4,0 - 15,2	15,2 - 20,2	>20,2
5 to 9	11,0 - 18,8	18,8 - 25,0	>25,0
9 to 13	12,5 - 21,5	21,5 - 28,4	>28,4

Having these values, it is foreseen to register large displacements on the marl slopes. Manual and digital-dynamic inclinometers have been employed and the data has been compared aiming to conclude its endurance against those displacements.

A similar approach was followed to analyse the behaviour of the Southern spoil dump. A modelling process was performed simulating the construction of dumping phases and the evolution of the pore pressure within the marl layer.

Firstly, an analysis of the pore pressure dissipation was undertaken. Models showed an increase in the pore pressure during and after the disposal of the different layers and it has been possible to extract the main representative values for displacements and pore pressure variations. Due to the influence of the dumping phases in the slope stability, the warning system has been established for every phase.

#### WARNING SYSTEM (cm)

Dumping Phase	Attention	Warning	Alarm
1	2,6 - 4	4 - 5,3	> 5,3
2	5,4 - 8,1	8,1 - 10,8	> 10,8
3	9,2 - 13,9	13,9 - 18,5	> 18,5
4	13,1 - 20	20 - 26,2	> 26,2
5	16,8 - 25,2	25,2 - 33,7	> 33,7
6	20,7 - 31	31 - 41,4	> 41,4
7	24,5 - 36,8	36,8 - 49	> 49
8	28,6 - 42,9	42,9 - 57,2	> 57,2
9	33 - 49,5	49,5 - 66	> 66
10	37,4 - 56,1	56,1 - 74,8	> 74,8
11	42,4 - 63,5	63,5 - 84,7	> 84,7
12	44 - 66	66 - 88	> 88

For the calculation of the pore pressure evolution at different depths, a reference point for the measurement of pore pressure with time was implemented in the design models. Based on the results of these models, a threshold system was established for the dumps, with the following values of Skempton B-bar:

#### WARNING SYSTEM (SKEMPTON B-bar)

Normal level	Attention	Warning	Alarm
--------------	-----------	---------	-------

<0,80 >0,80 - <0,90 0,90 – 0,98 >0,98

Every defined level will carry, based on its significance, different measures within a protocol. The scope of this study is the South Spoil, which is an appropriate scenario due to its size, height and nature of the material (similar to those studied in WP3). In addition, for spoil dumps, consideration of the value of the Skempton B parameter will be applied. This B-bar ratio allows to assessment of the variation of pore pressure when the total load changes; it represents a way of analysing the pore pressure dissipation during the dumping process.

Therefore, aiming to control this fact, the following thresholds have been defined after analysing the results of the numerical modelling:

Attention level: B-bar value in the bedrock (marls) is between 0,80 and 0,90;

Warning level: B-bar value in the bedrock (marls) is between 0,90 and 0,98;

Alarm level: B-bar value in the bedrock (marls) is higher than 0,98.

Monitoring and control process - For the purposes of the work undertaken in this WP and aiming to implement the methodology in the case of Slatinice Mine (CZ) in WP3, the following scheme will be applied to define the monitoring and data management process regarding spoil dumps and working faces, with the aim to be correlated to those results achieved in WP2 and WP3: Simulation using numerical models → Threshold definition; warning system → Data acquisition → Analysis and filter → Measures and actions.

Figure 2.21 shows the control evolution of the B-bar parameter with time in a piezometer installed in the Southern dump. It takes a long period of time after the dumping process to dissipate all the extra pore pressure.

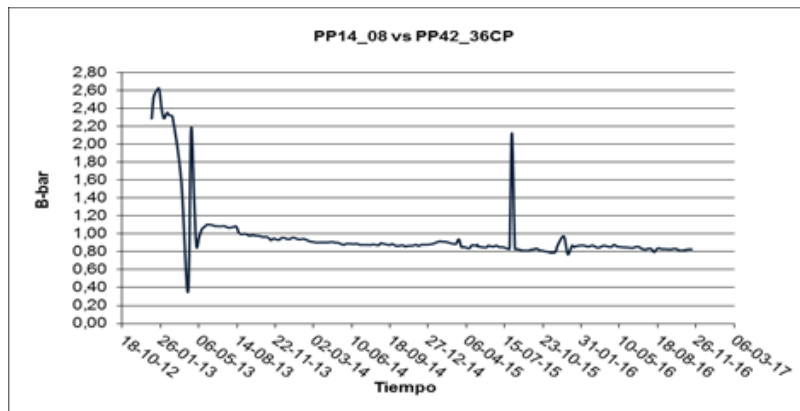


Figure 2.21: Example of the computerised recording of B-bar parameter against time.

A survey by means of topographic control points was performed, drawing the vector displacement in order to calculate displacements and deformation speed. A comparison between types of sensor to detect large displacements in a potential sliding area (where former instabilities were registered due to increases in pore pressure) has been performed with the aim of proving the accuracy of those methods and finding the differences between surface and depth displacements. The data from inclinometers in the Southern spoil were used. Results in Table 2.4 show the influence of the depth and the difficulty when registering large displacements by means of inclinometers. It is recommended to install both inclinometer and surface points in order to detect the instability and its velocity.

Table 2.4: Comparison of displacements recorded by automatic topographic control points and dynamic inclinometer.

TOPOGRAPHIC SENSOR	Average displacement (mm/day)	INCLINOMETER	Average displacement (mm/day)
ESPR-01	0,39		
ESPR-05B	0,83	INS-6	0,09
ESPR-08	0,91		
ESPR-42	0,45	INS-1	0,44
ESPR-43	0,56		
ESPR-10B	2,08	INS-7	0,33
ESPR-12B	3,67	INS-8	0,36
ESPR-11	26,54		

#### TASK 1.3: Application of laser scanning (INERIS, UNEXE, UoN, VUHU, POLTEGOR)

In this task, an overview of the different advancements in Light Interferometry Detection and Ranging (LiDAR) technology in the context of open pit mines is highlighted. This technology and

some examples of point cloud data analyses were presented for the three sites investigated: Polish open pit mine (Belchatow) undertaken by UNEXE in collaboration with POLTEGOR; open pit mine (CSA) in Czech Republic undertaken by UNEXE in collaboration with VUHU and an abandoned French lignite mine (Fosse Padène) undertaken by INERIS.

INERIS chose the abandoned French coal open-pit mine "Fosse Padène" to carry out the laser scan measurements with its own short-range laser scan. This site is one of the latest open pit coal mines in France that has not been transformed or backfilled. The objective was to provide additional results of this LiDAR technique: 1. using 3D laser scanner technology to collect the exact geometry and geotechnical data related to the fracturing of rocky slopes and mass displacement for coal mine deposits; 2. using the 3D point cloud data in the GRIDDE software (from Itasca software) to generate a good mesh to make calculations of slope stability at a local scale into a dedicated numerical modelling software.

The LiDAR campaign was organised between the 3rd and 4th of May 2017. The scanning operations were operated for two sites: the Fosse Padène (old open pit mine) and the dumps where a landslide has been occurred (north-east to the open pit). Both are located in the city of Graissessac (about 80 km west of Montpellier). Given the geological interest of the site (visible syncline), the Fosse Padène was not secured at the end of the mining operation: cliffs were not traced and the pit was not backfilled. Consequently, this open-pit has several types of instability: rock falls at cliff level; deep or superficial slides in the coal deposits and coal deposits erosion. The main features of this open pit are: two main orientations: (east face & north face cut by many faults) and its partial filling with open-pit waste at the base of cliffs. For the LiDAR survey three points of interest were studied, they are located in the Figure 2.22 to obtain slopes identification, geological analysis, discontinuities analysis and the slope analysis of one important landslide situated on the east face. A 3D numerical model, using geometry obtained by LiDAR data, was also calculated to assess the long-term stability of the landslide by identifying the critical zones.

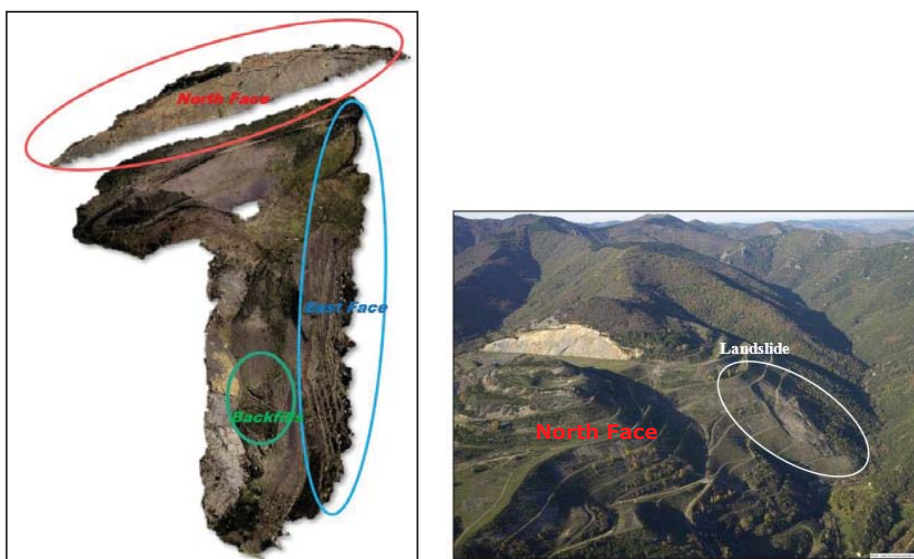


Figure 2.22: Top-left: view of the 3D colour point cloud realized by the Focus3D X330 and RealWorks software; Right: the position of one important landslide.

UNEXE produced a comprehensive document "Feedback and recommendations of the use of laser scanning technology for open pit mine stability diagnostics". The report covered in detail the development and application of technology, with focused discussion on deliverable outputs that can be generated from its deployment in open pit mining. For the purpose of this report, extracts of the deliverable have been selected specifically relevant to the case study sites in Poland and the Czech Republic.

Firstly, before undertaking any laser scanning campaign it is important to understand the site characteristics and the required output datasets needed. Therefore, UNEXE produced a scoping study on the deployment of laser scanning at Belchatow open pit mine in Poland. The failure areas at the mine are extensive, particularly on the south slope. Taking approximate measurements using Google Earth the failure is 600m wide and appears to have failed over approximately 2/3 of the full slope (from the bottom of the pit). As the pit is currently operating at a depth of 310m, the scale of the failure area could be characterised as approximately 600m wide and 200m high (vertical). With this in mind, the options for recording the slope could include multiple setups on the slope itself using a shorter range instrument or recording the slope from a distance using a long range instrument. However, due to the instability of the slope, size of the failure area and other safety implications deploying a short range instrument may not be the best solution. Therefore, a preferred laser scanning solution could be a long range instrument.

An investigation demonstrated that a number of different instruments currently available that would provide the accuracy and range of measurement that is required. These include: Riegl VZ-6000 (6km range, approximately 15mm accuracy, not eye safe) (Riegl, 2015f); Riegl VZ-4000 (4km range, approximately 15mm accuracy, eye safe) (Riegl, 2015d); Riegl VZ-2000 (2km range, approximately 8mm accuracy, eye safe) (Riegl, 2015c); Riegl VZ-1000 (1.4km range, approximately 8mm accuracy, eye safe) (Riegl, 2015b); Riegl Vz- 400i (0.8km range, approximately 5mm accuracy, eye safe) (Riegl, 2015e); Maptek I-Site 8820 (2km to a reflector, approximately 6mm accuracy, eye safe) (Maptek, 2015); Trimble TX8 (340m range, approximately 5mm at 50m accuracy, eye safe) (Trimble, 2015); Leica C10 (300m range, approximately 6mm at 50m accuracy, eye safe) (Leica Geosystems, 2015).

Following the scoping study a laser scanning campaign was undertaken using a Riegl VZ-4000. At the Belchatow site in Poland long range terrestrial laser scanning (TLS) of the East slope was undertaken. The laser scanning surveys were carried out in conjunction with 3D Laser Mapping (3DLM), who provided the Riegl VZ-4000. In view of the dimensions of the lignite operation the initial scoping exercises undertaken by UNEXE indicated that it was necessary to utilize a scanner with long-range capability. Numerous set-up positions were chosen and the coordinates of these locations were pre-established by the Mines' Survey Department. The known locations were strategically selected in order to provide significant overlap between the set-up positions and provide a basis to establish ongoing monitoring. Five fixed survey stations and one temporary position were selected in order to provide the density and overlap of data required to record the West slope. At each selected station multiple laser scan surveys were taken at differing levels of point spacing in order to provide over-arching information and additional data in specific parts where needed. Figure 2.23 illustrates the locations of the survey stations, where 1,2,3,4 and 6 were fixed positions and 5 was temporary.



Figure 2.23: Location of Laser Scan Survey Stations in Belchatow Mine

Following the site survey, post-processing was undertaken to register the different positions in order to create a complete model. Using the coordinates of the fixed survey stations the model was then translated into WGS84 reference system for dissemination of the dataset and provide a basis for comparisons.

During data collection of the scanning data using the VZ-4000, photographs were also taken using the in-built camera which were subsequently mapped onto the point cloud in order to provide visual realism. The entire laser scan dataset with photo texture is illustrated in Figure 2.24.



Figure 2.24: Photo Textured Laser Scan Data

Following the site visit to Belchatow, UNEXE then travelled to the site selected in Most, Czech Republic to undertake further laser scan surveys of the site. The scoping exercise highlighted that access on site was not restricted and allowed for personnel to operate in the landslide area. Therefore, a shorter range scanner was selected and used in the Czech site. UNEXE selected a Leica ScanStation C10 with a maximum range of 300m and carried out multiple laser scan

positions covering the majority of the landslide area. Approximately 60 laser scan positions were undertaken in order to transverse the landslide and the immediate surrounding area. Local control between the independent laser scan positions was established using Leica 'tilt and turn' targets which remained static between at least two adjoining scans. The targets were used to constrain the laser scans and provide common points in the subsequent registration process. The generated point clouds were again referenced to the WGS84 system for ongoing comparison of data following periodic surveys. This was achieved by establishing two DGNSS baselines at the north and centre of the site, which were then used to translate the local laser scans onto a grid system.

Evaluation of Slope Failure - Rockfall can be a major hazard particularly in areas where steep terrain is near developed areas or transportation corridors (Coggan and Eyre, 2013). With this in mind, it is important for the mining industry to consider rockfall as a significant hazard and undertake appropriate risk assessment to evaluate its effects (Coggan and Eyre, 2013). A laser scan dataset can be used in a number of ways in order to evaluate slope failure.

Failure and Source Modelling - If a failure has occurred, information relating to the source point is essential in order to understand what has happened, highlighting potential hazardous areas while mapping the source in which further incidents may occur. TL may be highly beneficial to this end. In particular, the accurate geometrical information can be incorporated into a Geographic Information System (GIS) environment to perform several spatial analyses essential for proper data interpretation. For example, GIS based analyses can be used for overcoming one of the main limitations of the traditional kinematic analyses, which is lack of ability to locate the source of a possible unstable block. In addition, as reported by Brideau et al. (2011), the results of a kinematic analysis are strongly influenced by the topography of the study area, especially in the case of a multifaceted shape slope. For this reason, in order to perform a complete and reliable study, a GIS-based spatial analysis can be performed using LiDAR data. In order to identify possible source areas it is necessary to combine different attributes, such as orientations of discontinuities, critical limit angle of the rock face, and slope angle and direction of the rock face. In this context, the orientation of discontinuities can be identified directly from point cloud data (using best fit patches to the point cloud surface), while the limit angle can be calculated through application of traditional kinematic analysis methods. The limit angle is very important in spatial analyses because it represents the angle from the horizontal that the slope can reach without causing a rockfall or potential failure event, and depends on the discontinuities direction and dip angle and shear strength characteristics. Finally, slope angle and direction of the rock faces can be calculated in a GIS environment using the TL as input data through the functions 'Slope' and 'Aspect'.

Slope function in ArcGIS - The purpose of this function is to identify the slope (gradient, or rate of maximum change in z-value) from each cell of a raster surface; this means that the point cloud must be converted to a raster before proceeding with the analysis. It is a cell by cell analysis, where the maximum rate of change in value from one cell to its neighbours is calculated. Basically, the maximum change in elevation over the distance between the cell and its eight neighbours identifies the steepest downhill descent from the cell (Esri, 2017).

Conceptually, the Slope tool fits a plane to the z-values of a 3x3 cell neighbourhood around the processing or centre cell. The direction the plane faces is the aspect for the processing cell. The lower the slope value, the flatter the terrain; the higher the slope value, the steeper the terrain. The Slope tool is most frequently run on an elevation dataset, steeper slopes are shaded red on the output slope raster (Esri, 2017).

In order to show the potential use of this function with TL data, Figure 2.25 shows an example of calculation for the Belchatow test site in Poland and at the CSA test site in the Czech Republic. Both examples use the laser scanning data acquired by UNEXE during WP1 of the SLOPES project.

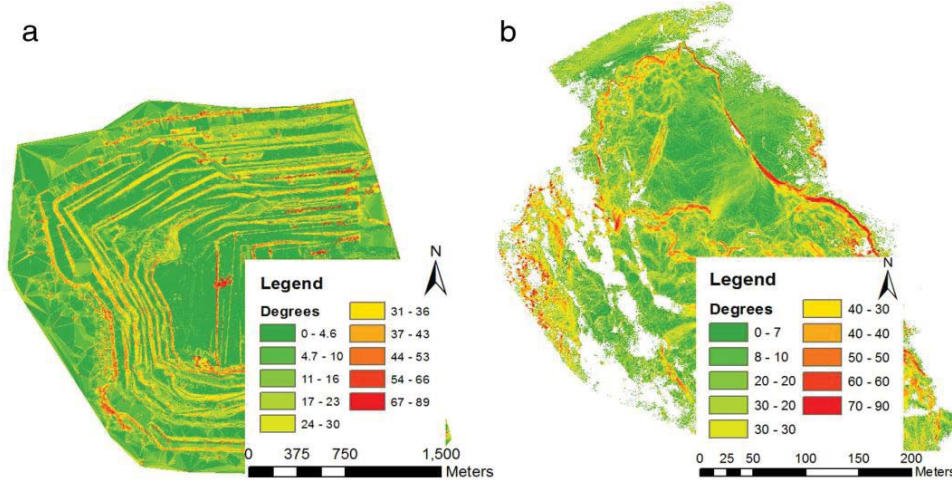


Figure 2.25: Application of Slope function using TL data acquired at (a) Belchatow test site in Poland, and (b) CSA test site in Czech Republic.

In addition, Figure 2.26 provides a 3D view of CSA slope analysis where the pixel with slope angles lower than  $26^\circ$  are not considered. Figure 2.26 shows how major and minor scarps within the site have been correctly identified.

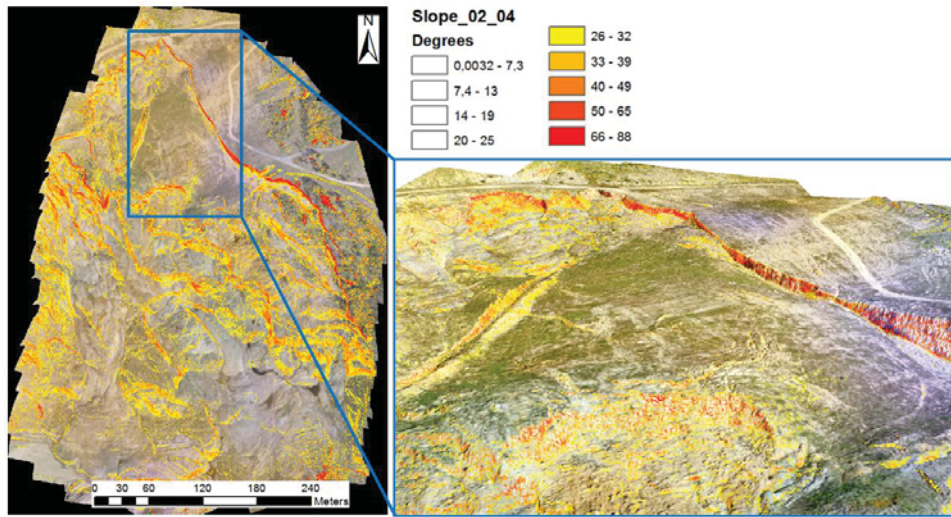


Figure 2.26: 3D representation of Slope function output carried out using TL data acquired at CSA test site in Czech Republic.

Aspect function in ArcGIS - The Aspect function is similar to the previous section, but is used for identifying the dip direction of a raster cell. The values of each cell in the output raster indicate the compass direction that the surface faces at that location measured clockwise in degrees from 0 (due north) to 360 (again due north), coming full circle. Flat areas having no dip direction are given a value of -1. Conceptually, the Aspect tool fits a plane to the z-values of a  $3 \times 3$  cell neighbourhood around the processing or centre cell. The direction the plane faces is the aspect for the processing cell. A moving  $3 \times 3$  window visits each cell in the input raster, and for each cell in the centre of the window, an aspect value is calculated using an algorithm that incorporates the values of the cell's eight neighbours.

Again, in order to show the potential use of this function with TL data, Figure 3.25 provides an example of calculation for the Belchatow test site in Poland (Figure 2.27a) and at the CSA test site in Czech Republic (Figure 2.27b). Both examples use the laser scanning data acquired by UNEXE during Work Package 1.

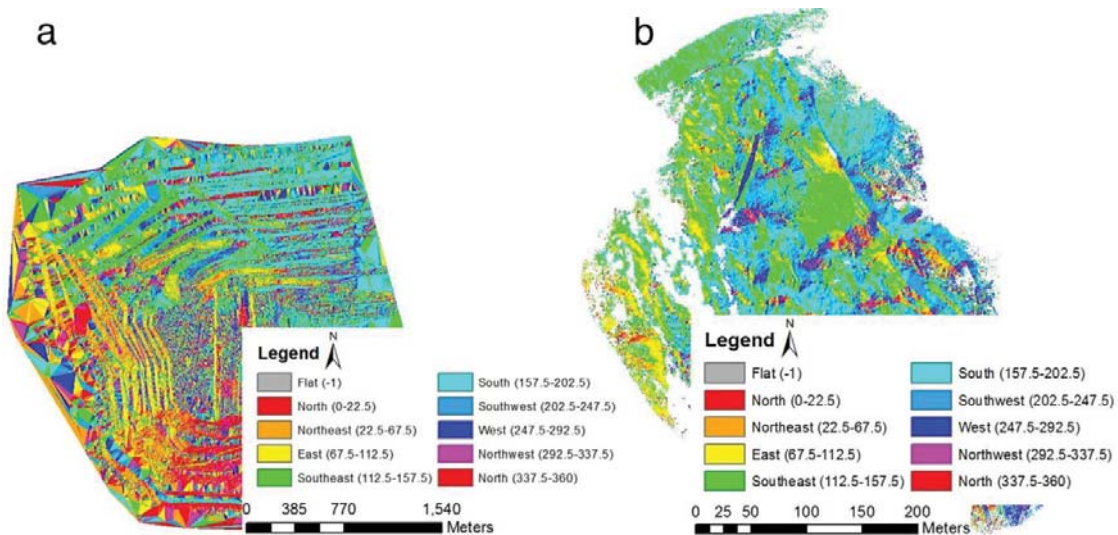


Figure 2.27: Application of Aspect function using TL data acquired at Belchatow test site in Poland (a) and CSA test site in Czech Republic (b).

## WP2 - Advanced modelling and risk analysis of open pit rock-face slopes

WP leader: CERTH

WP Partners: Geocontrol, SUBTERRA, POLTEGOR, UNEXE, INERIS

### TASK 2.1: Probabilistic analysis for reliability-based evaluation of risks (CERTH, UNEXE)

CERTH developed a slope reliability model, coupling the Monte Carlo simulation probabilistic method and the limit equilibrium method. Through this model, several aspects related to the risks of pit slope stability were thoroughly investigated. It was demonstrated that primarily cross-correlation between shear strength components, and secondarily, the statistical distribution type that random variables follow, both play a very important role in the probabilistic outcome. It seems that ignorance of the dependency between shear strength frictional and cohesive components leads to conservative probabilistic results. Lognormal distributions gave the lower calculated probability of failure values, whereas Normal truncated and Beta distribution yielded very similar probabilistic results. In addition, the non-linear relation of the failure probability with the mean safety factor was demonstrated for the most sensitive random variable of the slope examined. It is about the residual friction angle of the clay material that governs the compound mode of failure analysed. A slight alteration in mean values changes greatly the computed probability of failure, and thus, the slope safety conditions (Figure 2.28a). The latter inference is obscured when the deterministic safety factor is used as the sole indicator of slope safety. On the other hand, selection of a particular seed value of the random number generator (RNG) was found to induce only minor influence on the results (Figure 2.28b).

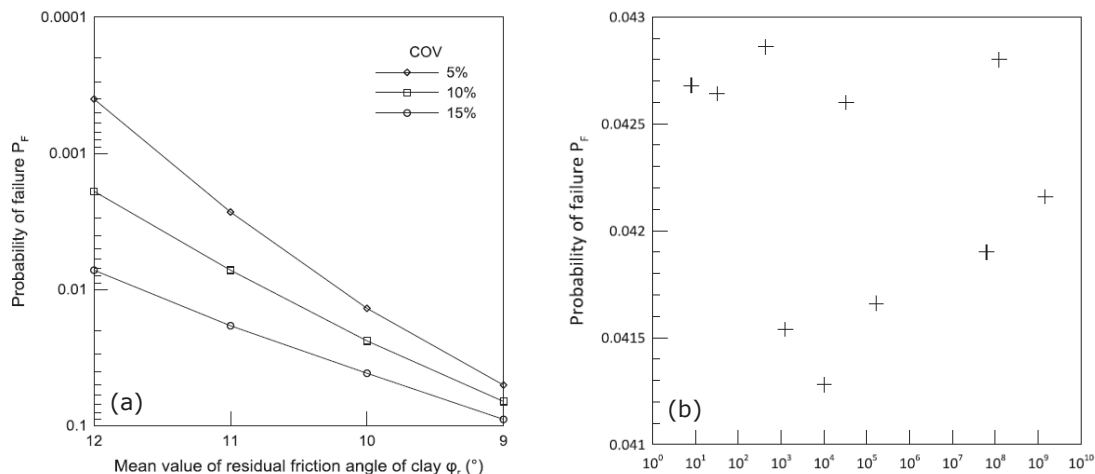


Figure 2.28: (a) Probability of failure with varying residual friction angle of clay; (b) influence of RNG seed value on the probability of failure

As for the critical design parameter of the overall pit slope angle, the non-linear relation of probability of failure and the deterministic safety factor with the overall pit slope angle was revealed through a series of parametric probabilistic analyses (Figure 2.29a). Considering the issue of the overall pit slope angle determination, through a design optimization approach, an optimization scheme was suggested that resulted in an optimum pit slope design angle, much close to the initial one of the baseline model (Figure 2.29b). Further information about the developed reliability model is provided in Deliveris et al. (2016) and Zevgolis et al. (2018a).

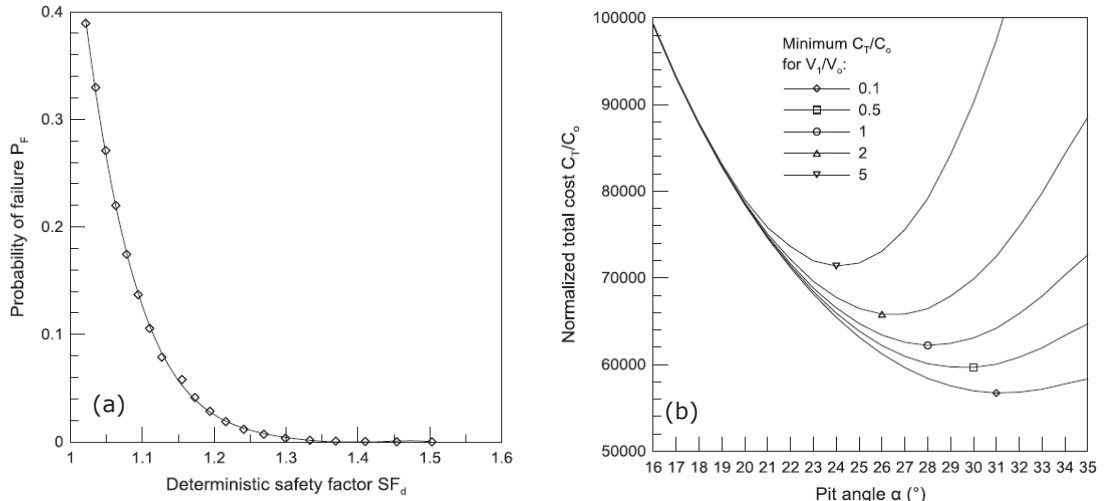


Figure 2.29: (a) Relation between probability of failure and deterministic safety factor

To complement the work undertaken by CERTH, UNEXE made a review of probabilistic approaches to plane failure analysis and slope stability acceptance criteria, and application of Eurocode 7 requirements in a mining context. The report entitled "Probabilistic approaches to plane failure analysis" was supplied to complement the deliverables of the SLOPES project. The review was based on example plane failure analyses typically of a limited size (e.g. benches) using a probabilistic approach and different methods of solution. The review considered the geotechnical aspects of the probability of failure and consequences were considered mainly for the scale of the slope. The cases studied did not include consideration of singular features such as major faults.

Plane failure analysis uses closed form equations; relevant examples are included in Wyllie and Mah (2004), based on the original work by Hoek and Bray (1974; 1977; 1981). Five cases were run using different models and two main input parameter distributions. In addition, the effects of shear plane length and spacing were considered as adjustments to the basic probability results. The models included the RocScience program RocPlane, used in probabilistic mode (with normal only or a variety of input distributions) and spreadsheets written at UNEXE using either a First Order Second Moment (FOSM) analysis (normal input distributions only) or using the add-in @Risk (normal only or variety of input distributions).

Basic plane failure analysis - The 5 cases were divided into examples where normal distributions only were used for the inputs (Cases 1 to 3) and where a combination of normal, triangular and negative exponential distributions were used (Cases 4 and 5). In all cases the mean input values were the same and the factor of safety for the mean block was in all cases close to 1.40. The full inputs for cases 1 to 3 are shown in

, which is an extract from the FOSM spreadsheet (Case 2). The full inputs for Cases 4 and 5 are shown in Table 2.6, which is an extract from the @Risk spreadsheet (Case 5). The variable inputs are highlighted in yellow. The cases examined did not include surcharge ( $W_s$ ), bolt tension ( $T$ ) or dowel shear capacity ( $D$ ), but these are available in all the models, as needed. It should be noted that the important detail of shear strength for the underlying discontinuity was based on the use of the non-linear Barton - Bandis equation (with parameters,  $\phi_b$ , JRC, JCS). It is UNEXE experience that this method is more practical than the linear Mohr-Coulomb equation (with parameters  $\phi$  and  $c$ ) for determining field-scale rock discontinuity shear strengths. All the models can use the Mohr-Coulomb equations if preferred. In all models the principle of effective stress was applied taking full account of the effect of water pressure on discontinuity shear strength and slope loading. The results of the analyses are shown in

Table 2.7 and commented on below.

Table 2.5: Input data for Cases 1 to 3

Input values:	Symbol	Mean		Sample	Standard deviation ( $\sigma_0$ )
Unit weight of water (kN/m <sup>3</sup> )	$\gamma_w$	9.81		9.81	0
Unit weight of rock (kN/m <sup>3</sup> )	$\gamma_r$	28		28	0
Surcharge (kN/m)	$W_s$	0		0	0
Height (m)	H	10		10	1
Crest to tension crack (m)	B	4		4	1
Face angle (deg)	$\phi_f$	70		70	2.5
Dip of failure plane (deg)	$\phi_p$	15		15	2
Bolt inclin. from horiz. (deg)	$\beta$	20		20	2.5
Bolt tension (kN/m)	T	0		0	0
Dowel shear capacity (kN/m)	D	0		0	0
Basic friction (deg)	$\phi_b$	25		25	4
Joint Roughness Coefficient	JRC	5		5	1
Joint Compressive Strength (MPa)	JCS	15		15	1.5
Water level ratio	$Z_w/Z$	0.5		0.5	0.1
Earthquake coefficient	$\alpha$	0.1		0.1	0.05

Table 2.6: Input data for Cases 4 and 5

Input values:	Symbol	Mean	Distrn.	Mean	Standard deviation ( $\sigma_0$ )	Min	Max
Unit weight of water (kN/m <sup>3</sup> )	$\gamma_r$	9.81	Normal	9.81	0.00	9.81	9.81
Unit weight of rock (kN/m <sup>3</sup> )	$\gamma_w$	28	Normal	28	0.00	28.00	28.00
Surcharge (kN/m)	$W_s$	0	Normal	0	0.00	0.00	0.00
Height (m)	H	10	Triangular	10	1.00	8.00	12.00
Crest to tension crack (m)	B	4	Normal	4	1.00	2.00	6.00
Face angle (deg)	$\phi_f$	70	Triangular	70	2.50	65.00	75.00
Dip of failure plane (deg)	$\phi_p$	15	Normal	15	2.00	11.00	19.00
Bolt inclin. from horiz. (deg)	$\beta$	20	Normal	20	0.00	20.00	20.00
Bolt tension (kN/m)	T	0	Normal	0	0.00	0.00	0.00
Dowel shear capacity (kN/m)	D	0	Normal	0	0.00	0.00	0.00
Basic friction (deg)	$\phi_b$	25	Normal	25	2.50	20.00	30.00
Joint Roughness Coefficient	JRC	5	Normal	5	1.00	3.00	7.00
Joint Compressive Strength (MPa)	JCS	15	Normal	15	1.50	12.00	18.00
Water level ratio	$Z_w/Z$	0.5	Neg. Exp.	0.5		0.00	1.00
Earthquake coefficient	$\alpha$	0.1	Neg. Exp.	0.1		0.00	0.20

Table 2.7: Summary of basic plane failure analyses and results. In Case 2 the output distribution of F has been taken as log-normal. In cases 4 and 5, triangular distributions were used for slope face and slope height; negative exponential distributions for water levels and seismic coefficient. MC is Monte Carlo simulation.

Case	Model	Input distributions	Fm	$\mu_F$	$\sigma_F$	p(F<1) %	p(F<1.5) %
1	MC RocPlane	Normal only	1.403	1.431	0.319	6.6	63.0
2	"Plane-FOSM" log normal F	Normal only	1.403	1.403	0.350	10.5	65.3
3	MC "Plane-@Risk"	Normal only	1.403	1.434	0.339	7.1	63.1
4	MC RocPlane	Normal, triangular and negative exponential	1.403	1.76	0.54	6.2	34.9
5	MC "Plane-@Risk"	Normal, triangular and negative exponential	1.403	1.75	0.53	6.1	34.9

Fm = mean F;  $\mu_F$  = sampled mean;  $\sigma_F$  = sampled standard deviation; p(F) = probability of failure

Case 1 RocPlane with normal input distributions - The inputs for this case were the same as for Case 3 (Table 2.5). The values of  $F_m$  and  $\mu_F$  were close to 1.4 and  $\sigma_F$  was about 0.32. The values of  $p(F<1)$  and  $p(F<1.5)$  were 6.3 % and 63 % respectively. By the above modified criteria the stability would be acceptable for Category 1 – non critical benches.

Case 2 FOSM with Excel spreadsheet normal input distributions - The values of  $F_m$  and  $\mu_F$  were close to 1.4 and  $\sigma_F$  was significantly higher than for Case 1 at about 0.35. Based the  $\mu_F$  and  $\sigma_F$  values and a normal distribution for  $F$ ,  $p(F<1)$  and  $p(F<1.5)$  were 12.5 % and about 61 % respectively. If the distribution was assumed to be log normal these were 10.5 % and 65 %. These clearly show the output distribution to be closer to log normal with the skewness for normal and log normal being 1.03 and 0.16 respectively. By the above modified criteria the stability may be acceptable for Category 1 – non critical benches, probably with the incorporation of suitable monitoring / instrumentation.

Case 3 @Risk with Excel spreadsheet normal input distributions - In essence the results were identical to those of Case 1.

Case 4 RocPlane with normal, triangular and negative exponential input distributions - The inputs for this case were the same as for Case 5 (Table 2.6). The values of  $F_m$  and  $\mu_F$  were 1.40 and 1.75 respectively and  $\sigma_F$  was about 0.53. The values of  $p(F<1)$  and  $p(F<1.5)$  were 6.2 % and 34.9 % respectively. By the above modified criteria the stability would be acceptable for Category 1 – non critical benches.

The significant increase in  $\mu_F$  and reduction in  $p(F<1.5)$  compared with Cases 1 to 3 was mainly due to the bias towards lower values in the negative exponential distributions used in the groundwater and seismicity inputs.

Case 5 @Risk with Excel spreadsheet, with normal, triangular and negative exponential input distributions - See Table 2.6 for the input data values. In essence the results were identical to those of Case 4.

For Cases 4 and 5 both Latin Hypercube and Monte-Carlo simulations were used with no significant differences in results (10,000 trials).

TASK 2.2: Application of advanced numerical methods (SUBTERRA, UNEXE, GEOCONTROL, CERTH, POLTEGOR, INERIS)

INERIS developed an original methodology to combine 3D laser scan data with a 3D mechanical numerical model to assess the stability of slopes. The laser scan data allowed the construction of a very precise model. The in-situ observation and laboratory characterization were then used for the different layers. The results can be the safety factor of the slope, strain, displacement and stresses. This methodology was applied on one case study of the landslide observed in the north east of the Fosse Padène. It occurred in the upper part 2 years after the dump building. This landslide is composed of argillite and sandstone and it is built with several 10 m height benches. Its 3D dataset was used to make a numerical model (Figure 2.30) for stability analysis. A basic 3D elasto-plastic numerical model using FLAC3D was carried out; the method of strength reduction was employed to determine the safety factor of the slope. The upper layer of the slope is mainly characterized by the friction angle and the cohesion of the soil ( $\phi = 31^\circ$  and  $c=8.2$  kPa). The deep layer is a competent limestone layer, which was considered as elastic. Shear and plastic deformation were analysed and compared to the displacement observations. The safety factor after the first instability is equal to 1.2. The local safety factor is smaller. Figure 2.30 presents the total shear strain obtained from the analysis. The maximum shear strain is located in the centre of the unstable zone. The thickness of the unstable zone is several meters and similar to the in-situ observations and measurements.

## FLAC3D 5.01

©2017 Itasca Consulting Group, Inc.

ColorScale of Max. Shear Strain Increment

1.0000E+00
9.5000E-01
9.0000E-01
8.5000E-01
8.0000E-01
7.5000E-01
7.0000E-01
6.5000E-01
6.0000E-01
5.5000E-01
5.0000E-01
4.5000E-01
4.0000E-01
3.5000E-01
3.0000E-01
2.5000E-01
2.0000E-01
1.5000E-01
1.0000E-01
5.0000E-02
6.0000E-04

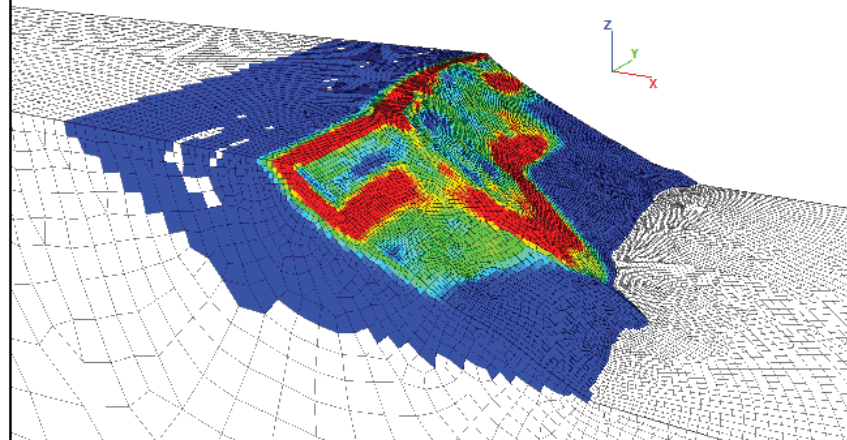


Figure 2.30: Numerical modelling results (left) of the slope and in-situ observations (right).

Terrestrial laser scanner technology appears as a very useful tool to characterize and analyse the stability of the inaccessible slopes with very reasonable costs comparing to classical displacement surveys. 3D datasets were also used to carry out a slope assessment and generate a numerical model. This innovative methodology, based on crossing and combination of 3D datasets, numerical modelling and in-situ observation, was successfully used for a real case study.

For the effective integration of WP1 data into numerical modelling, as part of Task 2.2, GEOCONTROL developed the methodology shown by Figure 2.31. According to this scheme, point-type data is processed separately to surface and 3D data. On one hand, both UAV-campaign point clouds (as outputs from WP1) and water table data are treated as point-type data and converted into geometrical surfaces to be imported to numerical modelling. This is possible mainly because UAV topography is already provided in a point cloud format (from photogrammetry results) and water data is usually provided for specific piezometers locations, where the combination of X-Y coordinates of the piezometer and water table height (Z) actually define a three dimensional point where the phreatic surface is known. This same approach could be considered for other cases where a higher amount of water data would exist or where an hydrostatic regime cannot be considered, for example if vibrating wire piezometers were installed to register pore pressures at certain locations (in these cases, more complex pore pressure tables could be created from interpolations, being again sets of points and pressures). For this objective, the free software CloudCompare (Girardeau-Montaut, 2017) was used, considering its strong orientation to process point clouds and its use in other parts of SLOPES project.

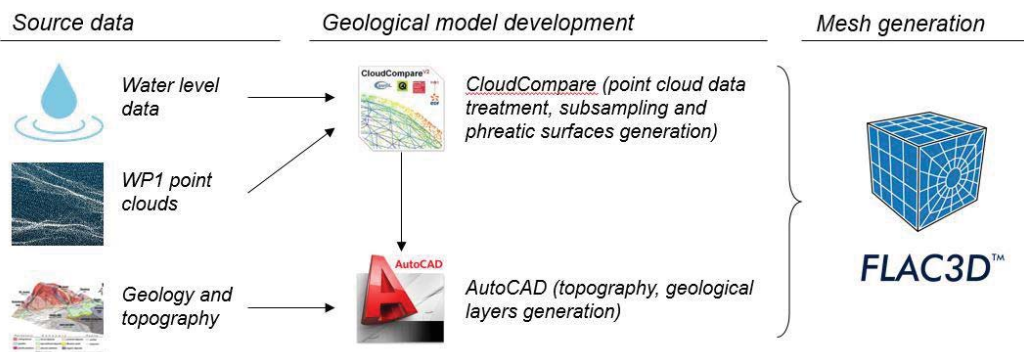


Figure 2.31: GEOCONTROL's approached scheme for integration of WP1 data into numerical modelling.

This scheme offers two main benefits. First, UAV clouds can be filtered and converted into subsampled surfaces, since original point clouds would be impossible to process using conventional CAD software, due to clouds size (over 5M points). On the other hand, coupling of high resolution topography (UAV clouds), piezometers data and other water-related elements as reported springs, allows the definition of interpolated water tables for numerical modelling of water variations influence on slope instability. Finally, mesh generation is achieved through FISH code in FLAC3D,

avoiding use of additional commercial software. This is applicable for cases of relatively simple geometry (defined by surface layers), being CSA slope a good representative example.

According to GEOCONTROL's proposed approach, controlling the slope evolution would require changing two main monitoring elements: the surface geometry, obtained through the UAV campaigns, and the water content of the slope, which plays a leading role in the instability. One of the most time-consuming steps in the model generation is mesh generation. Regarding this, available options for Itasca's software FLAC3D were reviewed, where two main alternatives were considered: automated meshing through octree partition and unstructured meshing with Griddle (Itasca's plug-in for Rhinoceros). Alternative to the octree partition, surface mesh extrusion was considered as automatable meshing process, as well. This type of 3D meshing is also supported by Itasca's software, as Figure 2.32 shows (Itasca, 2015). However, this type of mesh alternative presents a series of strong disadvantages, as the generation of elements with high aspect ratios. Besides, the mesh is also strongly dependent on the original surface, since it extrudes each triangle (in case a TIN surface is imported in DXF format).

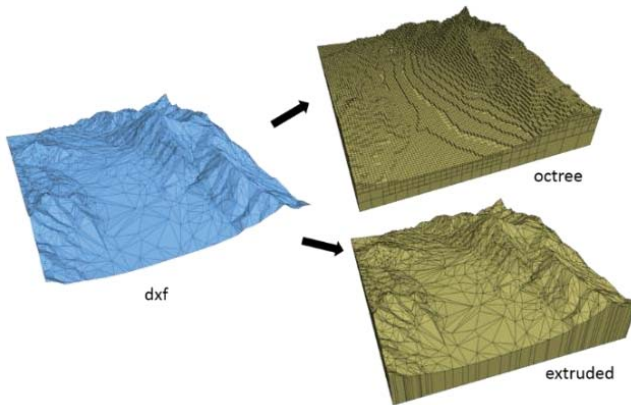


Figure 2.32: Comparative between octree and extruded meshes from a topographical surface.

Given the objective of periodic updating of the models for a correct monitoring of the slopes and in agreement with the use of low-cost aerial systems (avoiding further licenses for meshing), GEOCONTROL decided to use the octree partition system for the generation of its numerical model in Task 2.2.

For this task, GEOCONTROL also carried out works to study the influence of seasonal water content variations on slope stability. Real-data from CSA mine (Czech Republic), provided by VUHU, was used for the analysis, in coordination with the other project partners. First, the surface of the model was generated using general topography data of CSA mine and UAV flight point clouds from Task 1.1 to increase resolution within the active landslide area. On the other hand, geology of the slope was extracted from previous publications (Burda, 2011; Burda et al., 2011, 2013; Rajchl et al., 2008) and information provided by VUHU. With this data, GEOCONTROL created a 3D geological model of the landslide area, including Krusnohorský near fault and the contacts which separate, from top to bottom, quaternary sediments (Q), miocene stiff-fissured claystones (MSFC), miocene claystones (MCS) and the crystalline rock. Figure 2.33 shows a 3D view of the geological model used as input for the numerical tenso-deformational analysis.

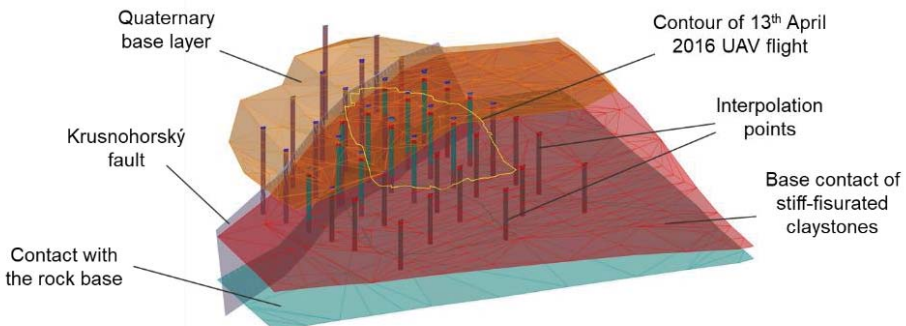


Figure 2.33: Geometry of the geological model created by GEOCONTROL.

After defining the geology and topography of the landslide, all geometries were exported to FLAC3D software (Itasca) for the development of the numerical tenso-deformational model. Model meshing was developed according to the octree approach. This allowed the later optimisation of calculation times, performing an analysis in two stages, one to determine the stress distribution of the area and the second one to focus in the active landslide.

Regarding seasonal water content variations, available data was analysed and it was observed that the most useful information was provided by four piezometers installed on top of the slope. According to these piezometers, highest seasonal variations of water content, as well as the most shallow phreatic levels, would be concentrated below Šramnický brook (shown by piezometer JZ241) and reduced towards the adjacent hill (unmined protective pillar adjacent to the active slope). In order to include these cyclical water variations in the numerical models, seasonal water levels were coupled with water springs information (Burda et al., 2013) and a series of season-dependent phreatic surfaces were generated with CloudCompare software and then imported to FLAC 3D. Once water data interrelations were examined, as well as numerical modelling results, further conclusions could be extracted comparing piezometers evolution during a 5-year period (from October 2012 to June 2017) to registered slope displacements (measured through ATR monitoring) and meteorological data retrieved at Jezeří station. As can be observed again in Figure 2.34, highest water level fluctuations were recorded at JZ241 piezometer, which, together with its location and shallow water table, proved it to be a useful indicator of water influence on slope instability. It was observed that most landslide reactivations during the recorded period were preceded by steep segments of the water table evolution curve, which would indicate that instability is not just conditioned by water levels themselves, but also by the speed of rise. The significant delay between precipitation periods and phreatic level rises could indicate a high component of snow melting water percolation.

On the other hand, taking into account not just the landslide events, but their overall cumulative trend, the average evolution of the active landslide could be partially conditioned by seasons with long periods of sustained precipitation. Figure 2.35 shows this overall trend, where it can be observed that intense precipitations during years 2014 and 2015 could be associated with an acceleration of the cumulative displacement curve, while a dryer period since the end of year 2015 would match the beginning of a possible landslide slowdown.

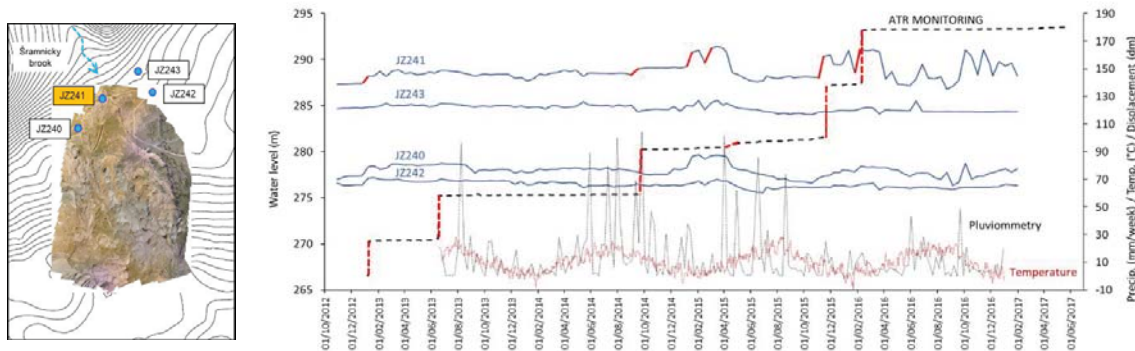


Figure 2.34: Influence of fast water table rises in landslide activity. ATR monitoring line indicates cumulative displacements. Landslide events marked in red dashed line and preceding rises of JZ241 in red continuum segments (October 2012 – June 2017).

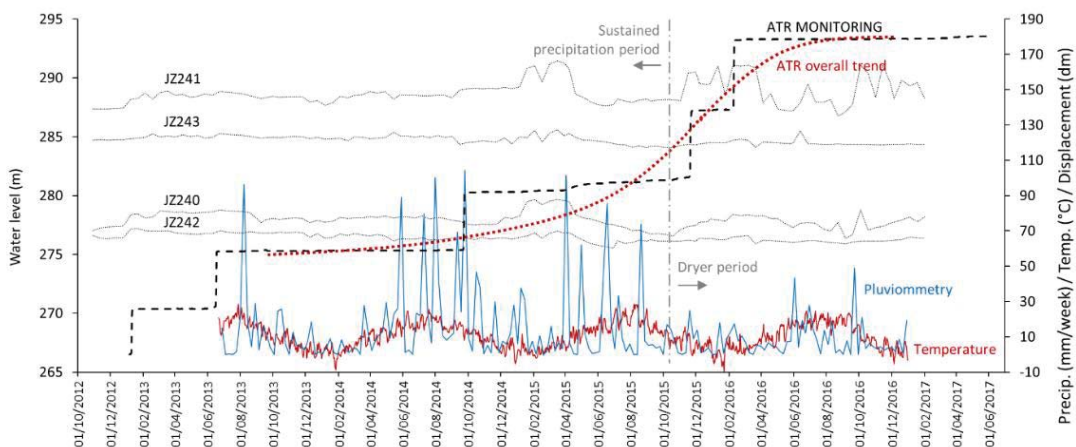


Figure 2.35: Observed influence of seasonal precipitation (week cumulated) in landslide displacement trend (October 2012 – June 2017).

Results from the analysis carried out with lower phreatic surfaces showed a general stability of the modelled region, with the localisation of most unstable areas on top of the active slope and above main scarp heads. This would be in concordance with the historical evolution of the headward erosion of the landslide, indicating that instabilities to develop during periods of lower water conditions could be localised within these regions above the landslide.

On the other hand, with high-phreatic levels, the analysis shows a general increase in shallow instability, as well as the propagation of the unstable areas to a wider region, mostly coincident with the surface of the landslide body and the area above the main scarp. In this case, the instability distribution extends to a region in concordance with the natural water course of Šramnický brook. Neither the model with the upper phreatic level nor the model with the lowest one showed the potential existence of deep-seated instabilities, all of them being developed within the quaternary sediments and the stiff-fissured Miocene claystones.

CERTH developed a slope reliability methodology, coupling the point estimate probabilistic method with the finite element numerical method. Taking advantage of finite element models to directly consider the construction sequence of slope formation, the operating stress states within the slope were determined. In this manner, both local and global slope safety levels along critical slip surfaces were evaluated. Via the probabilistic treatment of the above stability indicators by the point estimate method, local and global safety factors are matched with local and global probabilities of failure along certain critical slip surfaces. It was found that the probability of failure decreases from a slope's toe to the slope's crest (Figure 2.36a). Thereby, areas within a slope presenting significant potential for local overstress and progressive failure occurrence are manifested. The probabilistic simulation of progressive failure was attempted, and the updated global slope probability of failure during its development was computed (Figure 2.36b). A detailed presentation of the above is provided in Deliveris et al. (2018a) and Deliveris et al. (2018b).

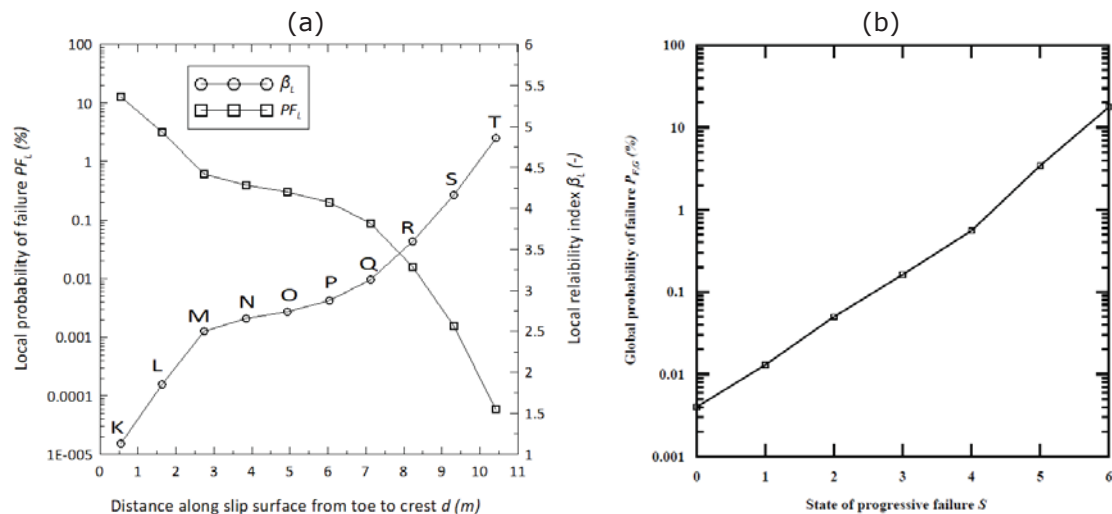


Figure 2.36: (a) Local failure probability and reliability index along slope slip surface; (b) global probability of failure at the states of progressive failure

Research conducted by POLTEGOR for Task 2.2 included field investigations and laboratory testing for numerical modelling of the Belchatow Mine. In recent years, due to high depth of exploitation, the reported risk for the south and west slope were significantly higher. This slope located near the Debina salt dome poses a threat for coal exploitation. Geotechnical investigations conducted by POLTEGOR within the SLOPES project on the west slope delivered new geotechnical data. Site investigations included drillings, in-situ inclinometer and pore pressure monitoring up to 100 m depth and index, compressibility and strength laboratory tests. The obtained results were used in numerical modelling using shear strength reduction (SSR) and limit equilibrium method (LEM) approaches. These results will be delivered to mine authorities to help with the management of risks associated with the instability of the west slope of Belchatow field. Characterization of strength parameters of rocks and soils for slope stability analysis required laboratory and field strength tests. Soils samples were taken from borehole located at west slope of Belchatow mine from level 42 m a.s.l. These included 31 undisturbed soil samples of 90 mm diameter, 500-700 mm length, collected from depths of 6.5-103.3 m. Index soil strength parameters are provided in Table 2.8.

Table 2.8: Results of field strength penetrometer and vane tests.

No	Soil type	Depth [m]	Penetrometer test (PP)			$C_u$ kPa	Vane test (TV-1)			$\tau_f$ kPa
			1	2	3		1	2	3	
1	Silty clay	0.5	4.4	4.4	4.3	43.67	0.90	0.85	0.90	42.20
2	Clay	4.5	4.4	4.5	4.5	44.67	0.90	1.00	0.90	44.59
3	Silty clay	29.5	4.0	4.1	4.2	41.00	1.00	1.00	1.00	47.77
4	Silty clay	54.4	2.5	2.5	2.4	24.67	0.55	0.50	0.45	23.89
5	Silty clay	56.7	4.0	4.0	4.1	40.33	0.90	0.87	0.90	42.52
6	Sandy silt	92.5	4.0	4.1	4.0	40.33	0.90	0.85	0.90	42.20

$C_u$  = undrained shear strength;  $\tau_f$  = shear strength

Laboratory tests included index, direct shear, IL oedometer compressibility, triaxial CIU and CID tests. Index tests covered grain-size, moisture content, unit weight, dry unit weight analysis. Tests cover also content of organic material and Attenberg limits. Results are provided in Table 2.9.

Table 2.9: Results of index, direct shear and compression tests

No	Soil type	Depth	M %	FOM %	$\rho$ g/cm <sup>3</sup>	$\rho_d$ g/cm <sup>3</sup>	WP [%]	WL [%]	LI [-]	$\phi$ [°]	C kPa	Mo MPa	M MPa
			1*	2*	3*	4*	5*	6*	7*	8*	9*	10*	11*
1	SL	0.50-0.60	15.4	2.65	2.20	1.91	11.9	31.4	0.17				
2	LS	16.4-16.8	21.1	3.29	2.12	1.75							
3	L	29.5-29.6	18.8	9.48	1.88	1.58							
4	SL	53.8-54.0	30.8	5.51	1.97	1.51	24.2	43.1	0.35	27.9	29.0		
5	LS	54.1-54.3	17.8		2.25	1.91							
6	LS	57.5-57.6	17.2	4.38	2.29	1.94							
7	SL	63.3-63.4	13.6		2.26	1.99							
8	SS	82.0-82.5	32.8	18.9	1.64	1.23	23.5	46.3	0.41	19.5	22.8	1.74	8.40
9	LS	92.5-92.7	24.5	19.3	1.74	1.39							
10	SL	93.5-94.0	16.3	5.06	2.15	1.85							
11	LS	103-103.3	28.8	7.53	1.96	1.53							

(\*) 1-moisture content, 2 - content of organic material, 3 - unit weight, 4 - dry unit weight, 5 - plasticity limit, 6 - liquid limit, 7- apparent friction angle, 8 apparent cohesion, 9 - constrained mod. primary consolidation, 10 - constrained modulus of secondary compression. SL=Sandy Loam; LS = Loamy sand; L = Loam; SS = Sandy silt

The triaxial tests were performed on 30 soils specimens taken from the borehole for on-line monitoring installation. It included one Consolidated Isotropic Undrained (CIU) and eleven Consolidated Isotropic Drained (CID) tests. All obtained results are presented in Table 2.10.

Table 2.10: Results of triaxial tests

No	Sample	Depth [m]	Soil type	Test type	Soil strength parameters			
					Friction angle		Cohesion	
					$\phi$	$\phi'$	c	$c'$
					[deg]	[deg]	[kPa]	[kPa]
1	2	4.0	loamy sand	CIU	42.87	42.98	0	0
2	3	16.4	sandy silt	CIU	33.51	34.13	27.75	19.66
3	4	29.3	loam	CIU	11.37	14.53	66.26	103.20
4	5	33.0	silty clay	CIU	21.83	30.29	129.17	32.53
5	5/1	33.5	lignite	CID		19.00		200.00
6	6	46.4	clay	CIU	8.54	9.85	6.31	18.71
7	7	47.5	loamy sand	CIU	55.13	28.64	0	0
8	8	50.5	clay	CIU	12.96	15.50	373.03	345.11
9	14	57.5	loamy sand	CIU	29.08	28.40	0	0
10	16cz	81.0	sandy silt	CIU	35.35	34.97	32.32	41.22
11	16m	81.5	Sandy silt	CIU	32.35	32.40	154.88	153.60

The results of total and effective strength parameters for different types of soils are presented in Table 2.11. Laboratory test results detected that the lowest strength parameters were recognized in clay 46.4-47.4 m depth. The highest in lignite 33.5-34.0 m depth and silty clay 33.0-33.5 m depth. However, in some cases it was not enough tests for comprehensive characterization.

Table 2.11: The results of total and effective strength parameters for different types of tested soils

Soil type	Friction angle		Cohesion		Depth [m]
	$\phi$ [deg]	$\phi'$ [deg]	C [kPa]	$c'$ [kPa]	
Loamy sand	42.8	42.9	0	0	4.0-4.5
	25.5	28.6	0	0	47.5-48.0
	28.4	29.1	0	0	57.5-57.6
Lignite		19		200	33.5-34.0
Silty clay	21.8	30.3	129.2	132.5	33.0-33.5
Clay	8.5	9.8	6.3	18.7	46.4-46.7
Loam	11.4	14.5	66.3	103.2	29.3-29.5
Sandy silt	33.5	34.1	27.8	19.6	16.4-16.8
	35.4	34.9	32.3	41.2	81.0-81.5
	32.3	32.4	154.9	153.6	81.5-81.7

For numerical modelling POLTEGOR analysed two cross-sections with the highest slope inclination. The cross-sections 18WE (near in-situ monitoring) and 20 WE were located on the west slope of Belchatow Field (Figure 2.37). In this region, seven risk areas were selected. The cross-section 18 W was located close the risk zone IV-W, VI-W, XXIIN, cross-section 20 W close to the zone V-W, VII-W, III-W and I-W. The analyses were performed using SSR Method and Flac 8.0 and LEM Bishop and Janbu method and Geostru Software. The SSR Method implemented in Flac tends to reflect the actual condition on the slopes leading to the reduction of shear strength of soil up to the

loss of stability. The implemented Mohr-Coulomb elastoplastic strength model required specification of bulk density, effective cohesion and effective angle of internal friction. Application of this method was based on the simultaneous reduction of the angle of internal friction and cohesion.

The SSR method is effective in terms of detection of the weakest zones of the analysed slopes. It allowed prediction of the relative factor of safety  $F_s$  with higher precision than the limit equilibrium method analysing the most probable circular slip surface. This way stress/strain relationship, tangential strain rate, shear strain rate contours [ $s^{-1}$ ], maximum velocity vectors [m/s] were calculated. These allowed the initial prediction of slip surface, the zones of occurrence of the greatest deformation and the velocity of movements within the analysed slopes. In LEM methods the software analysed the most probable 10 cylindrical surfaces for the every defined range of factor of safety ( $F_{oS}$ ) inside the slope. All the interpreted slope models included expected depth of the groundwater level. It was assumed that the stability factor above  $F_s = 1.5$  indicates very low likelihood of a landslide. The possibility of a landslide is more favourable with  $F_s$  below 1.3, and very likely if the  $F_s = 1.0$  and below. The principles of soil and rock classification recommended by the Eurocode 7 introduced general concepts in geotechnical design concerning derived characteristic and design values of effective strength parameters from so-called comparable experience. Therefore, the strength parameters used for the calculations were assumed on the basis of corrected values from previous investigations and modelling (Bednarczyk 2017) and laboratory tests. The method of correction related to the effective calculation parameters was estimated using the previous assessments and methods (Hawrysz 2013, Kulhavy 1992). For Mesozoic rocks, parameters were specified using Geological strength index (GSI) classification (Marinos and Hoek 2005). The complex geological structure of the slope required generalization of selected layers. These helped in the construction of representative slope models for the analysis.

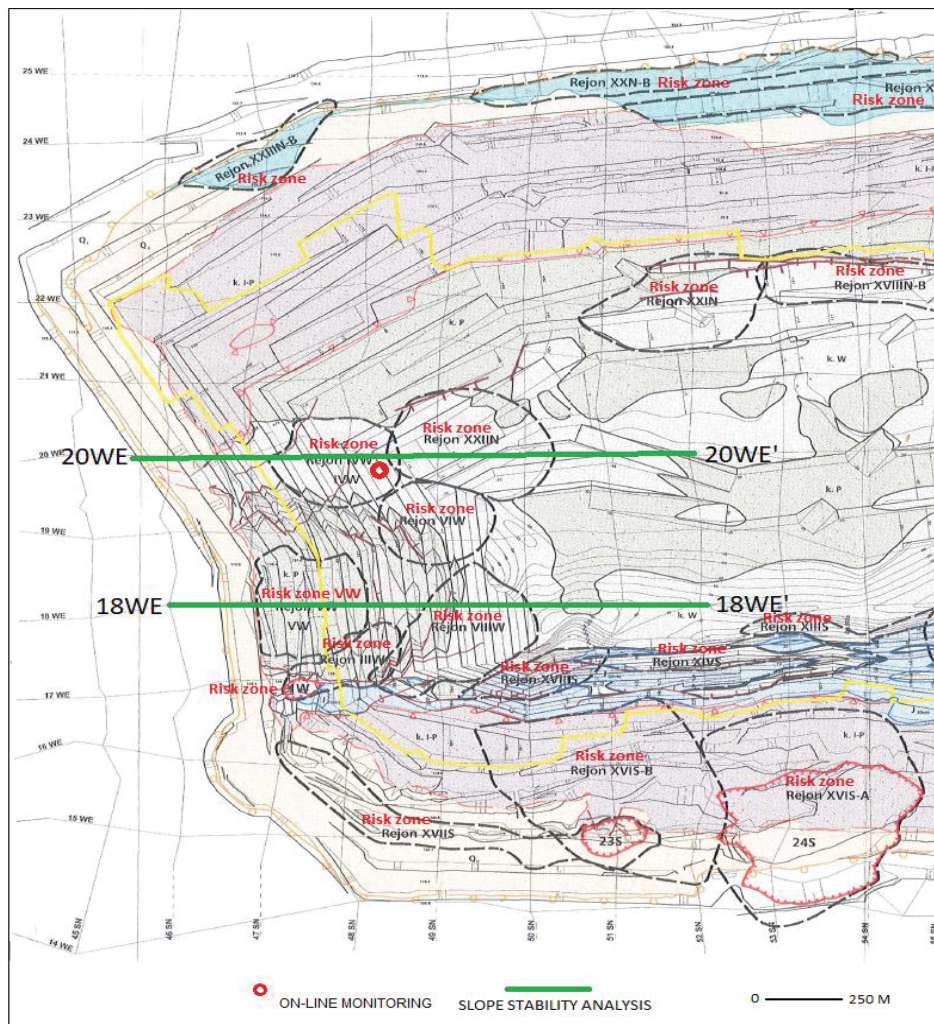


Figure 2.37: Location of slope stability analysis, risk zones and monitoring instrumentation

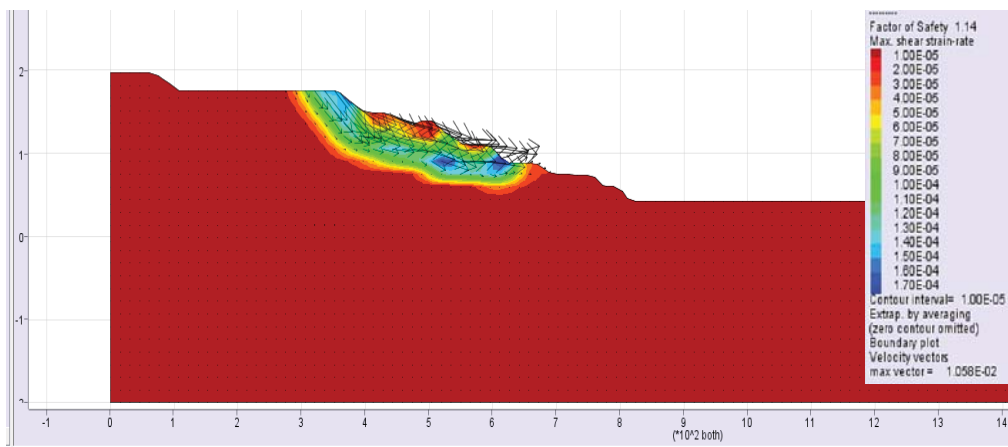


Figure 2.38: Results of slope stability analysis 20WE, FoS=1.14 .

An example of the analysis for cross-section 20 WE is shown in Figure 2.38, which included 9 geotechnical layers; cross-section 18 WE had 8 layers. The obtained values of factors of safety using SSR Method and Flac 8.0 were low ranging from 0.85 in cross-section 20WE to 1.14 in 18WE. The comparison of SSR and LEM method results is presented in Table 2.12. The results of LEM analysis using Bishop method indicated comparable results as SSR method for cross-section 18 WE. The FoS in cross-section 18WE using both methods was a low 1.14- 1.16 and slightly larger 1.27 using Janbu method. However, in LEM methods the most probable slide was located central part of the slope and cover very small area inside the slope in comparison with SSR method. In cross-section 20WE results of LEM analysis detected significantly larger values of FoS than SSR method, Fos=1.14. Using Bishop method it was 1.27 and using Janbu method. The most probable sliding surface were located in both method under the entire slope. The validation of slope stability analysis by field observations showed that better prediction compared to observed processes was obtained by SSR method.

Table 2.12: The results of numerical modelling by SSR and LEM methods

Method	FoS 20 WE	Comments	FoS 18 WE	Most probable slide
SSR Flac	0.83	slope middle part	1,14	slope upper and middle part
LEM Bishop	1,34	whole slope	1,16	slope middle part (small)
LEM Janbu	1,46	whole slope	1,27	slope middle part (small)

The analyses indicates that the west slope is a high landslide area. These results were confirmed by the monitoring field observations which detected activation of mass movements in these areas. The movements were caused by multiple factors such as mining, strength parameters, slope height and salt dome influence. The presented results are generally preliminary.

As part of Task 2.2 UNEXE produced a report on the “Application of advanced numerical methods”. The objective was to investigate the development of a methodology for effectively integrating data captured as part of WP1 into numerical modelling packages. Use of remotely captured data would provide valuable input for both two and three-dimensional simulations and provide representative simulation of the chosen case studies.

Three-dimensional model generation - UNEXE integrated data obtained from the work undertaken at the UK validation site, exploring the application of aerial and terrestrial laser scanning in an open pit mining environment. UNEXE investigated the development of a flowsheet or modelling approach for the different case studies highlighted within the SLOPES project i.e. develop a framework for incorporation of remotely captured digital data in slope stability analysis. The methodology of model generation from point cloud datasets is explained in depth in the report “Application of advanced numerical methods” and the process is summarised in Figure 2.39.

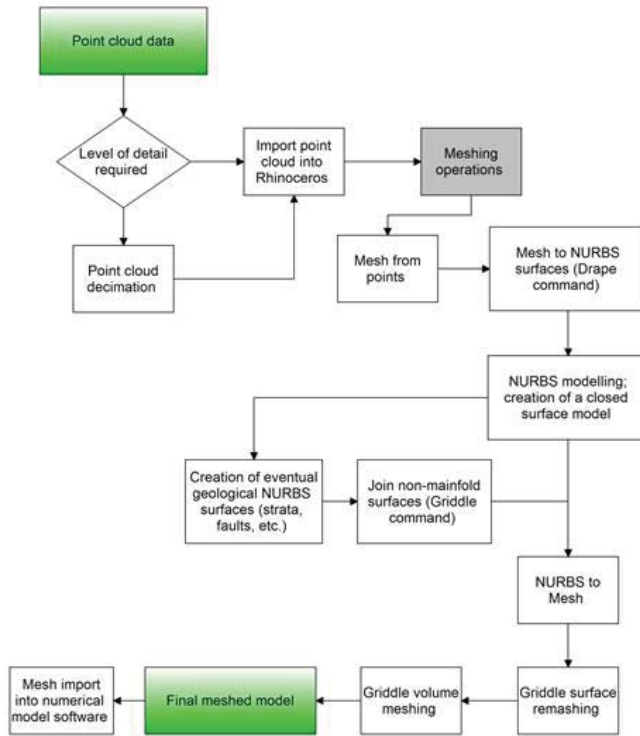


Figure 2.39: Flow chart

In reference to model generation, there is no difference between continuum and discontinuum geometry (except from the specific numerical software used), where the highlighted approach can be adopted in both cases. Nevertheless, it is important to differentiate between continuum, discontinuum and hybrid methods of numerical modelling/analysis. This is highlighted in Figure 2.40 which shows example modelling analyses for the SLOPES project, indicating the appropriate use of either continuum or discontinuum methods of analysis.

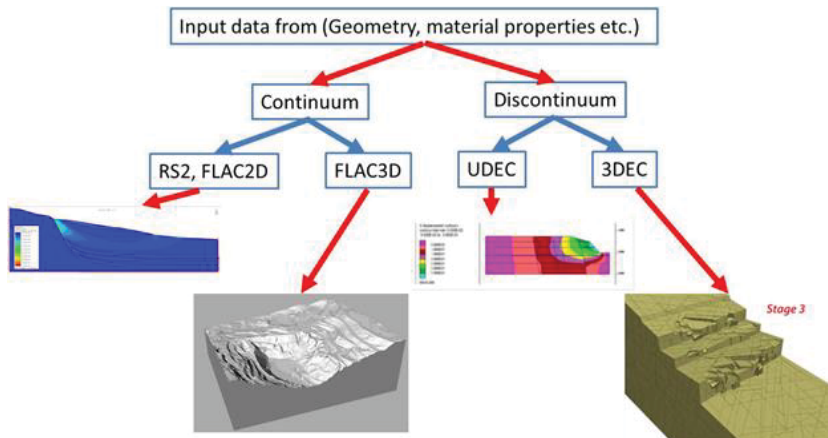


Figure 2.40: Modelling framework for continuum versus discontinuum modelling

Importantly, whichever method of analysis is adopted rigorous validation is necessary/essential to ensure confidence in the results. This validation could include comparison of model output with site based observations and instrumentation readings. Comparison should also be made with acceptability criteria for design (FoS, Probability of failure values). Where appropriate, comparison of results with more simple methods of analysis should also be undertaken to ensure confidence in output generated.

Validation is always important, even more so if models of great level of detail, achievable using modern geomatic techniques, are used. In most situations this can be seen as an advantage, but it is important to underline that geomatic data can be used to help understand the key features of a problem but that it is not always necessary to exactly re-create in the laboratory a natural phenomenon in its full complexity. Surprisingly, the detail obtainable by using remote sensing techniques can lead to the creation of a model that increases the level of uncertainty. For this reason every case study should have its own defined approach, in order to understand the level of resolution required to perform a cost-effective analysis.

With the aim of testing the illustrated methodology to a real case study, UNEXE applied a three-dimensional discrete element method approach to an example case study, identifying the critical parameters that influence direct toppling instability in an open pit environment. In this case, terrestrial laser scanning was used to obtain detailed three-dimensional geometry of a slope face and subsequent stability analyses undertaken. A series of sensitivity analyses on critical parameters such as friction angle, discontinuity shear and normal stiffness, discontinuity spacing and orientation was performed. Results of the analyses revealed the importance of undertaking three-dimensional analyses for direct toppling investigations that allow identification of critical parameters ignored by simple two-dimensional simulations. The study, illustrated below, highlights the importance of slope geometry and fracture network orientation on potential slope instability mechanisms.

A TLS point cloud survey was undertaken of the test bench at the UK validation site. The registration process indicated that the final accuracy achieved for the plano-altimetric alignment was sub-centimetre. A stereonet analysis using Dips 7.0 indicated three discontinuity sets, as detailed in Table 2.13; orientation and approximated spacing) identified on the point cloud, and average bench orientation (Dip/Dip Direction 75°/270°).

Table 2.13: Orientation and Spacing of major discontinuity sets identified within test bench in Melbur Pit

System	Dip (°)	Dip Direction (°)	Spacing (m)
J1	81	082	1
J2	83	321	2
J3	15	261	2

According to kinematic analyses and direct field observations it can be confirmed that J1, J2, and J3 cause the potential for direct toppling instability, with the centre of gravity of the formed blocks lying outside the outline of the base of the block, causing a critical development of an overturning moment. On the other hand, flexural toppling, even if geometrically possible, is unlikely to occur in this kind of competent rock. This is because for flexural toppling to occur the intact rock should be subjected to failure induced by inter-layer slip, but in this case, the low angle system J3 has a primary control on the instability and release the block. For this reason, the following stability analyses are focused on analysis of direct toppling.

Incorporation of representative slope face geometry from remote sensing - Previous results for the emphasized slope geometry highlighted that bench slope face angle may have a critical influence on the stability of the bench under study. Therefore, it was decided to perform a 3DEC analysis incorporating a more realistic representation of the slope face geometry obtained from the TLS and point cloud. In order to do this, the plug-in Griddle for Rhinoceros 5.0 was used to create a volumetric mesh that was imported into 3DEC. The results of the 3DEC simulation using the realistic slope face geometry is shown in Figure 2.41.

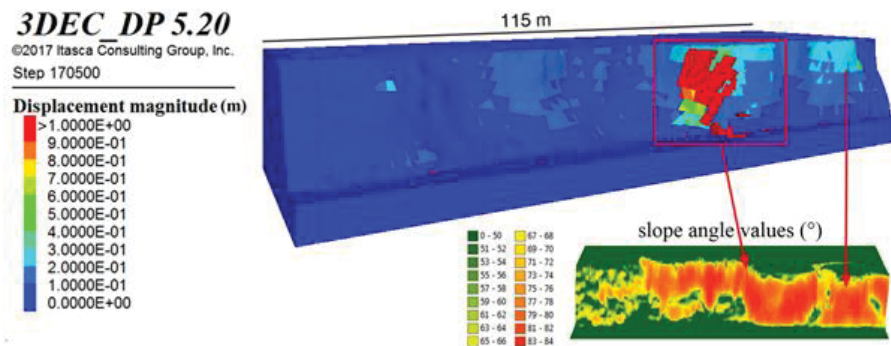


Figure 2.41: 3DEC simulation showing displacement magnitudes using bench face geometry from terrestrial laser scanning point cloud data. Lower right inset map indicates bench face slope angle values (°) calculated in ArcGis

The results indicate that direct toppling does not occur evenly throughout the model, but it is concentrated in regions that have a higher slope angle and instability occurs where rock blocks are confined by only one lateral discontinuity. The stability analyses undertaken provides improved understanding of discontinuity-controlled instability mechanisms affecting Melbur Pit. From previous engineering-geological investigation of the area (Carter, 2015; Keverne et al., 2015; Vanneschi et al., 2017) it was found that direct toppling is the likely dominant failure mechanism, therefore further investigation was carried out combining different methods of analysis. A detailed TLS survey of a selected location was performed in order to obtain accurate geometrical data for characterization of both the bench slope face profile and discontinuity orientations for use in subsequent analyses.

As direct toppling is a three-dimensional problem, controlled by 3 discontinuity sets (one basal plane and 2 sets forming block edges) a three-dimensional DEM analysis was undertaken. Initial deterministic 3DEC analyses performed on an idealised slope face geometry confirmed the possibility for direct toppling to develop within the model. This agrees with modelled results of previous 3DEC direct toppling/sliding investigation by Brideau and Stead (2012) that demonstrated the possibility of stepped-failure surfaces to develop in models with fully persistent discontinuity sets. Step-path surfaces are also common in slopes where rock bridges limit the persistence of the joints (Jennings, 1970; Einstein et al., 1983; Goodman, 2003).

A series of sensitivity analyses were then performed on discontinuity properties, the first of which was focused on the discontinuity friction angle. The results show that discontinuity friction angle has an influence on the modelled final horizontal displacements magnitude, but the underlying toppling failure always occurs for the range of friction angles simulated, even if with increased delay for higher friction angles. The second sensitivity analysis indicates that the model is very sensitive to  $K_s$  values. Such behaviour was also noted by Brideau and Stead (2012) and confirmed here, where a small increase of  $K_s$  leads to a stable condition within the model. Such factors should be carefully considered in development of numerical models as  $K_s$ , together with  $K_n$ , is one of the most uncertain parameters to determine in geotechnical investigations, and this may have implications for numerical modelling result interpretations.

Given the uncertainty related to geometrical setting in rock slopes, further sensitivity analyses were performed to investigate the influence of discontinuity spacing and dip angle of the toppling joint ( $J_1$ ) that according to LEM results would have the most influence on the model. Results indicated that an increase of the spacing aspect ratio by a factor of 1.5 is sufficient to prevent direct toppling to develop. This is due to the change of block size, with the centre of gravity acting within, or close to, the base of the new blocks. In addition, the inclination of the base surface ( $J_3$  set) is too low and the ratio of the shear to normal forces acting on the base does not exceed its friction angle, preventing sliding failure to develop. Therefore, neither direct toppling nor sliding failure can cause instability within the model. This is especially true for spacing configuration 3 ( $J_1/2m$ ,  $J_2/2m$ ,  $J_3/4m$ ), where no instability is reached even when changing both the toppling joint dip and slope angle, and using low  $K_s$ ,  $K_n$ , and friction ( $\phi$ ) values.

Nevertheless, a spacing configuration 2 ( $J_1/1.5m$ ,  $J_2/3m$ ,  $J_3/3m$ ) appears to be close to instability, since the sensitivity analysis show that an increase of the slope angle from  $75^\circ$  up to  $85^\circ$  can trigger direct toppling failure. This is an interesting result that was not detected by the LEM analyses, indicating that slope face angle may be a critical influential parameter, with possible important consequences on LoM decisions. In order to investigate the influence of this parameter, the 3DEC deterministic analysis was performed on configuration 1 but decreasing the slope angle value from  $75^\circ$  down to  $70^\circ$ . Results clearly indicate that if a lower bench face angle is considered, a fully stable model is obtained.

The importance of bench slope face angle was also confirmed by the 3DEC simulation performed using more realistic slope face geometry obtained from TLS point cloud data. The analysis indicated that zones of the slope characterized by high bench face angles are more susceptible to failure by direct toppling. In addition, instability first develops where blocks are only confined by one lateral discontinuity. The 3DEC analysis provided good representation of the observed instability mechanisms occurring within the Melbur Pit East face, as shown in Figure 2.42.

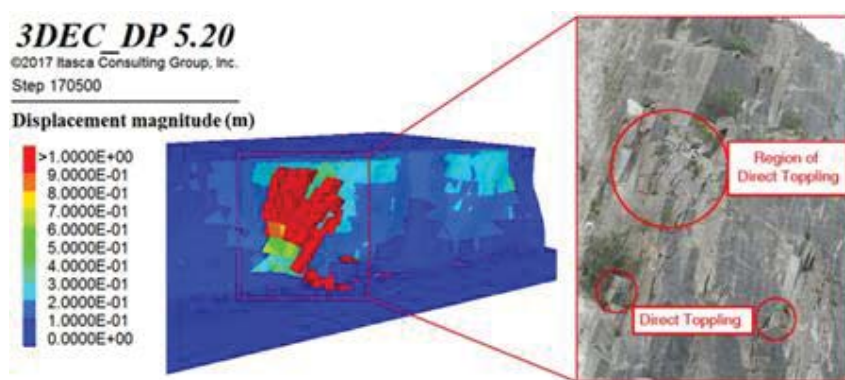


Figure 2.42: Comparison between results of 3DEC analysis and direct field observation

It is well known that persistence is one of the most influential parameters in geotechnics, and one of the most difficult to determine/obtain. Several authors have investigated the effect of rock bridges in numerical modelling (Nichol et al., 2002; Elmo et al., 2011; Brideau and Stead, 2012; Sturzenegger and Stead, 2012; Salvini et al., 2017) but, as recently reported by Tuckey and Stead (2016), an accepted standard for incorporation of rock bridges into slope stability analysis does not yet exist. In this case study, results of the persistence sensitivity analysis showed that a decrease of the joint persistence by 10 % lead to a fully stable model. Therefore, the model appears to be

very sensitive to this important parameter. The reason for this behaviour is explained in Figure 2.43.

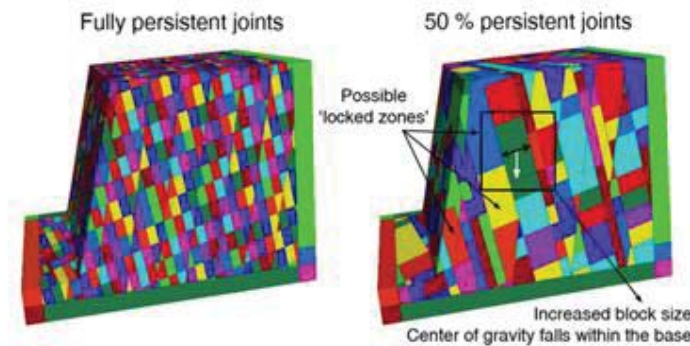


Figure 2.43: Increase in block size due to different persistence configurations in 3DEC

Figure 2.43 clearly shows the difference in block size when using the p option in 3DEC. As an example, a fully discontinuity persistent model is compared to a model with 50% persistent discontinuities. This means that in the second model only half of the possible blocks are actually formed. The consequence is similar to an increase of discontinuity spacing/block size. This means that, similar to what was discussed before, there are a number of blocks in the bench that do not have the potential for toppling, given that the centre of gravity is more likely to act within their base. In addition, persistence in this case is independent of "depth", and there is the same probability to find a non-persistent joint at surface or at depth. These conditions may create 'locked zones' within the slope, preventing block failures. This is not always correct in open pit environments, since excavation activity (i.e., blasting) can cause damage to the rock mass and influence the distribution of persistence values within the bench rock mass

To summarize, it was found that bench slope face angle in 3DEC has a major influence on the stability of the three-dimensional model, on a par with the effects of discontinuity Ks and spacing. While the latter cannot be changed, being intrinsic properties of the rock mass, the bench slope angle can be modified by the design engineer for safety purposes. Given the potentially unstable nature of the slope face and potential hazard identified from direct toppling a critical section of the East slope at Melbur Pit adjacent to a haul road underwent remediation through controlled blasting to reduce the overall bench slope angle, described in Keverne et al. (2015). The general failure mechanism for the slope orientation has been identified and useful information has been obtained for optimization of LoM excavation bench design, confirming the importance of the implementation of accurate three-dimensional data for appropriate mitigation strategies in contexts where two-dimensional simplification would lead to wrong conclusions. Importantly, the approach adopted during this investigation could be extended to other instability mechanisms and could be undertaken at different scales (to identify bench, inter-ramp and overall slope instability mechanisms).

SUBTERRA analysed the landslide that occurred in SAMCA Mine, Located in Teruel (Spain). Santa María Mine (property of SAMCA Group) is located in Teruel, Spain. Currently it is the largest active lignite open pit mine in Spain and has the second largest reserves of lignite in Spain and is one of the largest in Europe. The age of this coal basin is from Lower Cretaceous, and has been largely exploited by underground and open pit mining. Within the last four years several stability problems have been encountered within the exploitation of the North slope. The direction of the bed layers and their dip parallel to the natural slope is shown in Figure 2.44.

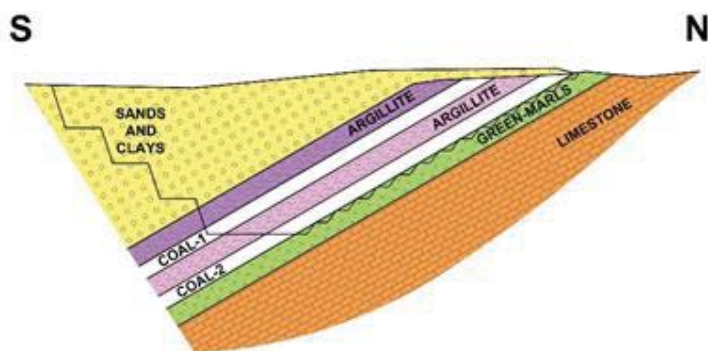


Figure 2.44: Schematic cross section of the materials involved in the Open Pit.

After the first slide on the North slope, a preliminary analysis showed the green marls layer as the main surface of the slide. After a rainy period, the saturation process of this layer remarks the

weakness on the strength properties of the marls. Slides cause severe damages to mine infrastructure as well as changes on the mining plan. The model has shown dependence on the pore pressure acting on the joint surface, limiting the possibility of a circular failure within the upper weak layers. The joint surface caused the development of higher values of shear strain in the head of the slope, and slight increase in horizontal displacements at the surface under saturation conditions. The process of back analysis carried out for Green Marls behaviour has shown the relative importance of the pore pressure on the joint, and the higher influence of the residual Mohr-Coulomb strength parameters. The parameters to explain the instability process according to the models performed, and to take into account for a control plan are the following are given in Table 2.14.

Table 2.14: Model parameters related to the instability process at SAMCA Mine

Parameter	Lower values	Higher values
Pore pressure excess on the marls layer (MPa)	0	0.25
Cohesion, $c$ (kPa)	0.15	0.52
Friction Angle ( $^{\circ}$ )	24	28
Residual Cohesion (kPa)	0.05	0.08
Residual Friction Angle ( $^{\circ}$ )	12	14

The results of the back analysis performed by means of numerical modelling showed the following conclusions for the real case considered. (1) The use of FLAC2D for the simulation of a failure surface of large dimensions (near 300m) and layers less than 2m thick is limited due to mesh restrictions. (2) The laboratory tests of intense fractured marl samples seems to lead to higher cohesion and friction angle values. This aspect has been analysed during several calculations employing Shear Strength Reduction. (3) Attention must be paid to the state of the joint between green marls layer and limestone bedrock. A proper characterization of this surface will facilitate the simulation and further detection of potentially instable areas. (4) The establishment of a piezometer, total pressure cell and inclinometer network is recommended in order to foresee future instabilities during rain season. Once the critical values are obtained, it will be possible to assess in terms of total displacements and B-bar evolution.

### TASK 2.3: Vulnerability issues (CERTH, INERIS)

The aim of this task was to present the characteristics of open pit mine instabilities and the damages of structures and infrastructures that may occur in the zones close to mine operations.

INERIS and CERTH considered the case of the open pit lignite mine of Mavropigi in the Ptolemais basin (northern Greece), where in 2010, the mine slopes and the resulting effects on the nearby area were raised. These concerns were triggered by the appearance of significant surface tension cracks at the crest of the southeast slopes of the excavation (northwest of the village, Figure 2.45). Because of this event, instrumentation and monitoring have been taking place since then (Papadaki et al. 2013), while counter-measures had been applied in order to ensure the stability of the mine slopes and the surrounding areas.



Figure 2.45. Cracks on the region northwards of Mavropigi.

To analyse the events, we started with the collection of data of the mine operations, as these have been reported by PPC (Public Power Cooperation) in various reports. From a geological point of view, the mine is located in the Ptolemais basin, which is a NNW-SSE elongated intramontane basin in the Pelagonian geotectonic zone. The basin sediments include Neogene formations and Quaternary deposits. Particularly, the area of Mavropigi belongs to the western border zone of Ptolemais basin and it has a strong complicated tectonic structure (Diamantopoulos et al. 2004). According to Monopolis et al. (1999), three series of sub-layers are included in the upper layers of the Neogene formations: (a) the upper series, composed of clay - marl clastic sediments, (b) the multi-stratified lignite-bearing series (including an intermediate waste sequence), and (c) the lower

series, whose uppermost part consist of marls with lenticular intercalations of marly limestones. In addition, towards the southeast slopes of the pit, there are the formations of limestones and schists. The above part of a local graben striking NW-SE intercepted by transverse faults (resulting to the fragmentation of the orebody in individual tectonic blocks).

In 2010, noteworthy surface tension cracks became evident at the crest of the southeast slopes of the excavation, very close to the village of Mavropigi (Figure 2.48). These cracks appeared in areas of pre-existing faults. At the same time, horizontal transverse movements were observed at the toe of the lower benches of the excavation. By 2011, persistent horizontal movements at an average of 1-2 cm/day (reaching 4-5 cm/day during heavy rainfall days) were recorded; the total volume of the kinematically unstable wedge was estimated to be about 6 Mm<sup>3</sup> (Kavvadas et al. 2013). The sliding mechanism was investigated thoroughly based on extensive monitoring, as well as back analyses using limit equilibrium methods. According to these investigations, the sliding mechanism was described as a movement of the southeast slopes of the mine (northwest with respect to the village of Mavropigi) on top of a near horizontal shear surface within the neogenes. The later one included a thin layer of high plasticity clay with a very low residual friction angle.

CERTH recorded the type of damages in Mavropigi village, which is located near an active open pit lignite mine operated by the Public Power Corporation (PPC). The establishment of a preliminary relation between the severity of structural building damages and their distances from the advancing pit walls was attempted. Two site visits were organized in 2011 and 2016 to identify damaged buildings in relation to mine activities. The main aim of this site inspection was to detect and record as many building damages as possible, and to identify their location in relation to the position and advancement direction of the pit mine. Figure 2.46 and Figure 2.47 present examples of damages in the ground and the buildings induced by the slope instability of the open pit mines. The first visit was organized (June-July, 2011) by Aristotle University of Thessaloniki (AUTH). Information and data were collected: the type of building, the owner, material of construction, number of floors, basements, the dimensions and shape of the base and other construction details were described. Of the 255 buildings, 45% of them were made of reinforced concrete, 38% of bricks or blocks and 17% of stone.

In September 2016, a second site visit to Mavropigi village was organized. For this reason, a topographic map of the village, with satisfactory surveying of the existing buildings and roads was sought, found and utilized for tracing purposes. Wherever possible, specific indicative and representative cases were recorded and correlated with the topographic plan view of the village. The number of the recorded cases raised to 17. It should be noted that the whole number of buildings into the village was not possible to be examined. Village and houses have long been abandoned after the reparation of its residents on behalf of PPC and the Greek state, and the empty houses have experienced significant looting and further severe damages. So, it was extremely difficult in many cases to distinguish if the damages in a specific building were due to the landslide phenomenon or the looting actions. The type of observed building damage was associated with the level of its functionality. Three levels of functionality were assumed, the green denoting safe conditions, the purple representing severe damage that could be repaired (the house probably being able to be returned to a safe status), and finally red that indicates irreversible building damage and a collapse situation. The plan view of the village with superimposed the recorded buildings, the present location of the pit slopes and their advancement direction, are all shown in Figure 2.48. As can be viewed, the distance of the pit mine slopes from the village is just 300 m.



Figure 2.46: Pictures of the region north of Mavropigi taken in December 2011



Figure 2.47: Observed damage in different buildings in Mavropigi village

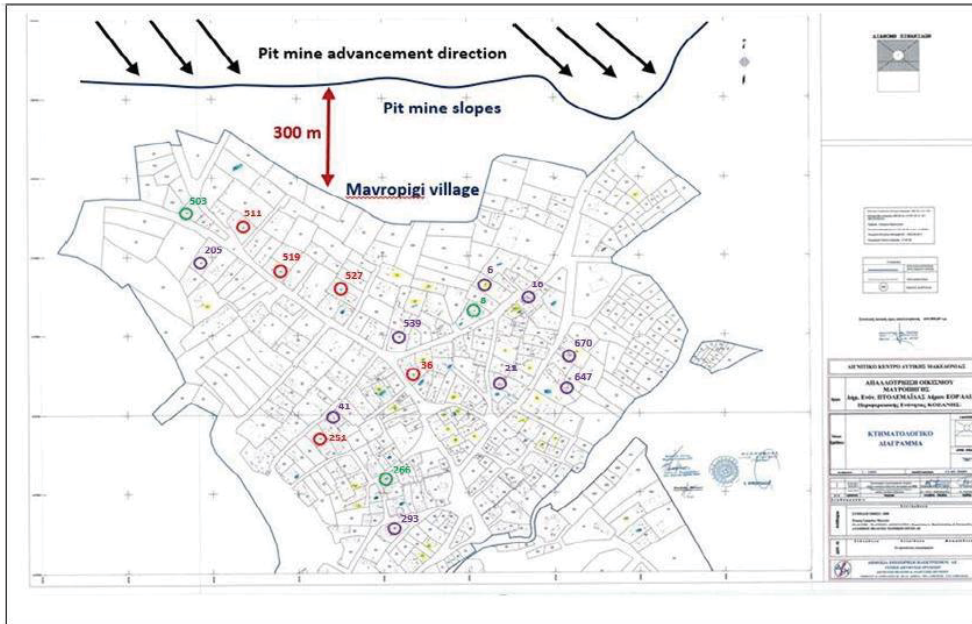


Figure 2.48: Mavropigi plan view and building damage recordings and classification. Damage levels: green: slight damage, purple -medium to severe damage, red – very severe damage.

An example of a fully damaged building (36, red) is given in Figure 2.49, which is a stone masonry house where the bearing wall has been revealed to a great extent. It was considered to be totally damaged and has been classified as red.



Figure 2.49: Red damaged building in Mavropigi village (CERTH)

The investigation results show that the damage increases with a decrease in distance from the open pit. The main damaged houses are very close to the mine, where the distance is less than

400 m. If we consider that the 17 houses represent the village buildings, we can note: 5 of 17 buildings = 30 % of the village present severe damage; 9 of the 17 buildings = 50 % of the village present moderate damage; 3 of the 17 building = 20 % present slight damage or without damage.

A large amount of research has been undertaken to identify the damage scales generally used to assess the damage level of structures due to ground movement and landslides. The damage due to mine activities and instability may be divided into direct damage and indirect damage, and into material and structure damage and human damage. In the case of open pit mines it is rarely that the land sliding induces direct fatalities for the population living near the mine because the velocity of such movement is low compared to landslide movement related to earthquakes. The level of damage depends on (1) the type of movement, its location, and its magnitude (in terms of volume and velocity); and (2) the building category, age, height/size, and type of foundation. The damage scales related to the landslide are based on the landslide velocity. The first damage class corresponds to a velocity of the movement less than 1 mm/day and the damages are very limited, the building damage starts when the velocity of the ground movement reaches a few cm/day. Alexander (1986) proposed an intensity scale for structural damage caused by subsidence, compression or extension of the ground during landslides. Both scales included eight grades, from 0 ("intact building") to 7 ("total collapse"). Geomorphological Services Ltd (1991) introduced a very simple graduation: "negligible", "slight", "moderate", "serious", and "severe". Figure 2.50 presents examples of different damages that can be observed in different buildings due to the ground movement and sliding. The slight and moderate damage are very difficult to observe and to relate to the ground movement and slope instability.



Figure 2.50: Examples of damage can be observed after a landslide, (A) very slight damage, (B) moderate damage, (C) severe damage (Frattini et al. 2013).

Antronico et al. (2015) introduced a macro damage index (ex. village or town). The Aggregated Damage Index (ADI), which is a weighted average of damaged buildings through the following simple equation  $ADI = (\sum(a_i \cdot B_i)) / (\sum B_i)$ , where  $B_i$  is the number of buildings located in the area belonging to a class of damages and  $a_i$  is the weight corresponding to the damage class: 0 for no damage; 0.2 for negligible damage; 0.4 for slight damage; 0.6 for moderate damage; 0.8 for serious damage; 1 for severe damage or destroyed building. ADI may vary from 0 (area without any damage) to 1 (completely destroyed or severely damaged area). The number of the damaged buildings concerned by the landslide depends on the area of the landslide (Ciampalini, et al. 2014) and a correlation may be observed in such cases. When the area of the landslide is less than 200 m<sup>2</sup> the damage for buildings is less than 0.2 (negligible damage) whereas landslides larger than ~10.000 m<sup>2</sup> produced a damage ranked as 0.5 or larger (functional to structural or total damage). Concerning major roads, a landslide less than 100 m<sup>2</sup> would cause a damage less than 0.2 and landslides exceeding ~1000 m<sup>2</sup> produced mostly a damage ascertained as 0.4 or larger (functional to total damage). For secondary roads, the majority of the landslides extending ~1000 m<sup>2</sup> produced a damage ranked as 0.4 or larger, and landslides smaller than ~1000 m<sup>2</sup> produced a damage ascertained as 0.4 or smaller.

The basic reasons behind the significant movements can be summarized as follows:

- During mine operations in the period 2009-2010, the excavation progressed in a non-conventional way due to expropriation limitations. More specifically, delays in the land acquisition of a small area in front of the excavation face, not only caused trouble in the production, but also imposed significant changes in the direction of the excavation (Roumpos and Papacosta 2013). These changes created an adverse steeply convex geometry in the excavation face and had adverse geotechnical effects.
- The geological conditions with steep inclined faults. More specifically, the mining field is separated by many NW-SE striking faults into individual fault blocks. Towards the village, the mining field is limited by one or several faults with dip towards the mine.
- The presence of near horizontal (unfavourably dipping) thin (just a few centimetres thick) high plasticity clay beds. These beds are often present in the marl - lignite intercalations of the Ptolemais mines, they are characterized by a significantly low residual strength (5° - 10°) and they often serve as part of the compound sliding mechanisms of the local mines.

In addition to the above, it is noteworthy to mention that a strong dependence of the movement's velocity on the level of precipitation was detected (Kavvadas et al. 2013). In other words, days of heavy rainfall were followed by increased velocities of slope movement. The analysis of building damages has been performed using of the Aggregate Damage Index (ADI). The first autopsy took place during the period of June - July 2011, by a research team on behalf of the Aristotle University of Thessaloniki, Greece (Tsapanos et al. 2011). The second autopsy took place in August 2011, by engineers of the Kozani Regional Unit (Region of Western Macedonia). It should be noted that the first ground fissures in the area between the mine and the village were noted in July 2010.

The scope of these inspections was to detect and record building damages, and to identify the location of these damaged buildings in relation to the position and advancement direction of the surface mine. In total, 255 buildings existed at the time of the first inspection (2011) in Mavropigi village. Different types of buildings according to their use, the construction material, and the number of floors are tabulated by Lialiabis and Dimoudi (2011), who indicated that the majority of the buildings (85%) were for residential use, made either by reinforced concrete (45%) or by bricks or concrete blocks (38%). Most buildings were either ground floor only (51%) or two storeys buildings (33%). Assessment of damages has taken place based on typical classifications from post-earthquake building damage assessments, with the basic criterion being the safety of people inside and outside the building. Overall, three categories were used during damage assessment:

- "Safe for use" buildings (green color), which refers to cases that have experienced negligible or none damage and do not indicate signs of reduction of their original bearing capacity.
- "Unsafe for use" buildings (yellow color), which refers to buildings with reduced bearing capacity, though not to the extent of being in risk of sudden collapse.
- "Dangerous for use" buildings (red color), which are buildings whose original bearing capacity has greatly decreased (and thus they might be prone to sudden collapsing).

Based on the assessment, 182 (i.e. 71%) buildings were characterized as green, 57 (22%) as yellow and 16 (7%) as red. The observed damage on the village buildings depends on the nature and the vulnerability of structure.

The Aggregated Damage Index (ADI) was calculated to estimate the situation of global damage of the village. According to the data, the ADI is equal to 0.47. According to this index, the damage is important.

A global damage index (GDI) has been proposed and can be used to compare different scenarios of mine operation. The GDI can also be used to compare different open pit mine projects and design options to minimize the damage on structures and infrastructure. The GDI is a score of points depending on 5 criteria:

- The safety factor value;
- The building distance or the urban zone and the class of the vulnerability of the village;
- The existence of faults, analysis outcomes concerning fault descriptions, distance, etc.;
- The natural or induced seismicity depending on the class of the mining zone or the recorded recent and historic seismicity;
- The water effect, relating to dewatering and rain consequences. The analysis is based on the likelihood of the potential to have significant periods of rain and water quantity.

The obtained score varies from 10 to 50 points; 10 points corresponds to a good configuration and 50 for a critical configuration. The total score varies from 50 to 250.

- for excellent open pit conditions, the score is equal to 50 points;
- for very critical open pit conditions, the score can be 250.

<i>GDI</i>	50	<100	<150	<200	<250
<i>Risk level</i>	Very low	Low	Moderate	Severe	Very severe

The GDI was estimated for the Mavropigi case study, which obtained a score of 120 points, corresponding to a moderate risk. This result of GDI is comparable to the method used to evaluate the damage of the Mavropigi village based on the classification of damage of individual buildings. Both approaches can be useful to predict and to assess the potential consequences of a mining project on urban areas. The qualification of these data should be prepared with the help and expertise of specialists. The GDI value can take into account the uncertainty of the site and the data.

A numerical model using 2D distinct element code UDEC (Figure 2.51) was carried out to study the consequences of the open pit mine on the Mavropigi village and its buildings. The model presented a section with the different geologic layers and the four faults. Two phases of the excavation were simulated. Table 2.15 presents the geotechnical parameters used in the calculation. In addition, sensitivity studies of the case study were done to identify the role of each one in complex conditions.

Table 2.15: Geotechnical parameters of the rock layers and joints (faults)

Layer	Density	Young's Modulus	Poisson's	Friction angle	Cohesion
-------	---------	-----------------	-----------	----------------	----------

	(kN/m <sup>3</sup> )	E (MPa)	ratio, v	$\varphi$ (°)	c (MPa)
Quaternary	18	100	0.25	20	0.1
Neogenic	22	1000	0.25	33	0.2
Limestone	25	3700	0.25	34	1.7
	Normal stiffness, kn	Shear stiffness, ks			
Faults	66 MNm	6.5 MNm		18	

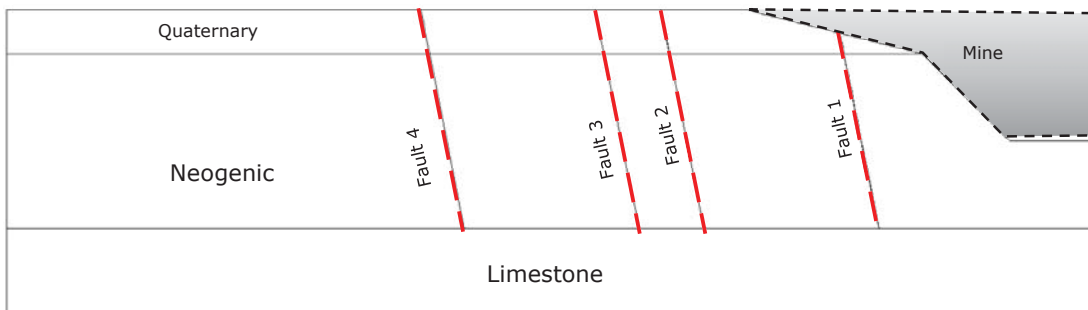


Figure 2.51: Numerical model (UDEC) of the Mavropigi open-pit mine.

The behaviour and the effect of faults under different geotechnical data: initial stresses, fault extension, dewatering and natural seismicity have been performed through sensitivity analysis. The results of the numerical modelling clearly highlighted the main role of the faults at the location of the village. The faults modified the influence of slope, horizontal and vertical displacements are identified, the magnitude of the displacement increases in relation to the dewatering, the initial seismicity.

The localisation of plastic points (Figure 2.52), obtained by the numerical model, presented the collapse of slope observed in the mine. In addition, differential displacement far from slope was calculated to vary between 3 to 5 cm mainly when the depth of the mine increased (Figure 2.53). Regarding the damage scales, these can induce severe damage on vulnerable masonry structures because it concerns short distance. The influence of slope increases by the influence of the natural and anthropic factors as the dewatering, natural seismicity and tectonic structure (faults and soft geological layers). The differential displacement amplitude is enough to induce a severe damage on masonry houses located near the position of the houses. Those results can explain the damage observed in both case studies in Greece. The open pit mine project should take the different factors to define clearly a safe zone for structures and infrastructures.

The work done in this task highlighted that the hazard and risk assessment approach should be performed considering the natural and operational factors. Since the coalfield is located in a populated region, detailed concepts must be worked out for the new landscape which will follow: the topography, the water drainage system, lakes and forests, and the intended land-use pattern are designed and specified in advance. Early, detailed planning makes it possible to coordinate mining and concurrent land reclamation activities. The comprehensive approach permits treating the overall problem as a whole rather than dealing with its separated aspects on a piecemeal basis.

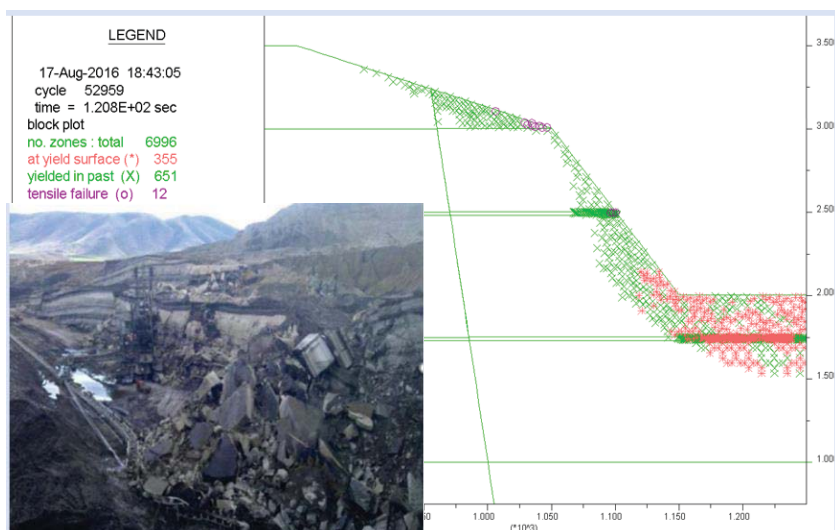


Figure 2.52: Plastic points (red and green) due to mine excavation and the 14th January of 2014 landslide in the mine Mavropigi open-pit.

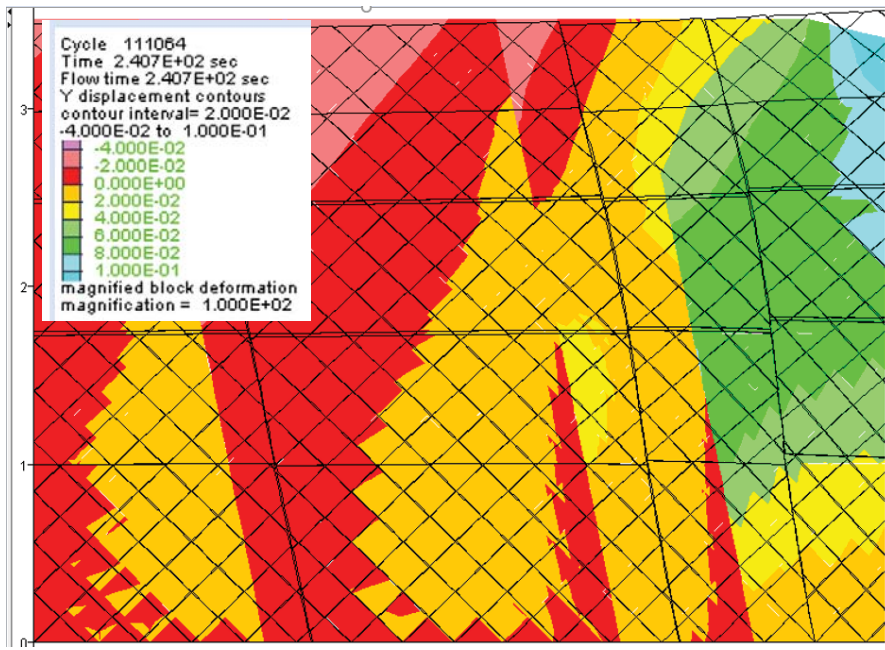


Figure 2.53: Vertical displacements along the faults in the area of the Mavropigi village.

The main conclusion, in term of risk management, is that the intensity as well as the extent of a potential instability can be predicted. Well-founded hydrogeological and geotechnical studies can determine the exact mechanism of the land subsidence by applying advanced modelling procedures. The decision-making authorities based on guidelines and the interest of the mine operators and the population can decide the proper steps to be made for the protection of the human environment, reducing or even eliminating the impact of the mining hazard. Decisions regarding the relocation of villages, as well as estimations, about their contentious restoration cost can be made. As a result, the uninterrupted exploitation of the natural resources can be conducted not only without damaging the local communities, but also by contributing to their development.

These results were presented during various project meetings. In addition, a paper was published in the international conference "Slope Stability 2018 | April 11-13, 2018 Seville, Spain".

### **WP3 - Stability and long-term behaviour of lignite mine spoil heaps and reclaimed ground**

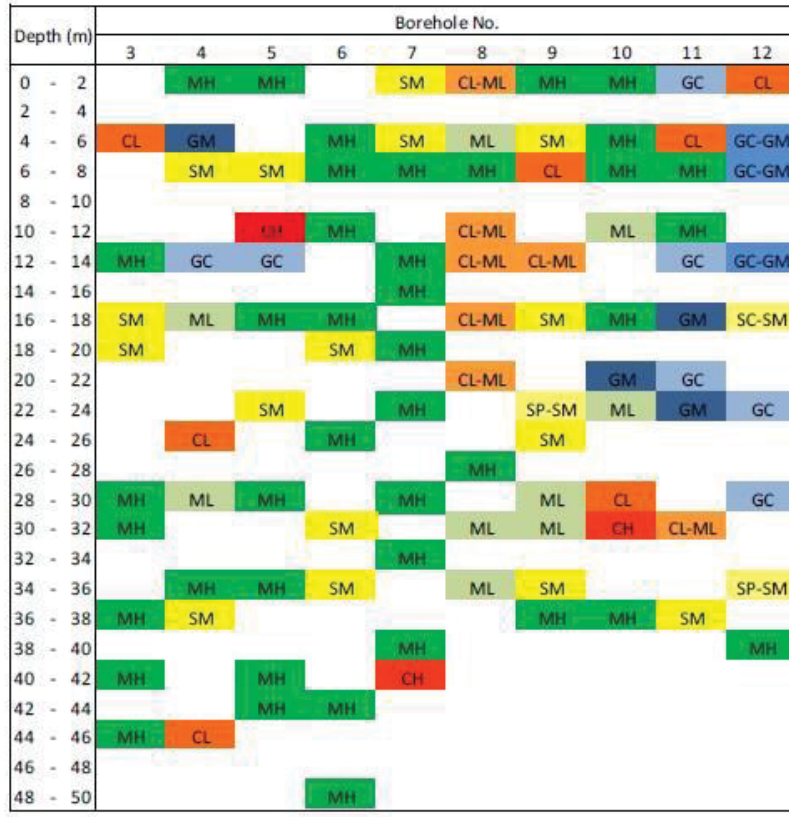
**TASK 3.1:** Collection of detailed data sets and material testing of lignite mine spoil heap materials (VUHU, POLTEGOR, UoN, CERTH)

CERTH collected and registered a large unified spoil property database, resulting from geotechnical laboratory tests, provided by the Public Power Corporation (PPC). PPC operates the two surface mines whose waste materials are discarded onto a dump. The dimensions of this huge waste embankment is about 5 km length, 1 km width, and a maximum height raising up to 150 m. A satellite plan view of the spoil heap (called Soulou's spoil dump such as the respective place name), with the sampling boreholes along its axis illustrated as yellow pins, is given in Figure 2.54.



Figure 2.54: Soulou's spoil dump plan view operated by PPC

Geotechnical identification and characterization of Soulou's spoil dump was based on laboratory tests performed by PPC, on samples from boreholes along the embankment axis, in representative and critically selected locations. Geotechnical laboratory tests included classification according to the Unified Soil Classification System (USCS), Atterberg limits, 1-D consolidation tests, and consolidated-undrained with pore-pressure (CUPP) measurements triaxial shear strength tests. In Figure 2.55, spatial distribution of spoil material type along the axis of the embankment and over depth is shown. It is evident that an explicit distinction among different stratigraphic layers cannot readily be made. Instead, due to the fact that spoil heaps' stratigraphy is greatly variable (or even nearly chaotic), from an engineering design point of view, a simplification of the problem would rather approve the consideration of a uniform geo-material within the waste dump. The spoil was managed as a uniform material, since as already mentioned, the distinction of different layers, and eventually, the determination of a certain stratigraphy about the embankment is for the time being practically impossible (Zevgolis et al., 2018). Due to the extreme difficult level of the examined problem, maybe this specific assuming approach is the most suitable one, provided that spoil heap's slope stability and performance calculations are accompanied by probabilistic principles and analysis methods.



Legend			
MH	CH	SM	GM
ML	CL	SP-SM	GC
CL-ML	SC-SM	GC-GM	

Figure 2.55: Spatial distribution of spoil material in Soulou's spoil heap

Herein, results derived from the statistical process of datasets according to the assumption of a uniform spoil material across the spoil dumps' mass are given. Attention could primarily be paid to the coefficient of variation  $COV$  of each random variable, defined as the ratio of standard deviation  $\sigma$  to the mean  $\mu$ . Minimum and maximum values are also included, since geotechnical parameters are random variables with physical finite limits of occurrence. Results of the statistical process, treating spoil as a uniform material within the dump's ground mass are displayed in Table 2.16. Further information of the examined case study is provided in Deliverable D3.1.1 detailing datasets related to spoil characteristics.

Table 2.16: Uniform spoil material geotechnical parameter statistics

Uniform Spoil	N	$\mu$	$\sigma$	COV	$\beta_1$	min	max	$\rho$
$\gamma' (KN/m^3)$	96	17.08	2.34	0.14	0.10	12.54	22.27	
$c' (kPa)$	17	21.9	22.2	1.01	1.13	0	72.5	-0.8
$\varphi'(^o)$	17	22.2	6.0	0.27	-0.86	8.2	29.0	
FP (%)	96	56	17	0.31	-0.29	11	94	
LL (%)	80	51	12	0.25	-0.30	22	84	
PI (%)	80	19	13	0.68	0.68	3	60	
w (%)	96	40.36	18.12	0.45	0.20	7.19	81.97	
$q_u (kPa)$	29	105.1	91.5	0.87	1.69	5.2	407.0	
$C_v (m^2/s)$	44	0.0000007	0.0000005	0.78	1.28	0.00000006	0.000002	
$E_s (kPa)$	44	2,754	1,538	0.56	1.33	951	8,093	
$m_v (1/kPa)$	44	0.00048	0.00025	0.52	0.74	0.00012	0.00105	
$k (m/s)$	44	0.000000003	0.000000003	0.98	1.56	0.000000002	0.00000001	
$C_c (-)$	44	0.2155	0.0862	0.40	0.46	0.0642	0.3977	
$C_r (-)$	44	0.0367	0.0142	0.39	1.05	0.0131	0.0899	

N = number of samples;  $\mu$  = mean;  $\sigma$  = standard deviation; COV = coefficient of variation;  $\beta_1$  = skewness coefficient;  $\rho$  = correlation coefficient;  $\gamma'$  = unit weight;  $c'$  = apparent cohesion;  $\varphi'$  = angle of friction; FP = Percentage of fines (clay + silt); LL = Liquid limit; PI = Plasticity Index; w = water content;  $q_u$  = Unconfined Compressive Strength;  $C_v$  = Consolidation Coefficient;  $E_s$  = Compressibility Modulus;  $m_v$  = coefficient of compressibility;  $k$  = permeability;  $C_c$  = Compression index;  $C_r$  = Recompression index.

In this task, UoN carried out a series of triaxial compression tests in using a hydraulic stress-path machine on the samples provided by VUHU and POLTEGOR. The primary purpose of these tests was to estimate the parameters of the critical state line to be used in numerical simulations. These tests can also be used for the evaluation of model-dependent parameters such as viscosity and destructuration parameters. Each triaxial test consisted of three stages: (i) saturation, (ii) consolidation, and (iii) shearing under drained/undrained conditions. Table 2.17 summarises the results of a series of triaxial compression tests. The slope of critical state line ( $M$ ) was the primary outcome of these undrained shearing tests. Using critical state friction angle ( $\varphi_c$ ),  $M$  can be defined as:  $M = 6 \sin \varphi_c / (3 - \sin \varphi_c)$ . Experimental data also showed that the coefficient of earth pressure at rest for normally consolidated soil ( $K_{0,nc}$ ) can be estimated using Jack's formula (Jaky, 1944):  $K_{0,nc} = 1 - \sin \varphi_c$ .

Table 2.17: Summary of triaxial test results on samples from Vrsany mine, Czech Republic

Sample	Location	Depth	$M$	$\varphi_c$	$K_{0,nc}$
#01	50°30' 12.5" / 13°35' 25.7"	12.50-13 m	1.3	32.3	0.47
#02	50°30' 12.5" / 13°35' 25.7"	12.50-13 m	0.38	10.3	0.82
#03	50°29' 21.7" / 13°36' 8.40"	31.30-31.59 m	0.49	13.1	0.77
#04	50°29' 21.7" / 13°36' 8.4"	31.30-31.59 m	0.54	14.3	0.75
#05	50°29' 41.145" / 13°35' 42.59"	6.2 m	1.6	39.1	0.36
#06	50°29' 40.145" / 13°35' 42.60"	16.6 m	0.94	23.97	0.59
#07	50°29' 40.145" / 13°35' 42.60"	32.4 m	0.55	14.1	0.75
#08	50°29' 35.77" / 13°35' 50.56"	40.65-41.00 m	0.58	15.3	0.74
#09	50°29' 35.77" / 13°35' 50.56"	61.65-62.00 m	0.39	10.55	81.69

$M$  = slope of critical state line;  $\varphi_c$  = friction angle;  $K_{0,nc}$  = at-rest earth pressure coefficient.

### TASK 3.2: Physical modelling of spoil heaps and reclaimed ground (UoN, VUHU, POLTEGOR)

This task involved work mainly being conducted at the UoN (1g and centrifuge modelling), with input from VUHU and POLTEGOR regarding the material characteristics and geometry of the models.

UoN constructed a meso-scale, 1-g physical model aimed at enabling a better understanding of the effects of water level variations and wetting-drying cycles on the stability of spoil material slopes. The steel model box has a dimension of 5m in length, 2m in height and 1.5m in width (Figure 2.56(a)). The box was designed to ensure controlled conditions within the container (e.g. no water losses). The sidewalls of the model box consist of 3mm thick steel plates which are braced to provide lateral rigidity to the sidewalls. A 12mm thick steel plate is used for the floor of the box. One sidewall has five Perspex windows (in three columns). Each window is 650mm wide by 750mm high. These windows are used for measuring deformations and movement via image processing. Three high definition, 8-megapixel webcams observe and record the soil movement inside the box through these windows. With each camera, there is a 50W LED light bulb to improve image quality. The cameras, the LED lights, and the windows are covered so that any interference from the ambient lights is prevented. The Perspex windows and the three high-definition webcams can be seen in Figure 2.56(b).

The water is fed into the box through a standpipe which regulates the rise and drawdown of water in the test box. The standpipe system is illustrated in Figure 2.56(c). In the box, the water first enters a layer of pea gravel with a thickness of about 50mm to provide uniformity of the water pressure distribution. This layer of pea gravel, as it can be seen in Figure 2.57, covers the floor and one of the sidewalls and is separated from the soil slope via a geotextile material. Changes in water level inside the model slope is controlled by injecting water into the pea gravel layer or drawing water out of it via the control valves on the standpipe. A valve was placed on the sidewall adjacent to the toe of the slope at an elevation of 450mm and is used to draw water from the box and measure the rate of the flow in the soil slope model.



Figure 2.56: (a) Test box for large scale 1-g physical modelling, (b) HD webcams and Perspex windows, (c) standpipe.

The soil used in this slope model experiment is sandy silt which was obtained from Scrooby Top Quarries in Doncaster, England. The particle size distribution was measured in a sieve analysis and hydrometer tests. This soil consists of 50% sand, 45% silt, and less than 5% clay size particles and has a specific gravity of 2.61. The soil has a maximum dry density of  $1720 \text{ kg/m}^3$  which is achieved at an optimum water content of 17%. The saturated hydraulic conductivity of this sandy silt is  $2 \times 10^{-7} \text{ m/s}$ . A large-scale slope model is prepared in the test box. The geometry of the model slope is shown in Figure 2.57. The slope model angle is  $60^\circ$ . Each lift of the soil was weighed before placing it in the box. The equivalent height for each lift of the soil for reaching to the desired wet density of  $1.70 \text{ g/cm}^3$  was calculated. No additional compaction effort was applied to the soil during the construction of the slope model. To examine this desired density, cores were taken from the slope model during the construction. These cores show that the model has a wet density of  $1.7 \pm 0.03 \text{ g/cm}^3$  with a water content of 18%.

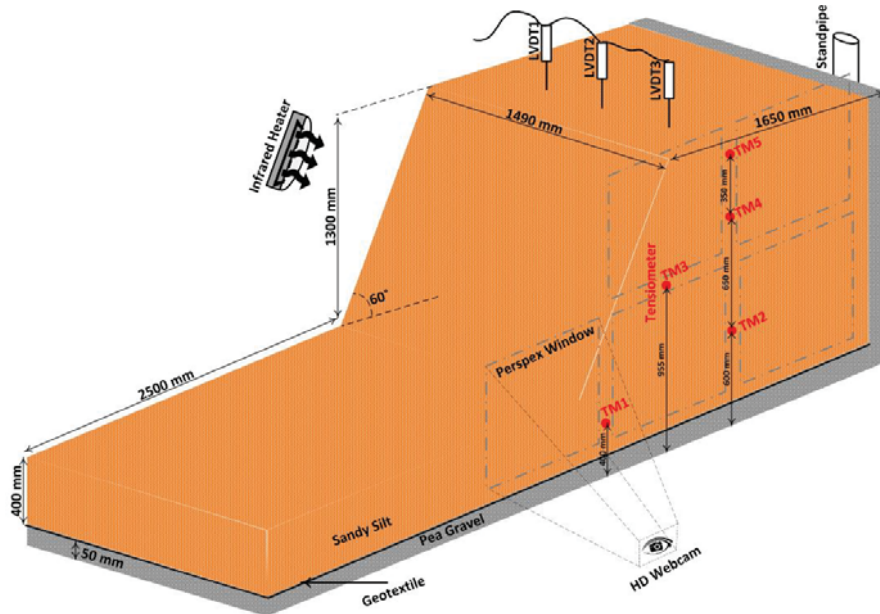


Figure 2.57: Schematic representation of the instrumented soil slope and its geometry

In addition to the high-definition cameras, LVDTs and tensiometers were also installed to monitor the behaviour of the slope model. Also, six infrared heaters, which are controlled via a thermometer measuring the temperature of the box, are installed inside the box to speed up the drying cycles. Tensiometers were installed along one section at elevations of 400mm, 600mm, 955mm, 1250mm, and 1600mm. The instrumented soil slope including the arrangement of the tensiometers along the slope model is schematically shown in Figure 2.57. Each instrument is calibrated prior to installation and is connected to a data-logger for automatic recording of data. All the instruments located inside the slope model were installed during soil placement. Each electronic instrument was logged at 1s intervals and the webcams took snapshots in 1min intervals.

The experimental program focused mainly on the performance of the slope model when the water level was raised and lowered and on the wetting and drying cycles. The water level variation consisted of four elevation steps with each elevation increment being 400mm. Each water level elevation was held for a period of almost 72h, followed by four draining stages which correspond to the elevation stages. During each stage, the readings from the tensiometers are checked for constant readings before initiation the subsequent stage.

Figure 2.58a shows the surface settlements monitored using 3 LVDTs installed on the crest of the slope. As it can be seen in this figure, settlement of the crest, during these stages, is between 1 to almost 5 mm. The observed settlements can be attributed to wetting-induced collapse of the unsaturated loose silt. It is also worth mentioning that, due to the boundary effects, the settlement values reported by LVDT1 and LVDT3 are smaller than those of LVDT2. Therefore, further surface settlement on the crest of the slope can be expected as the water level is further increased. The variation of pore water pressure was measured using five tensiometers (TM1-TM5). These measurements for the first two steps of water level elevation are presented in Figure 2.58b. As it can be seen, before putting water in the box, all tensiometers were reading suctions in the soil. As the water level was elevated, all tensiometers showed an increase of pore water pressure which is due to the saturation of the soil and the capillary rise of water in the slope.

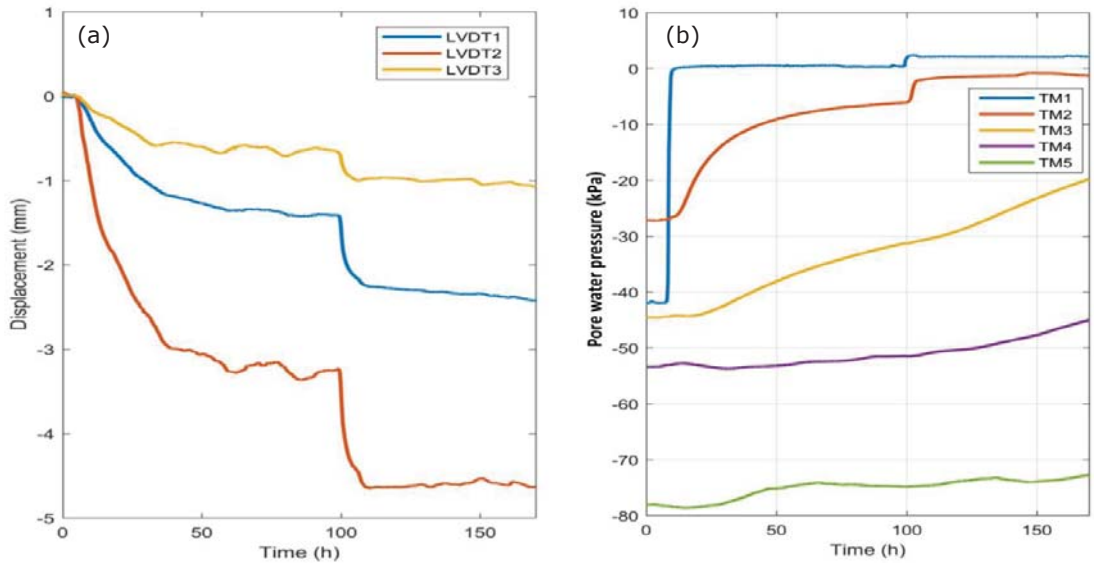


Figure 2.58: (a) Surface settlements measured by LVDTs; (b) variations of pore water pressure in the slope model

The UoN's 50 g-tonne geotechnical centrifuge with 2m radius was used to conduct the N-g tests for the SLOPES project. The centrifuge model tests simulated slope stability of spoil heap materials under specific rainfall and groundwater conditions. Studies have attributed rainfall-induced slope failures to two distinct mechanisms; the first is the build-up of positive pore pressure at the toe of the slope or at the weakest plane of slope (e.g. interface of superficial soil with the bedrock), which can lead to the static liquefaction; the second is related to the loss of suction within zones of unsaturated soil following rainfall infiltration, hence the saturation-dependent shear strength governs this failure process (Zhang et al., 2011). Previous centrifuge modelling studies have not considered the significance of grain size distribution on the coupled poro-mechanical response of the slope, for which pore pressure data is critical. The grain-size distribution plays an important role in determining the initial state and intrinsic properties of the slopes and can therefore influence the mechanisms of failure and rainfall infiltration. There are a relatively large number of studies investigating rainfall-induced slope instabilities using geotechnical centrifuges. Although some of these studies have considered different types of soil with different sand, silt and clay contents, they have not considered the significance of grain size distribution on the coupled poro-mechanical response of the slope. The closest attempt to study the effect of grain size on rainfall-induced slope instabilities is probably the paper by Ling et al. (2009), where slopes made of sand-clay mixtures were subjected to rainfall and post-failure deformations were analysed to estimate the failure threshold for rainfall characteristics, while no monitoring attempt was made on pore water pressure evolution. The pore pressure data is critical for developing links between failure mechanisms and underlying hydro-mechanical processes. The grain-size distribution plays an important role in determining the initial state and intrinsic properties of the slopes and can therefore influence the mechanisms of failure and rainfall infiltration.

The climatic chamber used for centrifuge tests is a plane-strain rigid container with a transparent Perspex window that allows acquisition of digital images of the sub-surface soil. A monochrome CCD camera (Allied Vision Prosilica GC2450) was placed in front of the Perspex window to take images (up to 15 frames per second), used to measure soil deformations using Particle Image Velocimetry (PIV) techniques. Rainfall is simulated by the flow of water at a pressure of 600 kPa through misting spray nozzles at the end of vertical aluminium hollow rods (Figure 2.59b) attached to the under-side of the container lid. The droplets have a mean diameter of 30 µm and the soil surface was covered with a 30 µm woven mesh to prevent erosion. The water for rainfall is supplied from outside the centrifuge through a 4-channel hydraulic slip ring; the flow is controlled and measured using a solenoid valve and flowmeter, respectively (Figure 2.59c). The vertical distance from the tip of the nozzles to the surface of the soil is between 70 and 100 mm to minimise the Coriolis effect and the erosion of the soil surface due to droplet impact pressure (Matziaris et al., 2015). The groundwater level is controlled using standpipes that allow drainage of water at specific elevations above the container base. Two water reservoirs made of perforated aluminium plates covered with woven mesh sheets allow the flow of water from inside the container to the standpipes. To monitor the subsurface pore water pressure during testing, two types of miniature pore pressure transducers (PPTs) were used: Druck PDCR-81 transducers and SWT5 tensiometers. These instruments are capable of measuring both positive and negative pore water pressures. The PPTs need to be saturated prior to testing (Take and Bolton, 2003) to ensure readings are able to quickly respond to changes in pore pressure. The PPTs are first subjected to dry air to remove moisture within the porous stones, then a vacuum (-99 kPa) is applied for nearly 30 minutes. De-aired water is then introduced to the PPTs under a pressure of up to 80% of the

PPT capacity for at least 24 hours. Different components of the container and the rainfall simulation instruments are depicted in Figure 2.59.

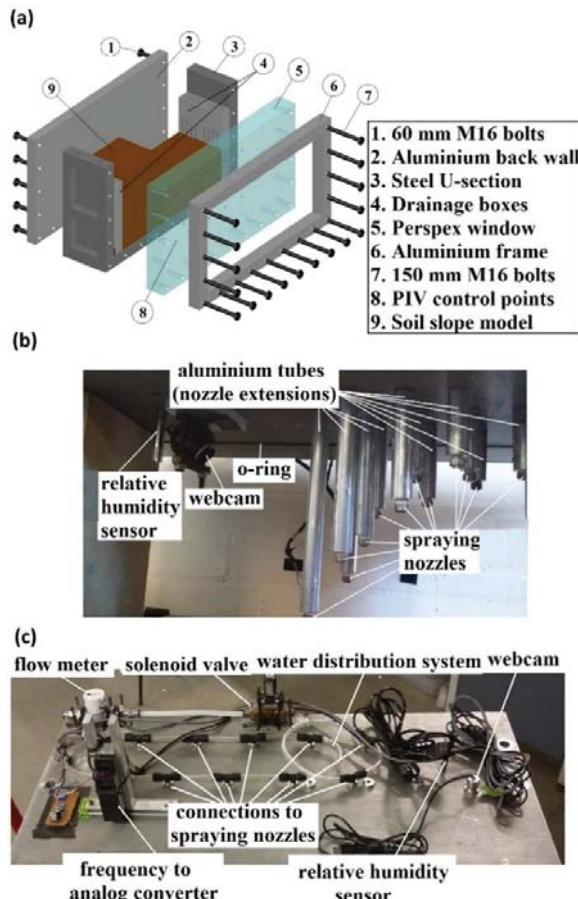


Figure 2.59: The centrifuge climatic chamber: (a) exploded-view of the plane-strain container (b) spraying nozzles and components inside the box (under container lid) (c) components on top of container lid, including the water distribution system, solenoid valve and flowmeter.

Three types of soils were used in this study: the first with 100% sand (Sa100), the second consisted of the same sand but with 10% silt added (Sa90Si10), and the third was the same silty sand used in the meso-scale models (Sa50Si45). Note that these soils do not completely represent the spoil materials, however this work focused on a more fundamental approach where the effect of sand, silt and clay contents are examined with the aim of eventually providing an understanding of how these affect slope stability in spoil heaps. All slopes were made at 50 degrees from horizontal. In order to study how different soil materials influence the results of centrifuge modelling, the soil types were tested under different rainfall intensities (low given by -L and high by -H) and at different compaction states. All tests were conducted at 60g (i.e. 60 times gravity).

Introducing rainfall to the model led to development of displacements in all models, due to the infiltration of water within the soil. In tests with pure sand, no failure mechanism was observed, whereas the Sa90Si10 silty sand exhibited failures under both low and high rainfall intensities; rainfall-induced displacements estimated from image analysis for these tests are presented in Figure 2.60. The main failure surface starts at the crest of the slope and continues to the mid height of the slope. These failures initiated at 1042 hr and 1.25 hr (prototype time) after the rainfall initiation in the low and high intensity rainfall tests, respectively. Analysis of the time-dependent displacements showed that the failure was sudden for high intensity while a more progressive failure was observed for lower intensity rainfall.

Unfortunately, pore water pressure readings were not obtained for all of the tests; only test Sa90Si10-H had reliable results. Figure 2.61 shows the PPT measurements during test SS-H. It can be seen that, prior to the onset of rainfall, suction (negative pore pressure) developed within the model at all locations, which is due to desaturation during the gravity increase to 60g. Upon rainfall initiation, pore pressure increased slowly at all points, with the first increase near the crest of the slope, indicating the rainfall infiltration and development of the wetting front. The advancement of the wetting front in the soil then leads to the increase in pore pressure at the other locations in order of their depth. The failure starts 1.25 sec after the onset of rainfall (1.25 hr in prototype time). As the rainfall continues, pore pressure increases, leading to positive pore pressures within the soil. However, PPT7 (the shallowest PPT, near the crest of the slope) indicated suction for the

whole period of rainfall, although the pore pressure approached a value of zero (nearly saturated) immediately before the rainfall was stopped.

In order to explain the differences between the results obtained for sand and silty sand, one may consider the effect of silt content on permeability and Darcy velocity. The conventional scaling law considering the macroscopic response of the soil under increased gravity deduces that the Darcy velocity ( $v_m$ ) in the N-g model is  $N$  times larger than that in the prototype (Taylor, 1994), where the flow path is considered to be  $N$  times larger in the prototype. However, according to Take et al. (2004), the underlying mechanism for static liquefaction of soil can be explained by the collapse of saturated voids which leads to a local and abrupt increase of the pore pressure, which in turn reduces the effective stress and strength of the soil, and consequently slope failure. Askarinejad et al. (2015) analysed the grain scale phenomenon of voids collapse and concluded that, if the structure of soil in an N-g model and prototype were the same, the scaling factor of length  $L$  at the grain scale is equal to one (i.e.  $L_p/L_m=1$ , subscripts p and m indicate prototype and model respectively). Thus, the scaling law for pore pressure dissipation time  $t$  in the model and the prototype can be written as follows:  $t_{dissipation,m} = L_m/v_m = L_p/(Nv_m)=t_{dissipation,p}/N$ .

In addition, Askarinejad et al. (2015) considered the collapse of the voids analogous to the free fall of particles, for which the time scaling law can be written as:  $t_{impact,m} = \sqrt{2L_m/a_m} = \sqrt{2L_p/(Na_p)} = \sqrt{1/N} t_{impact,p}$ , where  $a$  represents the acceleration, and  $L$  is the falling height. These relationships show that the pore water dissipation is  $\sqrt{N}$  times faster than the collapse of the voids, which may also be related to the grain-scale movements required to initiate failure along a slip-plane.

These scaling factors may be used to explain the differences between the types of soil used in this study. In case of sand, the pore water seepage is faster than the collapse of the voids and hence the time scale between the two coupled processes of dissipation and void collapse are incompatible. Thus, the pore pressure is dissipated before the void collapse occurs. In order to rectify this issue, Askarinejad et al. (2015) increased the viscosity of the pore fluid by a factor of  $\sqrt{N}$ . In this study, water is used as the pore fluid, but the use of silty sand provides models with a permeability ratio of 8.3 compared to the sandy models, nearly equal to  $\sqrt{N}=7.75$ . This suggests that adding 10% silt essentially reduces the permeability of the soil and is equivalent to the case where the fluid viscosity is increased by the same factor. In other words, if the viscosity of the fluid increases by a factor of 8.3 in case of sandy soil tests (Sa100-L and Sa100-H), failure is expected, similar to those observed in tests Sa90Si10-L and Sa90Si10-H. This may also explain why the test Sa90Si10-L with relative intensity of 1.71 led to slope failure whereas test Sa100-H with a higher relative intensity (2.44) did not result in a failure. In test Sa100-H, the pore pressure dissipation phenomenon is 7.75 times faster than that of a free falling particle, and hence the pore pressure dissipates before the void collapse can happen. On the other hand, in test Sa90Si10-L, pore pressure and void collapse have the same time scales which allow the test to properly simulate the prototype conditions. The presented interpretation and discussions, however, need further testing to validate the theoretical fundamentals discussed above, where pore pressure data are collected from a larger number of tests with enhanced spatial resolution.

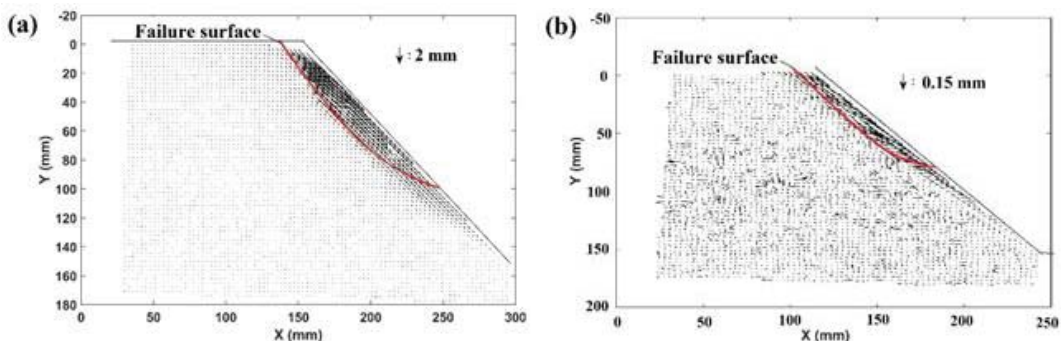


Figure 2.60: Rainfall-induced displacement vectors at failure initiation in (a) test Sa90Si10-Low intensity at  $t = 1042$  hr (b) test Sa90Si10-High intensity at  $t = 1.25$  hr (t is prototype time)

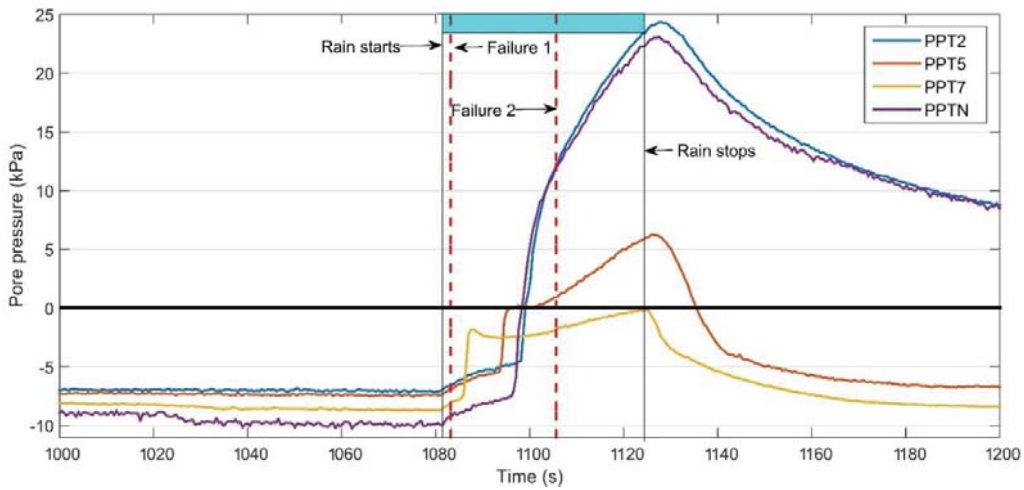


Figure 2.61: Pore water pressure measurement points for test SS-H

Several centrifuge tests were carried out on the Sa50Si45 soil, the same sandy silt used in the 1g physical model (obtained from Scrooby Top Quarries in the UK), which is representative of a spoil material. Two preliminary tests on loose dense sample proved problematic: the loose sample failed during centrifuge spin-up, whereas the densely compacted sample suffered problems related to surface erosion and clogging of the model drainage system. A range of improvements were made to the modelling equipment and procedures, however the issue of surface erosion of this type of soil during tests continued to hamper the ability to get reliable outcomes. The excessive impact force of the droplets on the surface is an ongoing modelling issue; this effect cannot be scaled properly on a higher gravity field experiment. To prevent erosion as much as possible, a metallic mesh was placed on the surface of the slope. However, the impact of the droplets on the mesh was still high enough to transfer their momentum to the soil. Erosion could be delayed but still occurred before complete infiltration of water in the soil. In the future, another solution for applying rainfall should be designed. Simulating rainfall only translates to applying a zero pore water pressure on the surface of the soil. Therefore, one suggestion would be to irrigate the surface instead of using nozzles for wetting the surface. Research is ongoing to design such an irrigation pattern and simulate rainfall without the negative effect of droplet impact.

**TASK 3.3: Numerical modelling of spoil heaps and reclaimed ground (UoN, UNEXE, SUBTERRA, GEOCONTROL)**

Each of the deterministic modelling exercises contained herein focused on the same case study from the Slatinice spoil dump located at Vrsany mine, Czech Republic. Geocontrol performed a stability analysis of an excavation profile by employing the software FLAC3D. UoN modelled the problem using an elasto-viscoplastic constitutive model. SUBTERRA developed a 3D model of the excavation (using the same sequence as Geocontrol) specifically analysing the variation of pore pressure distribution within the spoil material and the critical basement layer. UNEXE completed an analysis on the Slatinice spoil dump using two-dimensional Limit Equilibrium and Finite Element Method. In addition to the above, and driven by the outcomes of the project in terms of the evaluation of the characteristics and spatial variation of dump materials, an additional numerical modelling exercise was conducted by UoN in which stability was assessed using multivariate random fields.

The Slatinice spoil dump represents a challenge considering that the spoil heap is currently registering movements, in spite of the fact that its surface is not steep. There is potential for future re-exploitation of the dump and a previous historical event of significant instability make it an example worthy of study in terms of its long-term behaviour. GEOCONTROL first conducted an analysis of current movements of the spoil material focusing on the profiles A, B and C, shown in Figure 2.62. The rock strata, over which the dump is formed, has a long underground slope along the eastern part (area circled in Figure 2.62), rising up to the adjacent hill on the north-east region.

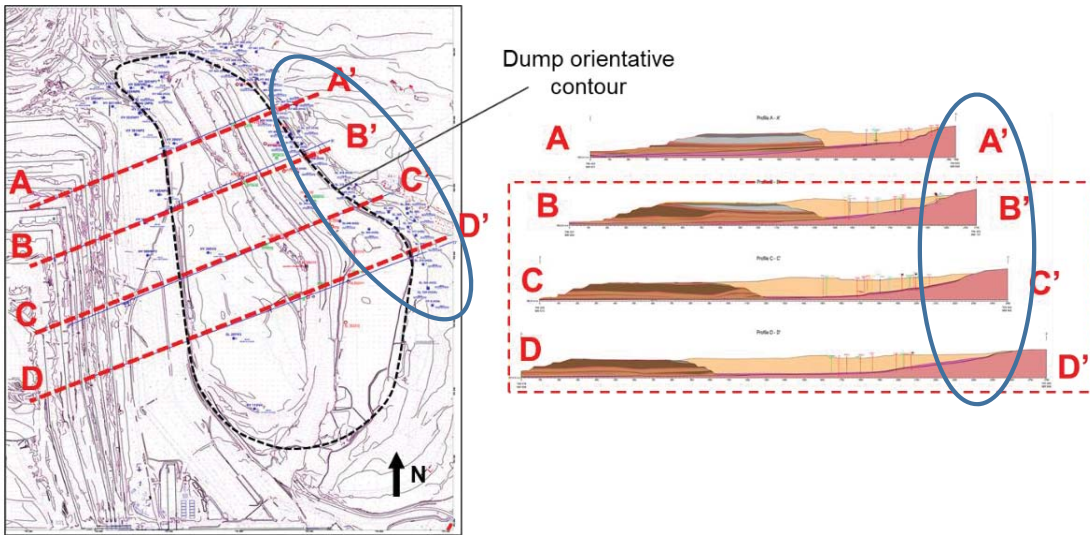


Figure 2.62: Geological profiles for the spoil dump analysis.

Some of the inclinometers showed a distributed deformation along the vertical direction of the spoil, decreasing with deepness. This could be due to a general deformation process of the material, possibly due to a consolidation process of the dump material resting on this rock slope, whose displacements would be directed towards the central and more stable parts of the dump. On the other hand, the second type of registered movements were localised displacements on points of the inclinometers which could cross potential slip surfaces.

In this example, with a steep rock base slope, various slip points were identified, with the conclusion that there was a clear localised instability at the contact layer of the bottom part of the spoil. This layer, which according to the geology is comprised of water-saturated clay, clearly represents a weak plane for the stability of the dump. Besides, displacements in this layer were higher than those located at lower deepness within the spoil material.

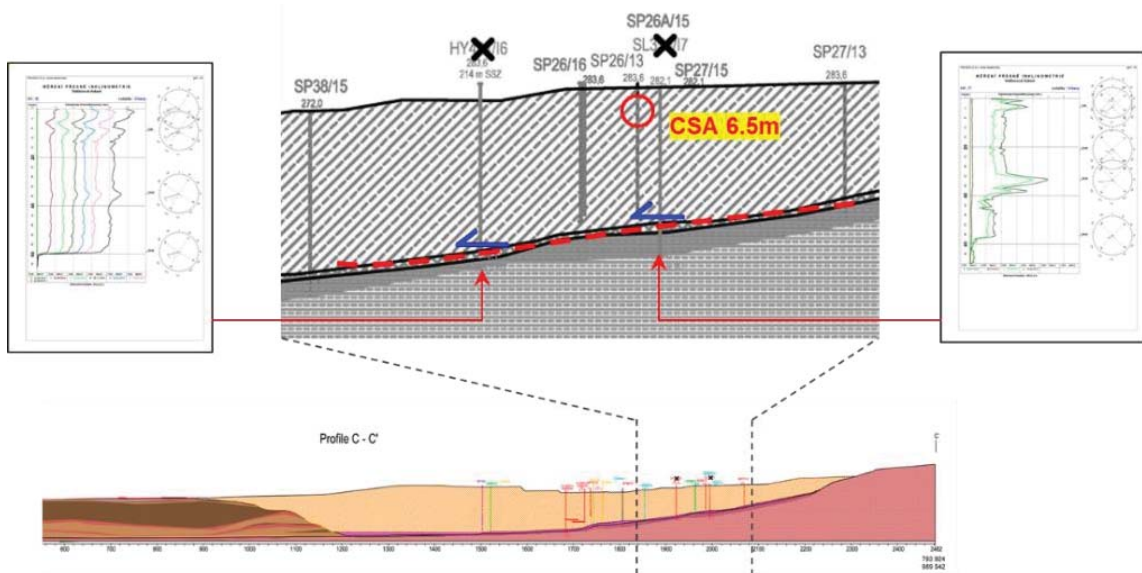


Figure 2.63: Localisation of displacements registered by inclinometers on section C-C'. Inclinometers and one of laboratory samples are marked in the figure.

For a better understanding of the case and prior to the tenso-deformational numerical modelling, GEOCONTROL also carried out a back analysis of 1983 landslide. Given the importance of the weak layer of the dump base, it could have played an important role in this landslide, which is the reason why it was decided to perform a Limit Equilibrium Analysis (LEA) of the historical event using Rocscience software application SLIDE. This analysis was carried out using Bishop simplified method, allowing slip surfaces to reach the weak layer. For the analysis, the geometry of the spoil in 1983 around the location of profile C-C' was chosen as representative due to its location in a central part of the mobilised area, as Figure 2.64 shows, where the marked area was the mobilised part of the spoil during the landslide, sliding towards south-west. In the cross section, the orange thin layer of the bottom represents the contact weak layer, a lighter orange is the spoil, brown colour represents the paleozoic bedrock and grey color represents the original unexploited

sedimentary material composed of interlocked layers of coal and claystones (not differentiated for the LEA model).

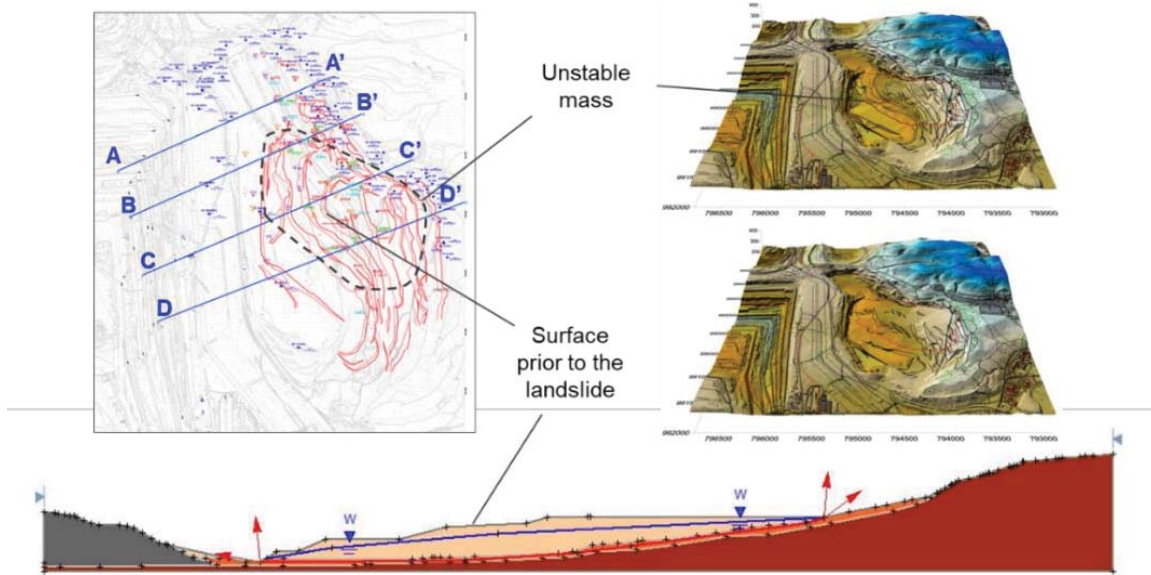


Figure 2.64: Analysis of 1983 landslide: geometry of the spoil surface prior to the landslide and displaced mass (top-left), 3D view of the landslide (top-right) and profile for the back-analysis.

Initial calculations run with SLIDE software obtained unexpectedly high values for the Factors of Safety along the section (above 2 for average scale regions), where it can be observed that the lowest FoS was 1.72. Based on these results, it was concluded that, for the geometry of the model, instability could not depend just on material properties calibration, thus leading to develop further work under the hypothesis that water conditions took a different configuration than initially expected.

According to water data, it was observed that there is a strong influence of the adjacent hill watershed on the expected water inflow in the dump base. This fact, together with the existence of the weak clay layer on the bottom and the main clayish content of the dump, could lead to the concentration of pore pressures above those expected from a hydrostatic water state. This point was also supported with reports from VUHU about cases where perforations up to the depth of the weak layer led to water springs even above terrain surface. Therefore, further analysis of 1983 landslide were carried by GEOCONTROL under the hypothesis of pore pressure concentration in the weak layer, using different approaches to represent it (pore pressure tables, specific phreatic levels for the water-saturated clay layer of the bottom, Ru method). It was finally decided to use an Ru coefficient for the back-analysis. This method simply models the pore pressure as a fraction of the vertical earth pressure for each slice, therefore leading to concentrations of pore pressure in deeper parts of the weak layer and null pressures for points in contact with the terrain surface, assumed representative of the potential pressure distribution for the dump base inflow. Values of the pore pressure leading to the initiation of the spoil instability were obtained by back-analysis and used for the later tenso-deformational models. This deep water content, being a potential response to water intake from the adjacent hill watershed, would be expected to depend on two phenomena: rainfall and snow melting on the watershed. Despite limited data available to assert this, GEOCONTROL examined annual registers from four piezometers located at the east part of the dump. Figure 2.65 shows the comparison between rainfall data and water tables evolution of these piezometers, from which some conclusions of interest can be extracted. First, it is observed that little variations are directly dependent on rainfall, except for piezometer (H22) whose levels rise fast after the four peaks of cumulative rainfall of the studied period (marked with red circles in the figure). Thus, it can be assumed that the water runoff coming from the hill watershed is less relevant for the variations of water content within the spoil material. On the other hand, all piezometers, show a clear trend of increasing water levels from the second half of February 2017. This sustained rise would probably be associated with a slow percolation process dependent on snow melting in the watershed, starting with the seasonal and temperature changes, with a delay depending on the hydrogeological conditions of the infiltration paths. Water table rises in this region within January and February have been mentioned before by Burda et al. (2011) and in January 2011 there was an important landslide reactivation in CSA mine active landslide, precisely due to a rapid snow melting (Burda et al., 2013). These cyclical water changes could directly compromise the stability of spoil dumps in the long term, defining season-dependent pore-pressure distributions.

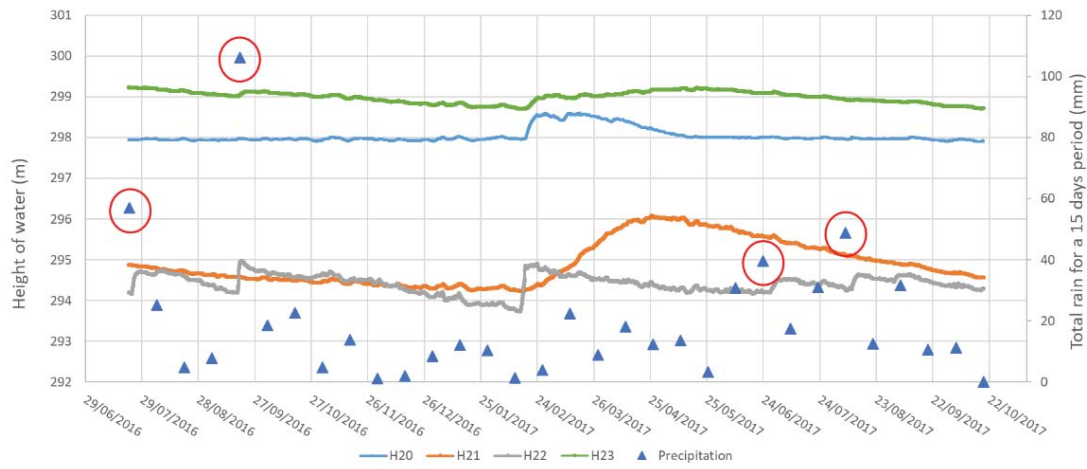


Figure 2.65: Cyclical changes of water content for the period between July 2016 and October 2017.

To continue with the research, a 2D numerical modelling simulation was performed using FLAC3D (Itasca) under plane strain conditions. The developed model has a length of 1700 metres and a height of 200 m, with approximately 13000 elements. Element meshing was achieved according to the octree partition system available in FLAC3D and also used by GEOCONTROL for WP2 numerical modelling. For the model development, there were considered as well the potential excavation stages for the future re-exploitation of the mine, in order to analyse the potential behaviour of the dump for the long term.

Regarding the water conditions of the dump, it was decided to study two different situations or hypothesis. The first one would consider a shallow water table and hydrostatic pore pressure distribution within both the spoil material, while the other case would be developed with a pore pressure concentration at the contact layer, according to previous back analysis. Eight excavation stages were considered and each of them was modelled until reaching stability and the evolution of strains and displacements was analysed. Once stabilized, a routine created by GEOCONTROL within the FISH programming language was used to calculate the Factor of Safety for potential failure mechanisms and slip surfaces. This routine identifies masses which could be mobilised after the reduction of mechanical properties of the materials, in a magnitude equal to the Factor of Safety associated.

Results for the hypothesis of the hydrostatic distribution of pore-pressure according to a shallow phreatic level showed the existence of a potential instability for the last two excavation stages, where a factor of safety of 1.1 was obtained for the final state of the slope (eighth stage). The possible initiation of higher scale failures can be observed in Figure 2.66, with shearing concentrated within the slope toe and two curved surfaces in the central part of the remaining spoil body.

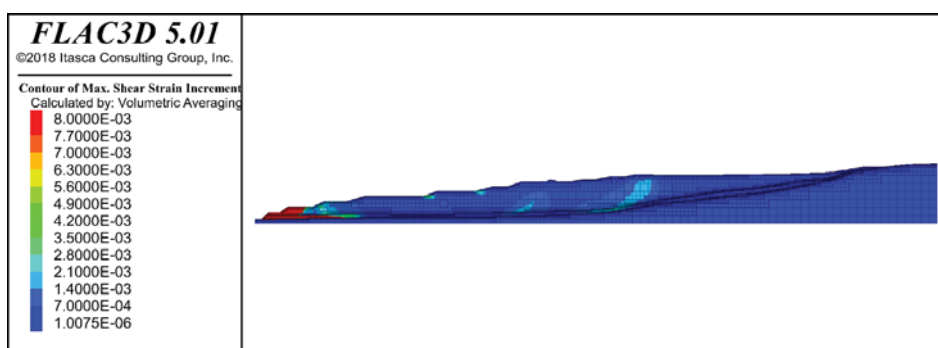


Figure 2.66: Shear strain plot for the shallow water table hypothesis.

However, results for the model with pore pressure concentration at the contact layer showed a significant progress of strains associated to the higher scale failures. Potentially unstable masses and their associated Factors of Safety for this second hypothesis are shown in Figure 2.67. In this case, two main bodies associated to low factors of safety could be identified: first, the toe failure already existing without pore-pressure concentrations (red area associated to a failure with  $FoS=1.05$ ) and, secondly, a deeper and higher scale failure initiated in the shearing region where the dump rock base changes its slope (orange mass associated to a failure with  $FoS=1.2$ ). Figure 2.68 shows the aforementioned concentration of shearing strain, coincident with the limit between the high scale potential failure shown in Figure 2.67 ( $FS=1.2$ ) and regions without failure for strength properties reductions above 2 ( $FS>2$ ).

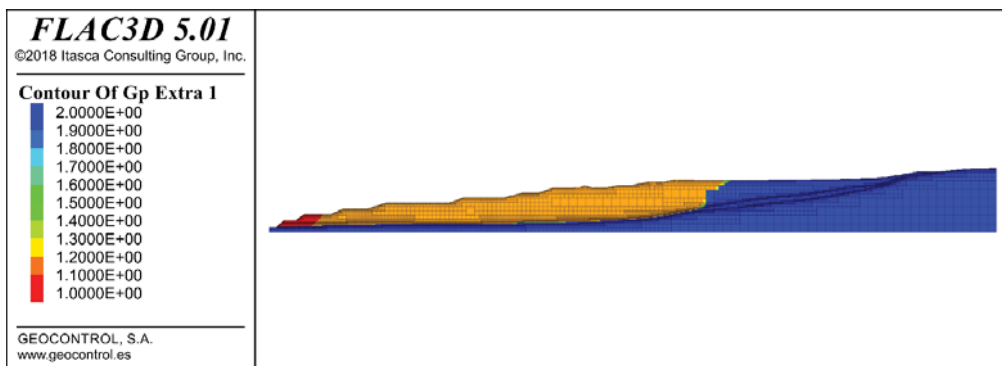


Figure 2.67: Potential sliding masses coloured based on their associated Factors of Safety, which represent the required strength reduction for the initiation of each instability mechanism (final state of Vrsany dump re-excavation under the pore-pressure concentration hypothesis).

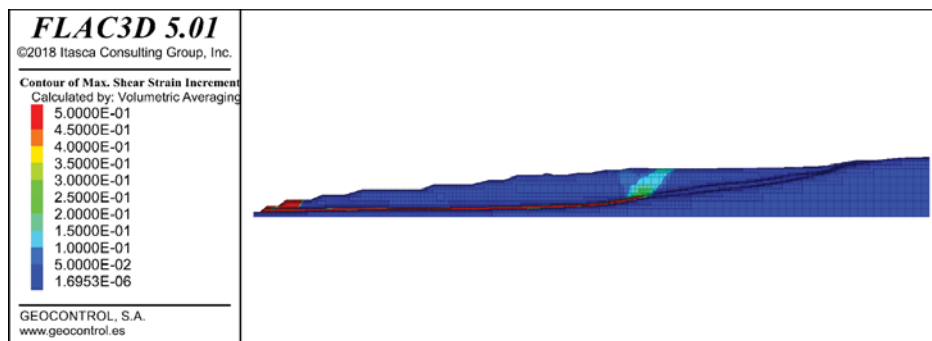


Figure 2.68: Failure mechanism associated to FoS calculation.

From these results, it is clear that the existence of pore pressure concentrations within the contact layer, dependent in seasonal water content changes, plays a leading role in the development of large scale failures of the dump. Monitoring of these pressures, as well as the use of mitigation strategies should be considered for cases similar to Vrsany spoil dump.

SUBTERRA worked in parallel to GEOCONTROL in the analysis of the inner dump of the Slatinice Mine. According to the proposed method, both 2D and 3D approaches were considered in order to conclude the reliability and calculation time/resources spent in each case. However, the initial premises were similar, by calibrating both material properties and pore pressure from the back-analysis of the former landslide that occurred back in 1983. The first step of the calibration process was based on reproducing the conditions (geometry, water content and material properties) of the former dump, as shown in Figure 2.69. The surface of the failure was reproduced with information provided by VUHU. This model allowed consideration of a reliable range for the properties of the water-saturated layer. As previously indicated, this area is strongly influenced by weather cycles; mostly during January and February. The snow melting process in the surrounding hills add an important water inflow which impacts on the pore pressure distribution and contributes to the saturation process of the contact layer.

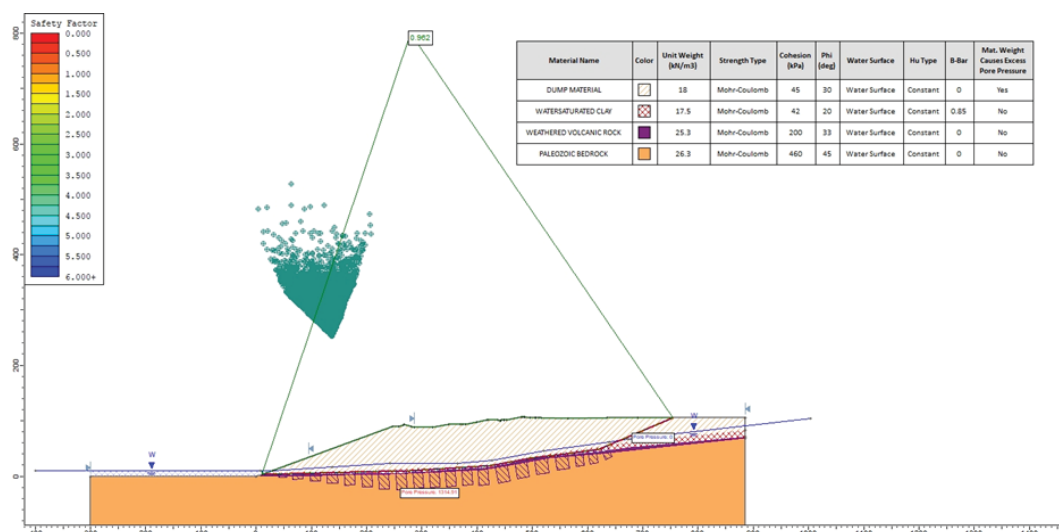


Figure 2.69: Calibration Model reaching a FOS of 0.962.

The most representative profile, as well as the excavation sequence, were then applied to the current geometry of the dump to be re-excavated. Several benches were considered, both in X and Y directions, in order to obtain a 3D analysis of the stability of the spoil during the excavation. The initial geometry of the model, as well as the main phases, are shown in the following figures. For the analysis, the two bottom benches were taken into account, which are the critical ones due to the proximity to the contact layer, as well as because of the inter-bench angle. During the excavation process, a comparison between dry conditions and a scenario where the water table was lowered by seepage pumping to the bottom of the spoil material was conducted. In the second scenario, the contact layer accumulates the pore pressure of the water column above it.

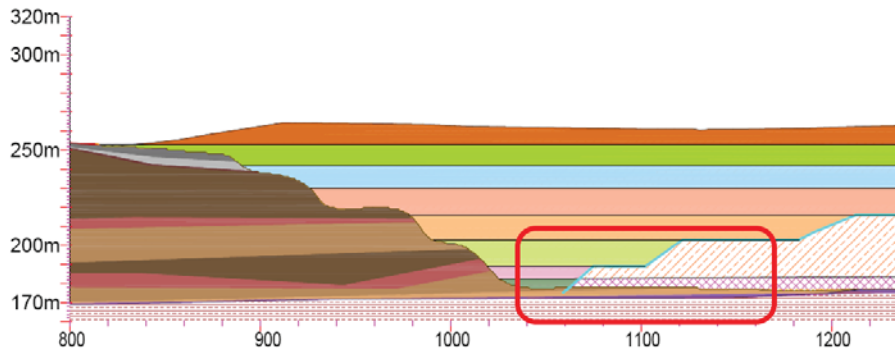


Figure 2.70: Detail of the phases for the excavation of the dump, and the selected area for FLAC3D analysis.

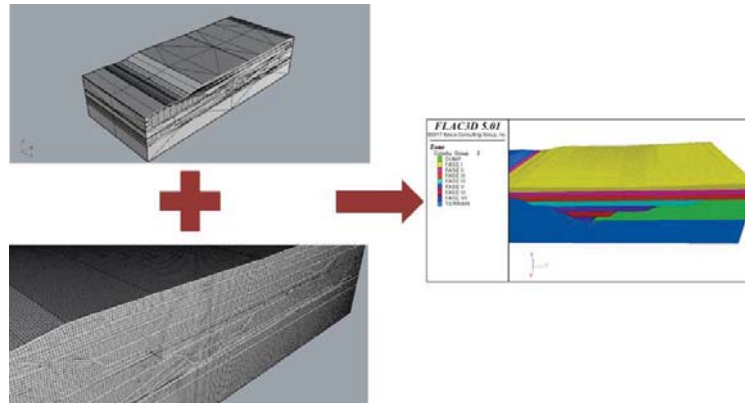


Figure 2.71: Meshing process employing Griddle-Rhinoceros

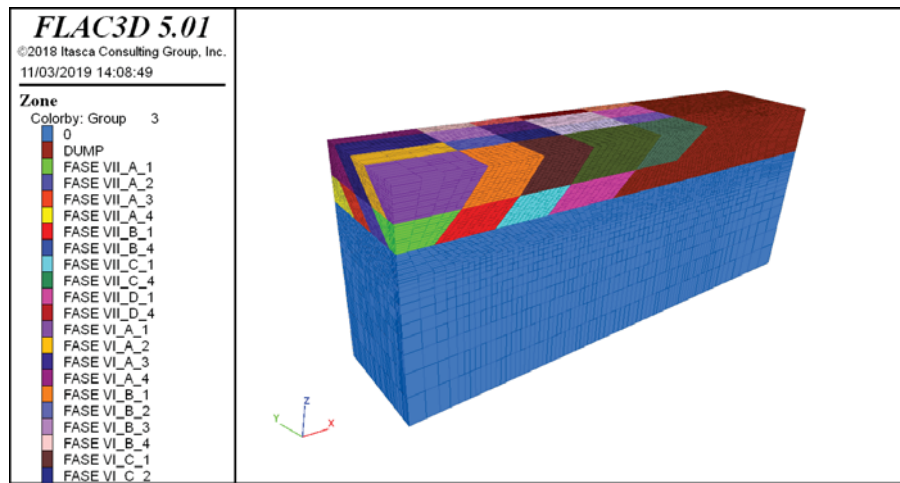


Figure 2.72: Multi-phase excavation for the analysis of the influence of the sequence in the slope stability.

Results obtained in dry conditions - Although it is known that the behaviour of the designed slopes will be influenced by the water inflow from the surrounding hill slopes (see above conclusions of the piezometer analysis), a comparison of the pore pressure state of the contact layer has provided clear conclusions. In order to assess to mine operators at Slatinice, the analysis was focused on displacements, pore pressure/water saturation and shear strain of the bottom benches to obtain an overall Factor of Safety.

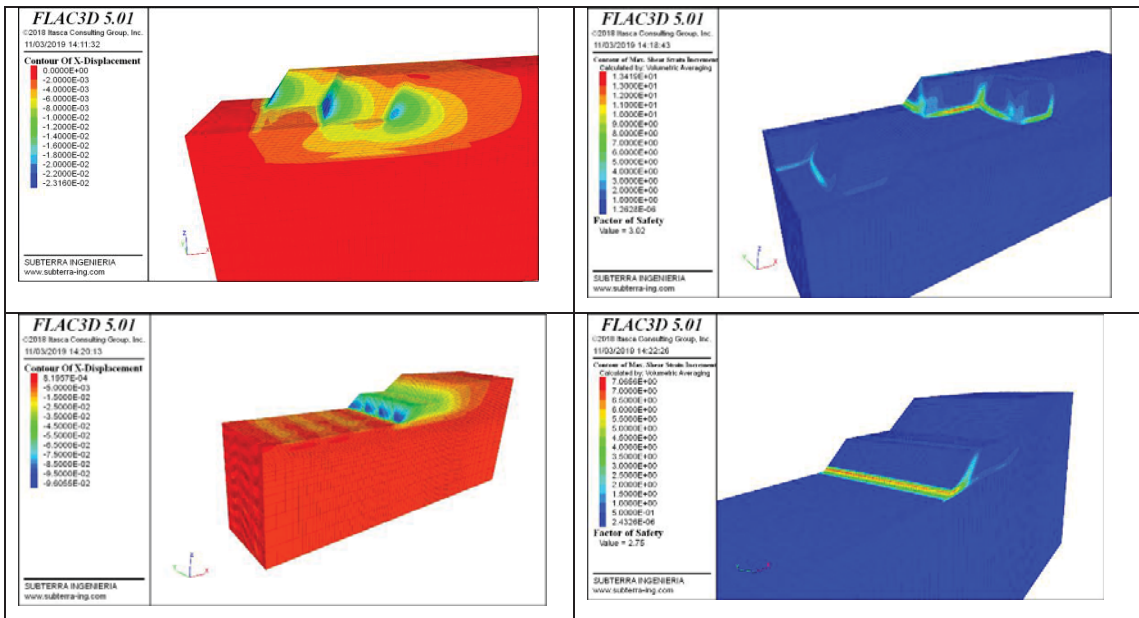


Figure 2.73: Left-side pictures show displacements during the phase excavations and final configuration, and right-side pictures shear strain contours in the same phases. Special attention must be paid to displacements in the toe of final benches for the accumulated volumetric shear strain increments.

Results obtained in saturated conditions - A first approach for the behaviour of the whole slope has been carried out, concerning the pore pressure evolution when lowering the water table as the excavation evolved. In order to check the global stability, the B-bar coefficient by Skempton was employed, having the advantage of considering pore pressure evolution with the burden discharge of the excavation process. Figure 2.74 illustrates the critical influence of the water inflow (from raining seasons or for contribution from hill slopes after snow melting) in the behaviour of the contact layer. B-bar values were calculated from the vertical load and pore pressure at every excavation stage. The focus was then placed on the bottom benches in order to estimate potential threshold values for the excavation control and monitoring.

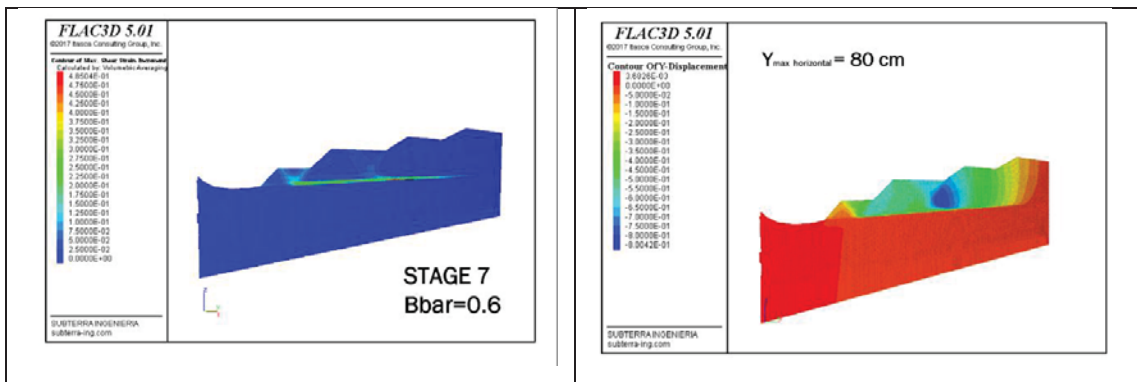


Figure 2.74: Left-side picture shows shear strength increment along the contact layer when Skempton B-bar coefficient reached 0.6. Right-side picture shows horizontal displacements.

Table 2.18: Results of the B-bar evolution simulation when excavating the inner dump

Excavation Stage	B-bar value applied to contact layer	Maximum displacement (cm)
5	0.4	19
6	0.4	54
7	0.4	68
5	0.6	41
6	0.6	79
7	0.6	80

In light of the above analyses, it was concluded that excess pore pressure in the weathered and saturated clay is a key factor for global stability for Slatinice Mine re-excavation. Even small values of B-bar over weathered and saturated clay could trigger global instability. A 30 % increment in B-bar value lead to a 15% increment of horizontal displacements. Recommendations for re-

excavation of Slatinice Mine are based on pore pressure and total cell pressure instrumentation, trying not to exceed  $B\text{-bar} > 0.75$ . By means of advanced modelling techniques, based on 2D back-analysis and 3D detailed calculation, it was possible to assess the influence of water changes in spoil stability. There is always uncertainty when characterizing these materials, and special attention should be paid to interbedded clayey layers and to the water inflow process. Monitoring activities should be driven to detect pore pressure evolution and horizontal displacements, especially at the final stages of the excavation.

Advanced numerical models offer the benefit of the potential to match more complex soil behaviour than more conventional (i.e. Mohr-Coulomb or Cam-Clay) models. Their use, however, has the drawback of the requirement for additional soil parameters, some of which can be difficult to obtain using standard field or laboratory test methods. UoN adopted the use of an advanced elasto-viscoplastic model that uses an improved iteration of the EVP-SANICLAY model in this project. The model uses a novel rotational-hardening (RH) law that guarantees the uniqueness of the critical state line, prevents excessive rotation of yield surface, and is sufficiently simple that it could be adopted for some practical applications. The elasto-viscoplastic anisotropic constitutive model was implemented in the commercial software PLAXIS.

A comparative study using the EVP-SANICLAY, Mohr-Coulomb, and Modified Cam-Clay constitutive models was undertaken using Plaxis 2D based on the Slatinice spoil dump. The geometry of the model is shown in Figure 2.75. The properties of the contact layer and coal seam layers are defined in Table 2.19. The dump material was simulated with three different models for comparison: Mohr Coulomb, Modified Cam-Clay and the EVP-SANICLAY model, with parameters provided in the following tables.

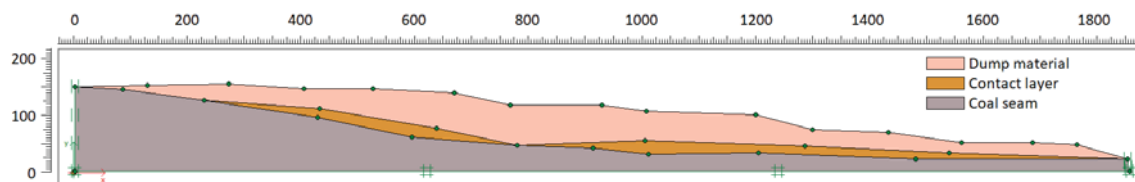


Figure 2.75: Model profile of the numerical analysis

Table 2.19: Model parameters for the contact layer and the coal seam

Contact layer	Cam-Clay Model
Unsaturated unit weight: $\gamma_{\text{unsat}}$	16.0 kN/m <sup>3</sup>
Saturated unit weight: $\gamma_{\text{sat}}$	18.5 kN/m <sup>3</sup>
Initial void ratio: $e_{\text{init}}$	0.5
Compression index: $\lambda$	0.36
Swelling index: $K$	0.01
Poisson ratio: $v$	0.15
Slope of critical state line: $M$	1.09
Coal seam	Linear Elastic Model
Unsaturated unit weight: $\gamma_{\text{unsat}}$	17.0 kN/m <sup>3</sup>
Saturated unit weight: $\gamma_{\text{sat}}$	21.0 kN/m <sup>3</sup>
Initial void ratio: $e_{\text{init}}$	0.5
Young Modulus: $E'$	17.73 MPa
Poisson ratio: $v'$	0.15

Table 2.20: Soil classification of the different layers

Percentage	< 2 µm	2 µm – 50 µm	50 µm – 2mm
Dump Material	70	13	17
Contact layer	10	13	77
Coal seam	10	13	77

Table 2.21: Mohr Coulomb parameters for the dump material

Unsaturated unit weight: $\gamma_{\text{unsat}}$	15.0 kN/m <sup>3</sup>
Saturated unit weight: $\gamma_{\text{sat}}$	18.0 kN/m <sup>3</sup>
Initial void ratio: $e_{\text{init}}$	1.0
Cohesion: $c'_{\text{ref}}$	15.0 kPa
Friction angle: $\phi'$	25.0°
Young Modulus: $E'$	18.26 MPa
Poisson ratio: $v$	0.15

Table 2.22: Cam-Clay parameters for the dump material

Unsaturated unit weight: $\gamma_{\text{unsat}}$	15.0 kN/m <sup>3</sup>
Saturated unit weight: $\gamma_{\text{sat}}$	18.0 kN/m <sup>3</sup>
Initial void ratio: $e_{\text{init}}$	1.0
Compression index, $\lambda$	0.40
Swelling index: $K$	0.01
Poisson ratio: $\nu$	0.15
M	1.00

Table 2.23: EVP-SANICLAY parameters for the dump material

Unsaturated specific weight: $\gamma_{\text{unsat}}$	15.0 kN/m <sup>3</sup>
Saturated specific weight: $\gamma_{\text{sat}}$	18.0 kN/m <sup>3</sup>
Initial void ratio: $e_{\text{init}}$	1.0
Poisson ratio: $\nu$	0.20
Swelling index: $K$	0.01
Compression index, $\lambda$	0.40
Critical state constants: $M_c, M_e$	1.07
Over consolidation ratio: OCR	2.00
Destructuration viscosity term: N	2.00
Destructuration viscosity term: $\gamma$	2x10-8
Rotational hardening parameter: $a_0$	0.02
Rotational hardening parameter: C	12
Rotational hardening parameter: X	1
Structuration factors: $S_{l0}, S_{f0}$	1
Destructuration factors: $k_l, k_f$	1
Destructuration factor: A	0.5
Step size	1

Some results from the analyses are demonstrated in Figure 2.76. The results demonstrate some important differences between the Mohr-Coulomb, Modified Cam-Clay, and EVP-SANICLAY models. The location of the predicted ground movements in the EVP-SANICLAY model is quite different to that from the Mohr-Coulomb model, but similar to the Modified Cam-Clay model (though magnitudes are considerably different).

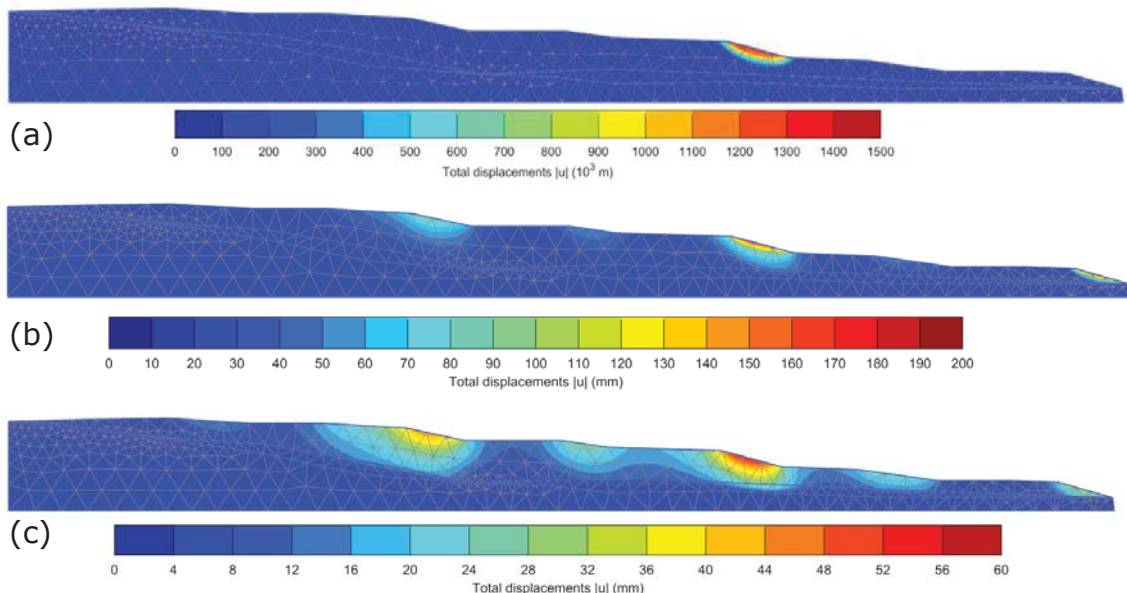


Figure 2.76: Total displacement field for (a) Mohr-coulomb, (b) Modified Cam-Clay, and (c) EVP-SANICLAY models

In addition to the above work, due to the observed variability of the spoil material, an additional numerical modelling exercise was conducted by UoN in which stability was assessed using multivariate random fields. Soils are variable over space and their variability must be considered for numerical models to realistically represent the actual conditions. Despite the relatively large number of studies on rainfall-induced slope instabilities in partially-saturated soils, only few studies have considered the spatial variability of geotechnical properties. The present study considers four dependent random variables of void ratio, dry unit weight, cohesion, and friction angle which are cross-correlated using a multivariate Gaussian copula. The spatial correlation of random variables is based on a Gaussian auto-correlation function. The numerical model used here is a fully coupled

transient hydro-elasto-plastic model constructed in Abaqus, where saturated permeability is related to the random field of void ratio through the Kozney equation.

The first step in generating the conditional random field is to identify the dependence structure of multiple properties as observed in the field. This enable a rigorous characterisation of the cross-correlation among multiple geotechnical properties. A dataset from Soenksen et al. (2003) was used to estimate the dependencies between four variables: cohesion, friction angle, dry density, and void ratio. Figure 2.77 shows the data points in red circles and the estimated probability distribution in blue.

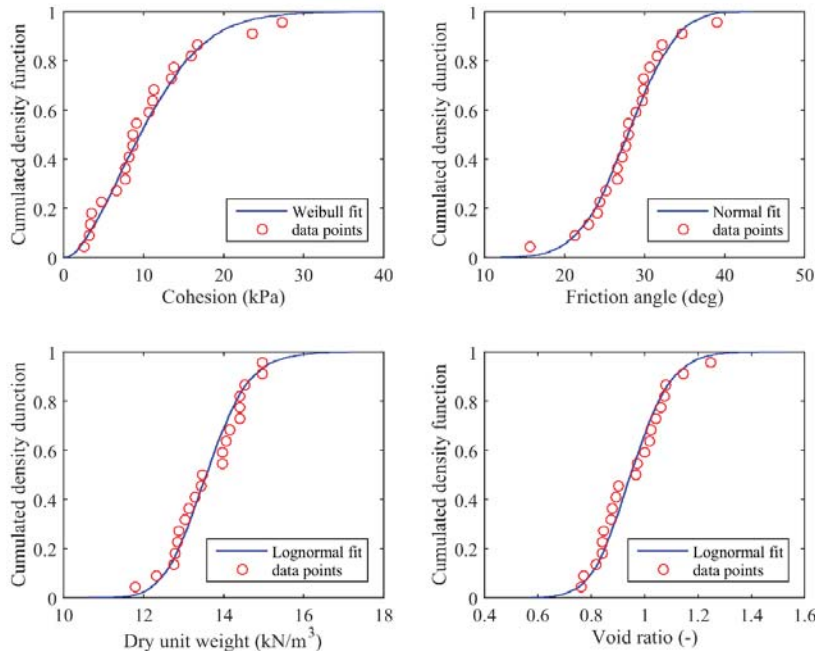


Figure 2.77: Marginal (one-dimensional) cumulative distribution functions of the dataset presented in Soenksen et al. (2003)

The second step is then to find the parameters for the corresponding 4-dimensional Gaussian copula using these fitted marginal distributions. Table 2.24 shows the result of the multivariate copula correlation matrix.

Table 2.24: Estimated multivariate copula correlation matrix for the dataset presented in Soenksen et al. (2003)

Variables	Cohesion	Friction angle	Dry unit weight	Void ratio
Cohesion	1	-0.3868	0.1692	-0.1592
Friction angle	-0.3868	1	0.2641	-0.2942
Dry unit weight	0.1692	0.2641	1	-0.9982
Void ratio	-0.1592	-0.2942	-0.9982	1

In order to construct a random field, the relationship between any two observations in the field needs to be considered through their separation distance and scales of fluctuation. There are several correlation structures, such as Gaussian. The product of this process is the multivariate cross-correlated random field for the four variables of cohesion, friction angle, dry unit weight, and void ratio. A typical set of random field realisation generated with this method is given in Figure 2.78. The set of random fields are then exported to Abaqus where the numerical simulation is carried out. 1,000 different random fields have been generated and simulated using Abaqus. Using MATLAB, an analysis of the most likely failure surface and its safety factor is carried out.

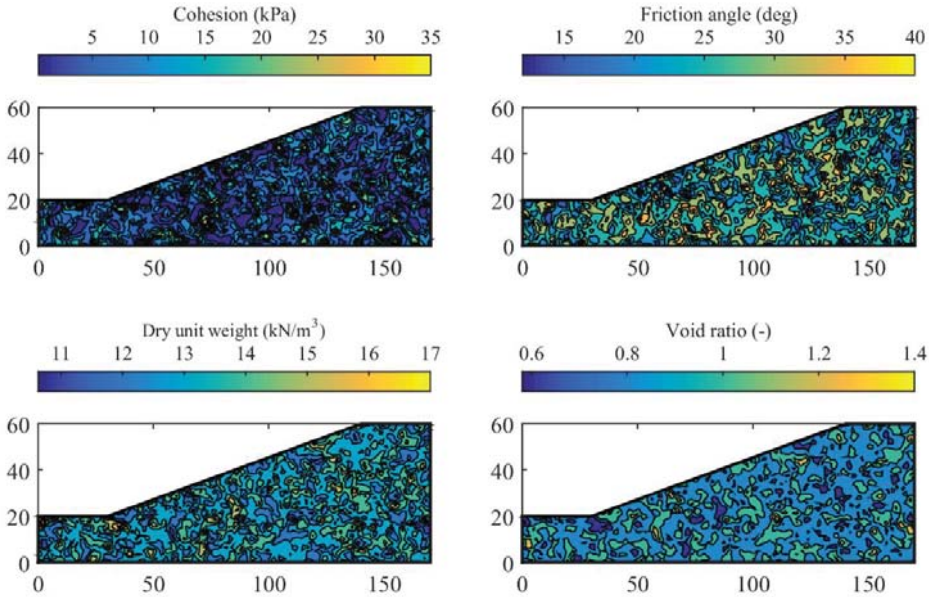


Figure 2.78: A typical set of random fields generated with multivariate copula and Gaussian auto-correlation function

Stress and strain matrices, pore pressure, and total displacement data is found using Abaqus. This data is collected and in MATLAB the minimum safety factor is calculated as follows. Each random field simulation is taken at a simulation time in multiples of 6 hours. For each of these time snapshots, an optimization problem is calculated to find the minimum safety factor. The safety factor for a path  $S$  is defined as:

$$F_S(S) = \frac{\int_S \tau_{max}(s) ds}{\int_S \tau(s) ds} \quad \text{Equation 2-1}$$

where

$$\tau_{max}(s) = c' + \sigma'_n(s) \tan \varphi' \quad \text{Equation 2-2}$$

where  $\tau$  is shear stress along surface  $s$ ,  $c'$  is cohesion intercept, and  $\varphi'$  is friction angle.

The stress  $\sigma$  matrix data collected from Abaqus is given by  $\sigma'_x$ ,  $\sigma'_y$  and  $\tau_{xy}$ . Therefore, a change of coordinate system must be considered using:

$$\sigma'_n(s) = \sigma'_x(s) \sin^2 \alpha(s) - 2\tau_{xy}(s) \sin \alpha(s) \cos \alpha(s) + \sigma'_y(s) \cos^2 \alpha(s) \quad \text{Equation 2-3}$$

$$\tau(s) = \sigma'_x(s) \sin \alpha(s) \cos \alpha(s) + \tau_{xy}(s)(\sin^2 \alpha(s) - \cos^2 \alpha(s)) - \sigma'_y(s) \sin \alpha(s) \cos \alpha(s) \quad \text{Equation 2-4}$$

where  $\alpha$  is the angle of the slip line at the position  $s$  in the slip line. The path  $S$  is first defined as a circle and optimised. Afterwards, 5 equally distributed points are taken from the circle and a spline is defined and optimised. Then, 9 points are optimised and then, finally, 17 points.

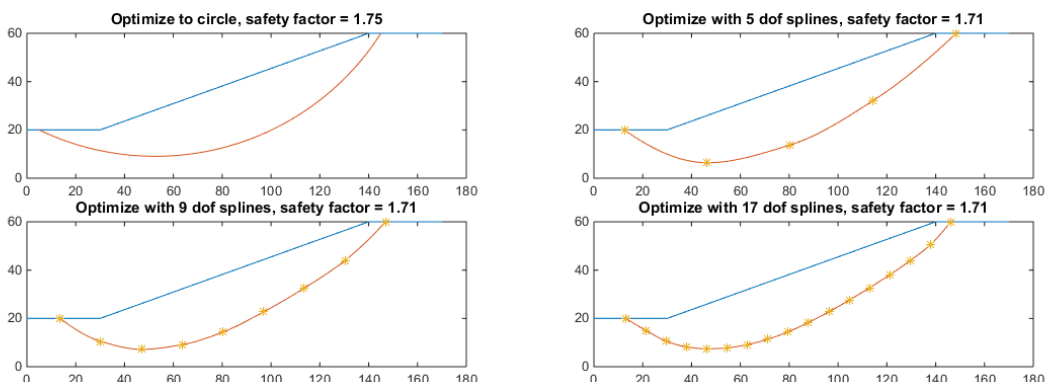


Figure 2.79: Safety factor optimization with a circle then 5, 9 and 17 points splines

After obtaining a 17-point spline as a slip line, the failure line is considered sufficiently accurate. The optimization is made via the pattern search algorithm. The homogeneous case is also

considered to understand the importance of heterogeneity. In the homogeneous case, the following parameters are taken:

Table 2.25: Variables taken for the homogeneous case

Variables	Cohesion (kPa)	Friction angle ( $^{\circ}$ )	Dry unit weight ( $\text{kN/m}^3$ )	Void ratio
Homogeneous case	10.43	27.80	13.57	0.947

Results are shown as a heat map in Figure 2.80. The slip lines are superimposed with the slip line of the homogeneous case. The homogeneous case gives a slip line smaller than most of the simulations, therefore showing the importance of considering heterogeneity. The heat map also shows a concentration of failure lines going until the crown of the slope. All failure lines start near the toe of the slope.

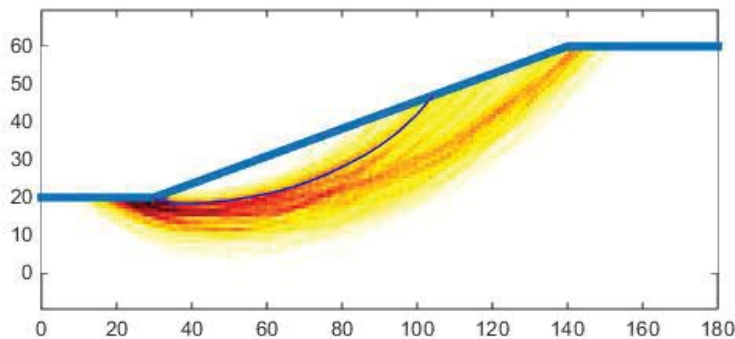


Figure 2.80: Heat map of slip line of all 1000 simulations, the homogeneous case is shown in blue

Figure 2.81a shows the decrease of safety factor during rainfall. The homogeneous case shows a slightly higher safety factor. It can also be seen that the safety factor decreases to 1 at different rainfall times. Those failure times range from 4 to 10 days rainfall whereas the homogeneous case tends to 1 at approximately 6 days. Figure 2.81b shows the histogram of the volume of failure for each simulation. The volume of failure of the homogeneous case is  $560\text{m}^2$ . More than 80% of the failure lines show a larger volume of failure than the homogeneous case.

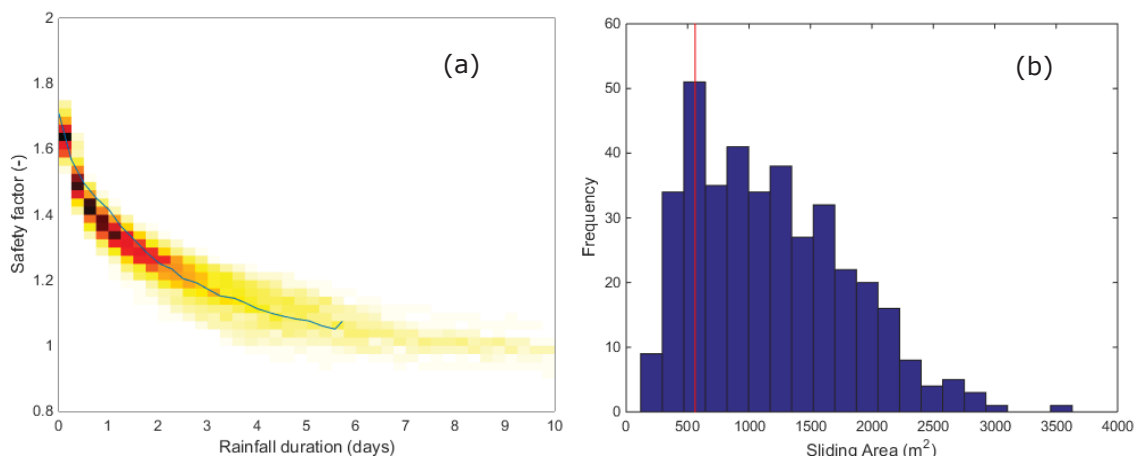


Figure 2.81: (a) Safety factors as a function of time with the homogeneous case shown in blue line; (b) volume of failure for all simulations, the red line shows the homogeneous case

The outcomes of the multivariate random field evaluation of rainfall induced slope stability is being used for the preparation of a journal paper under review within Computers and Geotechnics.

UNEXE produced a document as part of the D.3.3.1 and D.3.4.1 detailing the integration of numerical modelling of spoil heaps and reclaimed ground. The document included numerous numerical modelling simulation using Limit Equilibrium and Finite Element Methods of the Slatinice spoil dump in Vrsany mine (Czech Republic).

Deterministic and sensitivity LEM analyses - For this case study, given the variable nature of the dump material, the major source of uncertainty is associated with data input relating to the material properties (parameter uncertainty). The first step of the sensitivity analysis was to vary the parameters, focusing on the dump material, across a range of values, observing the effect on the final calculated FoS. Using this methodology, it is possible to determine which parameters have the most influence on the stability of the slope. For a sensitivity analysis in Slide7.0 it is necessary

to determine relative MINIMUM and relative MAXIMUM (distance from the mean value) values across which the analysis can be performed. This can also be expressed in terms of standard deviations away from the mean value. The values used in the sensitivity analysis for a preliminary evaluation, based on previous analyses performed on WP3, are shown in Table 2.26 (only values relative to the geological layers actually included in the model are reported).

Table 2.26: Sensitivity analysis: values for each geological formation (with indication of relative MINIMUM and MAXIMUM values for dump material)

Material	Property	Mean	Rel. Min.	Rel. Max
Dump material	Cohesion(kPa)	4	4	10
Dump material	Unit Weight(kN/m <sup>3</sup> )	17.5	3	3
Dump material	Phi(°)	22	7	7
Rock basement	Cohesion(kPa)	460	-	-
Rock basement	Unit Weight(kN/m <sup>3</sup> )	26	-	-
Rock basement	Phi(°)	45	-	-
Contact Layer	Cohesion(kPa)	35	-	-
Contact Layer	Unit Weight(kN/m <sup>3</sup> )	20	-	-
Contact Layer	Phi(°)	20	-	-
Volcanic rocks	Cohesion(kPa)	200	-	-
Volcanic rocks	Unit Weight(kN/m <sup>3</sup> )	25	-	-
Volcanic rocks	Phi(°)	33	-	-
2 Coal seam	Cohesion(kPa)	50	-	-
2 Coal seam	Unit Weight(kN/m <sup>3</sup> )	15	-	-
2 Coal seam	Phi(°)	25	-	-
4 Coal seam	Cohesion(kPa)	50	-	-
4 Coal seam	Unit Weight(kN/m <sup>3</sup> )	15	-	-
4 Coal seam	Phi(°)	25	-	-
Coaly clays	Cohesion(kPa)	50	-	-
Coaly clays	Unit Weight(kN/m <sup>3</sup> )	17.5	-	-
Coaly clays	Phi(°)	30	-	-

The water table was also initially considered in the deterministic analysis, results of which (mean values) and associated sensitivity analysis are provided in Figure 2.82.

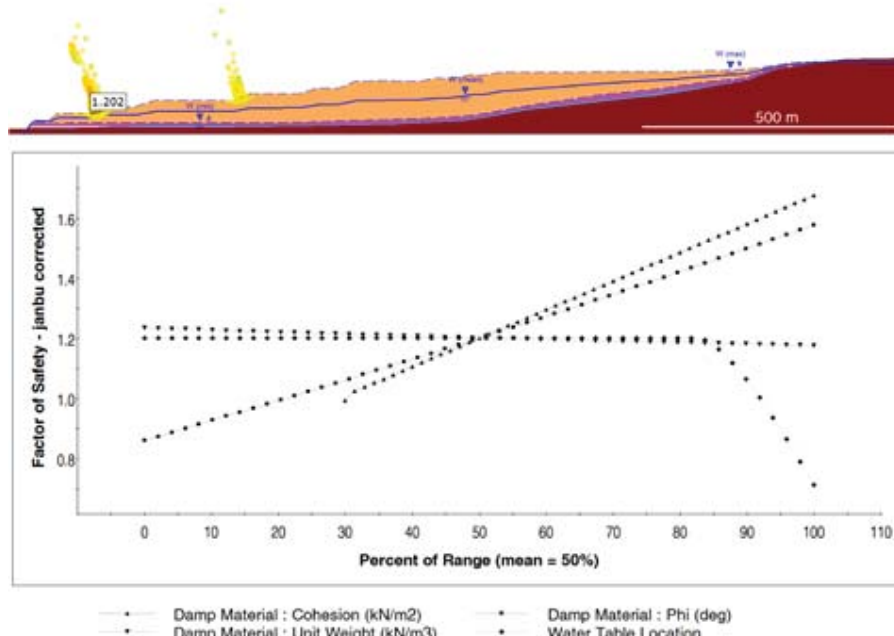


Figure 2.82: Slide7.0 LEM deterministic stability analysis results with indication of mean FoS (above) and LEM sensitivity analysis results (below). Only failure surface with FoS lower than 2 shown.

As observed in Figure 2.82, the detected failure surfaces (only surfaces with FoS lower than 2 are shown) are connected to local possible instability at bench scale, while the overall slope appears to be stable (i.e. there is no evidence of deep failure surfaces). According to the stability analysis results, the parameters that showed the highest influence on the FoS are the friction angle and cohesion (FoS ranging from 0.85 to 1.6), while the unit weight does not seem to significantly affect results. In addition, it can be seen that the modelled water location has an important influence on the FoS results, that decrease with the water table approaching the ground surface.

Deterministic FEM analysis - In keeping with the previous study, the first FEM deterministic analyses were carried out using the same profile shown earlier, this time considering 5 different water table locations (a-dry condition; b-water table location 15 meters below ground surface level; c-water table location 10 meters below ground surface level; d- water table location 5 meters below ground surface level; e-water table location at ground surface level). For the critical Shear Reduction Factor (SRF – calculated with the SRT; in this work SRF and FoS are used as synonyms for convenience), the detected value is equal to 1 and it decreases down to 0.9 when the water table approaches the ground surface. In this case, the analyses showed development of shear strain values in correspondence of the hypothesized benches, similar to that observed from the LEM analysis. It is possible to note also that in the case of a fully saturated slope a higher number of benches is affected, developing higher values of shear strain.

Therefore, the critical SRF (critical area of maximum instability) refers to localized shear strain concentrations, without any evidence of a potential deeper failure surface. The FE software RS2 allows consideration of a search area to define the potential location of different SRF factor, excluding or including the search area from the calculations. In order to investigate the critical SRF at an overall slope scale an additional series of simulations were performed excluding the contribution of the "superficial" critical area previously identified. Utilizing this new configuration, the modelled critical SRF passes from 2.3 in dry conditions to 1.2 if the worst case scenario is considered (fully saturated slope). Nevertheless, even if SRF is always higher than 1, more analyses are necessary. In fact, given the uncertainty of the dump material involved in the analyses, a SRF of 1.2 may not be considered acceptable for safe design, and a more in depth study, with the use of probabilistic analyses is required.

Discussion - The approach adopted during the investigation utilized both LEM and FEM stability analyses for evaluation of possible landslide failure mechanisms in consequence of hypothesized excavation activities in dump material on an open pit lignite mine. The approach reduces uncertainty by using sensitivity and probabilistic analyses in order to identify the critical factors that influence the results of analyses. The LEM results have then been compared with FEM analyses results.

The initial sensitivity analyses based on LEM indicated that friction angle and cohesion of the dump material have an influence on the stability analysis results, in addition to the influence of water level. Results indicate that possible instability is connected to critical failure surfaces at a bench scale, while the overall slope appears to be stable (with  $FoS > 2$ ). The mean detected FoS is equal to 1.2, but a decreasing of friction angle and/or cohesion decreases it down below 1. In addition, it should be noted that the effect of water is significant when it approaches the ground surface. This is a consequence from that the benches are characterized, according to Slide7.0 results, by a low FoS in dry conditions, and when the water level intersects the failure surfaces identified by the software the FoS drops down below 1. However, critical deep failure surfaces at an overall slope scale does not develop even in the worst case scenario, with the water table intersecting the ground surface. After LEM analyses, more complex deterministic FEM analyses were carried out. Results indicated lower FoS ( $<= 1$ ) compared to LEM analyses, with shear strain concentrations localized in correspondence of the hypothesized benches, without evidences of deep failure surfaces. In order to investigate this aspect, a new series of deterministic FEM analyses was conducted focusing on deeper instability. Results indicated a minimum SRF of 1.2 if a fully saturated slope is considered, while SRF is higher than 2 for all the other water conditions. Therefore, results of the deterministic overall slope analyses show a stable slope, with low values of shear strain that affects the whole material thickness, and increases from condition (a) (dry slope) to condition (e) (fully saturated slope).

In summary, the most critical condition of the slope is related to the superficial instability involving local benches. According to the results of the analyses (both LEM and FEM), instability occurs even in dry conditions, but a higher number of unstable benches are detected if the slope is considered fully saturated (1 in dry condition, 5 in wet conditions). This is due to the fact that the presence of water decreases the strength properties of the material and in the case of abundant precipitations (rainfall) and snow melting during spring time, if the slope become saturated, the critical bench angle may significantly decrease and instability occur.

#### TASK 3.4: Probabilistic analysis of reliability-based evaluation of risks (CERTH, UNEXE)

The developed methodology of local and global slope reliability for excavations (open pits), is implemented herein for the case of spoil dumps. The reliability methodology developed by CERTH was presented in detail in Deliverable D.2.2.1: Results of numerical modelling related to rock-face slopes. Sequential bottom-up construction of a typical 6m-height dump is represented through an incremental finite element numerical model by PLAXIS 2D software (Plaxis b.v., 2018). Slope inclination raises to  $45^\circ$ . Dump's construction is simulated through the successive placement of six distinct layers of spoil material of one meter each, as shown in Figure 2.83.

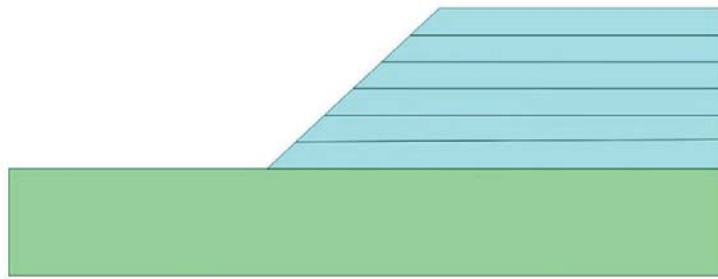


Figure 2.83: Spoil dumps incremental construction numerical simulation

The dump is placed upon an elastic bedrock material, assuming that foundation influence on the stability of the spoil dump is insignificant. As a result, the developing failure mechanisms are not allowed to propagate into the dump foundation, and are solely limited into the spoil dump's mass. Geotechnical properties of the elastic – perfectly plastic spoil material, and the elastic bedrock material are shown in Table 2.27.

Table 2.27: Bedrock and spoil geotechnical parameters

	Drained elastic modulus , E' (kPa)	drained Poisson's ratio, v' (-)	Unit weight, γ (KN/m <sup>3</sup> )	Cohesion intercept, c' (KPa)	Friction angle, φ' (°)
Bedrock	500,000	0.3	24	-	-
Spoil	15,000	0.3	20	20	25

Since in this study the reliability of the spoil dump will be considered in terms of stability, only the shear strength parameters of the spoil material will be treated as random variables of assumed variation. Statistics of the effective shear strength parameters  $c'$  and  $\varphi'$ , expressed in terms of mean value  $E$ , standard deviation  $\sigma$ , and coefficient of variation COV, are given in Table 2.28.

Table 2.28: Shear strength parameters statistics

	Mean, E	Standard Deviation, σ	coefficient of variation, COV
Cohesion $c'$ (KPa)	20	4	0.2
Friction angle $\varphi'$ (°)	25	5	0.2

Merging probabilistic analysis with the above slope stability numerical model, the imminent variation in the calculation of local safety factors is determined, and its distribution upon the slope's slip surface is shown in Figure 2.84. Variation of computed local slope safety factors ranges between the extremes of 16.1% at the third point, and 18.0% at the tenth point (from the slope's toe to crest along the assumed slip surface). The variation values regarding the calculation of local slope safety factors are consistent with the statement of Meyerhof (1970) that conventional safety factors' variability in stability analysis of earthwork engineering projects lies around COV values of 10% and 30%.

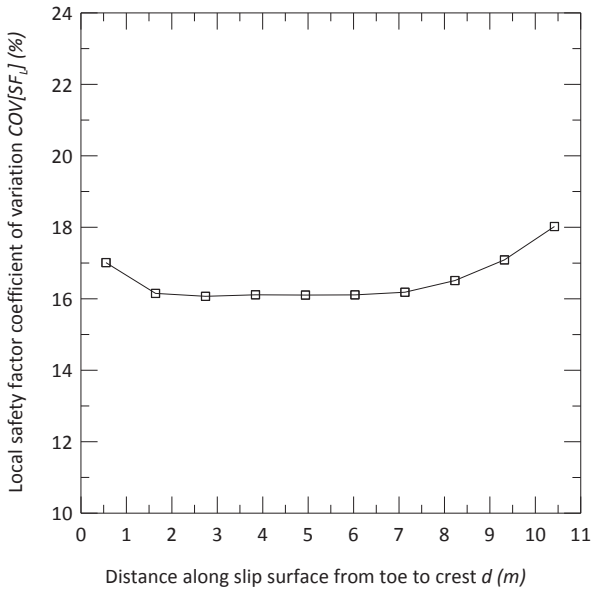


Figure 2.84: Local slope's safety factor variation along slip surface

By means of local safety factors' statistics, and in particular, the first two statistical moments of the mean value and the coefficient of variation, local probabilities of failure along the slope slip surface are evaluated and shown in Figure 2.85. Local probabilities of failure remain relatively constant for half of the slip surface. A remarkable reduction of local failure probability is observed starting at the seventh point.

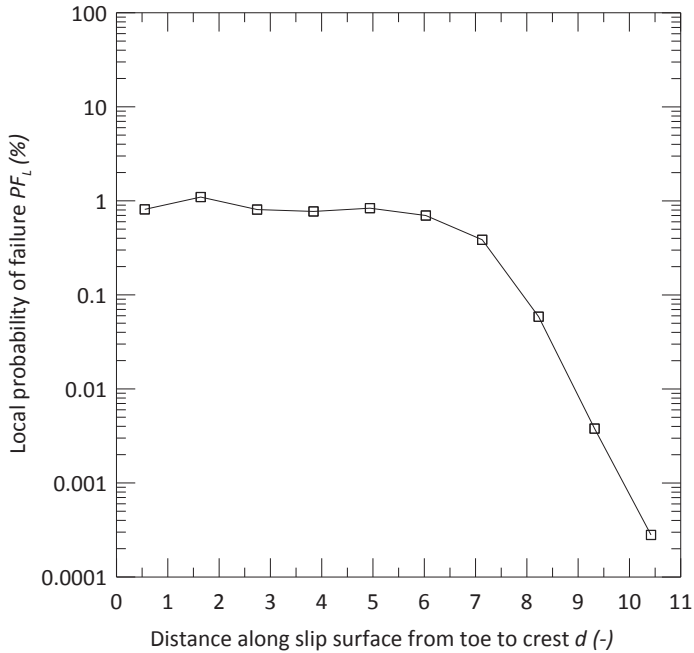


Figure 2.85: Local slope's safety factor probability of failure along slip surface

Regarding the global aspect of the problem, statistics of global slope safety factor  $\text{SF}_G$ , and global failure probability  $\text{PF}_G$  are given in Table 2.29. For comparison purposes, relevant results concerning a cut slope with exactly the same geometrical and geotechnical parameters are also tabulated.

Table 2.29: Global slope safety factor statistics and probabilities of failure

Slope type	Mean, $E [\text{SF}_G]$	Coefficient of Variation, $\text{COV} [\text{SF}_G]$	$\text{PF}_G$
Embankment slope	1.877	16.32%	0.210%
Cut slope	1.984	16.63%	0.143%

Concerning the global slope mean safety factor, and the global slope failure probability, the difference is noteworthy. This noticeable difference in the mean values of global slope safety factors, which in turn justifies the difference in the global failure probabilities, has to do with the

different construction method adopted for the two slopes under consideration. The global slope safety factors' variability has a smaller effect on the calculated global probabilities of failure. It would be normal for the cut slope to present a greater failure probability than the embankment slope, due to the larger uncertainty involved in the determination of relevant global safety factors ( $\text{COV}[\text{SF}_G]=16.63\%$  versus  $\text{COV}[\text{SF}_G]=16.32\%$ ). However, this fact does not occur due to the fairly greater value of the cut slope's mean global safety factor ( $E[\text{SF}_G]=1.984$  versus  $E[\text{SF}_G]=1.877$ ). Either subtle or noteworthy, difference in the probabilistic outcomes is mainly attributed to the different slope construction method assumed (excavation versus back-filling). These two different construction methods (possible to be simulated by a finite element numerical model) are yielding different stress states within the slope and upon its slip surface, leading to diverse safety factors and associated probabilities of failure.

The reliability methodology developed for the case of pit wall stability was herein applied for the case of spoil dumps. The primary benefits derived from this slope reliability methodology may be found in the following two issues: (1) in the capability of disclosing both local and global slope reliability levels; and (2) in the possibility for considering slope's construction method in the stability analysis. Finally, since the evaluation of safety factor levels is performed for slopes under operating conditions, the formers may be directly associated with corresponding deformation risk levels. Thus, the proposed methodology would be further extended in the future, for the establishment of a unified slope stability-performance reliability framework, considering jointly stresses and deformations within a slope, independently of the construction method followed.

UNEXE's aim in this task was to provide insight into material behaviour, predicting its long-term evolution, to be used within risk analysis. The analyses included the application of probabilistic methods set out in Task 2.1 and 2.2, which is essential in consideration of the complex heterogeneous nature of the spoil heaps material. In fact, understanding the impact of data uncertainty is a fundamental part of ensuring safe design of man-made excavations. Despite high levels of knowledge achievable from field investigations and experience, a natural geological environment is subjected to an intrinsic variability that may compromise the correct prediction of the system response to the perturbations caused by mining activity, with direct consequences on the stability and safety of the operations. To complement the work undertaken in Task 3.3, probabilistic analyses were undertaken on the same section of mine dump to evaluate their effect on the results. The key factors affecting system behaviour were identified with specific Limit Equilibrium sensitivity analyses, studied in further detail by Finite Element probabilistic analyses and the results compared. Such an approach aims to reduce system uncertainty and provide an improved understanding of the spoil dump material behaviour over time and in consequence of system perturbation.

Probabilistic LEM analysis - The sensitivity analyses (shown in Task 3.3) indicated that the most critical situation in this model is relative to local multiple failure surfaces in correspondence of the hypothesized new benches. Friction angle and cohesion of the dump material appears to affect the results significantly, as well as the water table location. Consequently, probabilistic stability analyses were carried out considering cohesion and friction angle variability (according to results of WP3) for four different water table locations (1-dry condition; 2-water table location 10 meters below ground surface level; 3-water table location 5 meters below ground surface level; 4-water table location at ground surface level). In a probabilistic analysis, it is possible to associate a statistical distribution to the model input parameters, accounting for the degree of uncertainty in the parameters values. In Slide7.0 input data samples are randomly generated, based on the user defined statistical distribution. This results in a distribution in the FoS from which probability of failure for the slope can be calculated. The default random sampling in Slide7.0 is the Latin Hypercube Sampling method (used for this analysis). With reference to the Slide7.0 user manual, the Latin Hypercube method is based upon "stratified" sampling, with random selection within each stratum. Typically, an analysis using 1000 samples obtained by the Latin hypercube technique will produce comparable results to an analysis of 5000 samples using Monte Carlo method. In this case the probabilistic analysis is focused on cohesion and friction angle of the dump material for different water content configurations. The material statistics, which reflect significant variability, are provided in Table 2.30. Results of the probabilistic analyses are given in Figure 2.86, where the critical failure surfaces are again located in correspondence of the hypothesized new benches.

Table 2.30: Statistical properties used in the probabilistic analysis for the dump material.

Property	Distribution	Mean	Std. Dev.	Rel. Min.	Rel. Max.
Friction angle $\phi'$ (°)	Normal	22	5.6	16.8	16.8
Cohesion (kPa)	Normal (truncated)	4	6.6	4	19.8

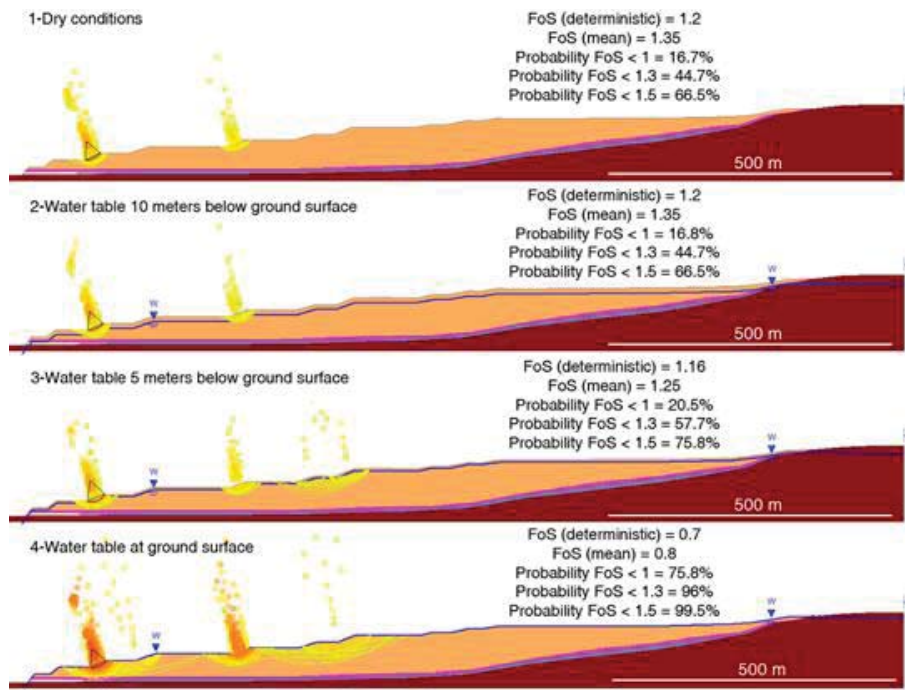


Figure 2.86: Results of Slide7.0 LEM probabilistic analyses performed for different water table locations (only failure surfaces with FoS < 2 are shown).

However, the results are similar for water configuration 1 (dry conditions) and 2 (water table 10 meters below water surface), with a probability of FoS < 1 of 16%, a probability of FoS < 1.3 of 45% and a probability of FoS < 1.5 of 66.5%. In addition, the water table has an effect on the results of the analyses when water configurations 3 and 4 are considered. Specifically, in water configuration 3 there is a probability of FoS < 1 of 20.5%, a probability of FoS < 1.3 of 57.7% and a probability of FoS < 1.5 of 77.8%. Considering the worst case scenario instead (water configuration 4) there is a probability of FoS < 1 of 75.8%, a probability of FoS < 1.3 of 96% and a probability of FoS < 1.5 of 99.5%. Figure 2.87 shows scatter plots where FoS values are plotted against dump material friction angle and cohesion for water configuration 1 and 4. In addition, FoS values less than 1 are highlighted. It should be noted that complex slope movements, with different deformation mechanisms, cannot be fully replicated and simulated with LEM analysis. This is because plastic deformation and degradation of material properties are not considered in such an analysis. Therefore, more complex numerical modeling analyses should be carried out to fully understand the implications of possible material deformation.

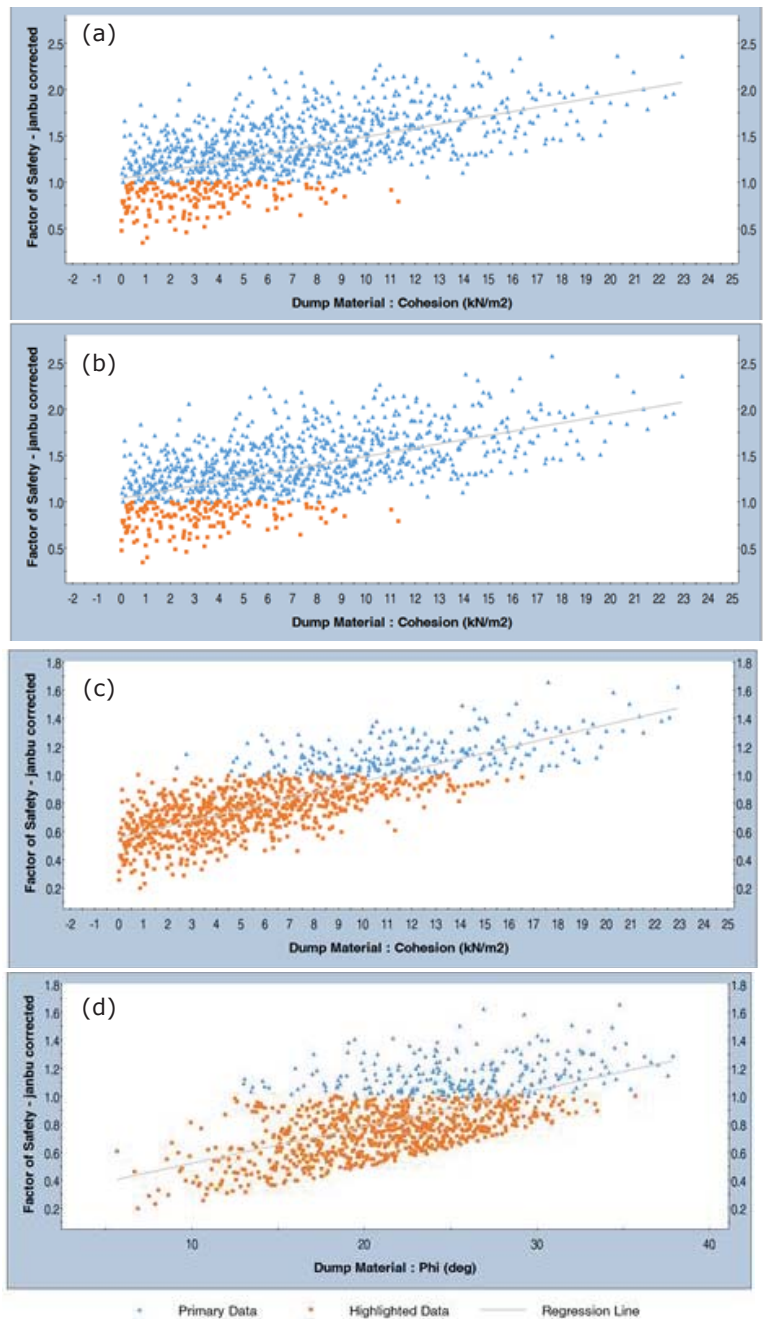


Figure 2.87: Scatter plot of FoS versus: (a) cohesion, water configuration (WC) 1; (b) friction angle, WC 1; (c) cohesion, WC 4, and (d) friction angle, WC 4.

Probabilistic FEM analysis - Following the previous considerations, probabilistic analyses were performed using the parameters shown in Table 2.31. Following the same logic as the previous probabilistic analyses, the random sampling method used was the Latin Hypercube, with 1000 samples. A normal distribution was also incorporated, and the Standard Deviation (SD) values chosen according to Task 3.1 and 3.2 results and following a conservative logic. The results of the probabilistic analysis refer to three different water conditions: a) dry slope, b) water table 15 meters below ground surface, and e) fully saturated slope (which are considered as the most representative for this study).

Table 2.31: Statistical properties used in the probabilistic analysis for dump material.

Property	Distribution	Mean	Std. Dev.	Rel. Min.	Rel. Max.
Peak friction angle (°)	Normal	22	5.6	16.8	16.8
Residual friction angle (°)	Normal	17	5.6	16.8	16.8
Cohesion peak (MPa)	Normal (truncated)	0.004	0.0066	0.004	0.0198
Cohesion residual (MPa)	Normal (truncated)	0.002	0.0066	0.002	0.0198
Young's Modulus (MPa)	Normal	80	15	45	45
Poisson's ratio	Normal	0.15	0.03	0.09	0.09

A low critical SRF, <1 was obtained for all the water conditions considered. In detail, condition (a) (dry slope) obtained a critical SRF of 0.9 with a probability of failure of 66.4% considering minimum FoS of 1, a probability of failure considering a minimum SRF of 1.3 of 98.5 % and a probability of failure considering a SRF of 1.5 as a minimum acceptable value for a safe design of 99.9 %. Condition (b) (water table 15 meters below ground surface) obtained a critical SRF of 0.9 with a probability of failure of 66.4% considering minimum FoS of 1, a probability of failure considering a minimum SRF of 1.3 of 92.2 % and a probability of failure considering a SRF of 1.5 as a minimum acceptable value for a safe design of 98.6 %. Finally, condition (e) (fully saturated slope) obtained a critical SRF of 0.8 with a probability of failure of 69.2% considering minimum FoS of 1, a probability of failure considering a minimum SRF of 1.3 of 95.2 % and a probability of failure considering a SRF of 1.5 as a minimum acceptable value for a safe design of 99.2 %.

The results are very similar for all the water conditions. This means that the hypothesized excavation may be unstable even in dry conditions. Nevertheless, it should be highlighted again that in case of a fully saturated slope, a higher number of benches are affected developing higher values of shear strain. In addition, similar to previous results, the observed critical SRF refers to superficial instability connected to the bench realizations, and investigation of possible deeper failure surfaces is needed. In order to investigate the critical SRF at an overall slope scale an additional series of simulations was performed excluding the contribution of the "superficial" critical area previously identified. Utilizing this configuration, the modelled critical SRF passes from 2.5 in dry conditions to 1.6 if the worst case scenario is considered (fully saturated slope). Probability of failures are very low for simulations in condition a and b, even considering a SRF of 1.5 as minimum acceptable condition. Higher values of probability of failures are detected when condition (e) (fully saturated slope) is applied; for example, the probability of  $SRF < 1.5$  is 41.4%. Therefore, results of the probabilistic overall slope analyses show again a stable slope, with low values of mobilized shear strain that interests the whole material thickness, and increases from condition a to condition (e).

Investigation on possible instability induced by deep pore pressure - The previous analyses revealed the possible influence of pore pressure in the spoil stability both at a bench and overall slope scale. Such indication is essential in a geological context characterized by high variability. Nevertheless, it should be noted that the dump material in this case is generally composed by a large content of fines. On the other hand, the contact layer at the base of the dump material is mainly composed of sand material and has been observed to contain water at pressure. This suggests that the dump material may behave as an aquitard/aquiclude in some part of the slope, even if the high heterogeneity of the material does not allow to draw precise conclusions. In order to investigate this scenario, a series of deterministic FEM analyses was carried out for evaluating the influence of a deep water pressure (affecting the contact layer) in the spoil heap stability in consequence of the hypothesized new excavation. The slope was therefore considered dry, and possible presence of critical pore pressure investigated by adopting the Ru method, which has been used for many years in slope stability analyses. With the Ru coefficient, pore pressure is simply modelled as a fraction of the vertical earth pressure. The vertical earth pressure is estimated from the unit weight and height of each material directly above a given point.

The first step was to perform a sensitivity analysis, using different Ru values, for identifying the critical pore pressure which may induce instability in the slope after the systems disturbance induced by the excavation. The analysis was carried out using the same properties of the previous simulations, with the same profile and excavation stages. In addition, a search area was again used for excluding the contribution of the "superficial" critical areas previously identified (benches) from the calculations, focusing on the overall slope stability, which may be directly affected by the deep pore pressure. The result of the analysis is shown in Figure 2.88, where SRF is plotted against the Ru coefficient adopted in each analysis. Results show a clear trend, indicating a decrease of the SRF if deep pore pressure is considered in the model. In particular, it can be observed that the SRF decreases from 2.3 to 1.5, if a Ru coefficient of 0.2 is used, and to 0.9, if a Ru coefficient of 0.3 is used. Such Ru values mean a theoretical maximum pore pressure respectively of 0.31 MPa and 0.46 MPa.

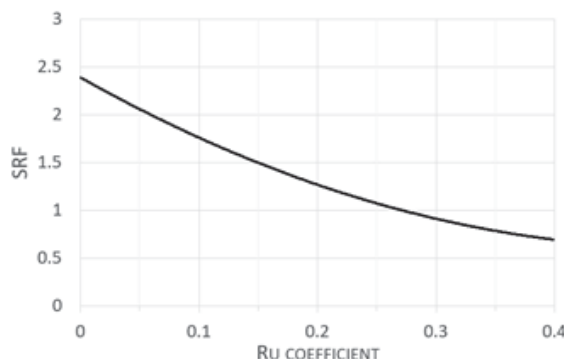


Figure 2.88: Sensitivity analysis of possible pore pressure in the Contact layer.

Following the same logic of previous analyses, the effect of uncertainty in the model has been again evaluated by performing two different probabilistic analyses. Since the critical pore pressure value is presumably included between 0.31 and 0.46 MPa, the probabilistic analysis was focused on the Ru 0.2 and 0.3 conditions. The statistical parameters used for the dump material are the same used in previous analyses, derived by previous tasks and deliverables. Nevertheless, this new analysis is also focused on the contact layer, which is lacking of specific variability analyses. Therefore, the values have been chosen by considering, without evidence for any other distribution, a normal distribution, with SD values estimated using  $\sigma = (\text{HCV}-\text{LCV})/6$ , where HCV is highest conceivable value of the random variable, and LCV is the lowest conceivable value of the random variable (Duncan 2000). Again, the random sampling method used was the Latin Hypercube, with 1000 samples. The contact layer statistics, which reflect significant variability, are provided in Table 2.32. Results showed that the modelled critical SRF passes from 1.55, when Ru coefficient of 0.2 is used (maximum theoretical pore pressure of 0.31 MPa), to 0.9, when Ru coefficient of 0.3 is considered (maximum theoretical pore pressure of 0.46 MPa). In detail, condition Ru 0.2 shows a critical SRF of 1.55 with a probability of failure of 12.8% considering minimum FoS of 1, a probability of failure considering a minimum SRF of 1.3 of 30.5 % and a probability of failure considering a SRF of 1.5 as a minimum acceptable value for a safe design of 46.2 %. Condition Ru 0.3 instead, shows a critical SRF of 0.92 with a probability of failure of 59.2% considering minimum FoS of 1, a probability of failure considering a minimum SRF of 1.3 of 87.5 % and a probability of failure considering a SRF of 1.5 as a minimum acceptable value for a safe design of 96.1 %. The results indicated that the hypothesized excavation may be unstable if a certain value of pore pressure in the contact layer are reached, with increased mobilization of shear strain that interests the whole material thickness.

Table 2.32: Statistical properties used in the probabilistic analysis for Contact layer.

Property	Distribution	Mean	Std. Dev.	Rel. Min.	Rel. Max.
Peak friction angle (°)	Normal	20	1.66	4.98	4.98
Residual friction angle (°)	Normal	10	1.66	4.98	4.98
Cohesion peak (MPa)	Normal	0.035	0.01	0.003	0.003
Cohesion residual (MPa)	Normal	0.01	0.003	0.009	0.009

Conclusions - Limit Equilibrium and Finite Element analyses (undertaken in Task 3.3 and 3.4) have been used to assess the effects of data uncertainty on a spoil heaps at a lignite operation in the Czech Republic. The case study provides valuable insight into the effects of geological parameters and model uncertainty. A sensitivity analysis was undertaken to understand the controlling influences of input parameters on model behaviour. The results highlight, as expected, that water table level and material input parameters have the greatest influence on stability of the slope. The potential for both deep-seated instability and superficial landsliding have been investigated. More detailed probabilistic analysis suggests that possible instability is connected to local bench failure, while there is a minor possibility for deep-seated instability in case of fully saturated slope. Nevertheless, if the presence of deep pore pressure affecting the contact layer at the base of the dump material is considered, possible instability may occur even in case of dry slope. However, such a hypothesis has to be validated with field monitoring data. In particular, the real pore pressure value should be evaluated with specific in situ tests.

The modelled results, using LEM and FEM, demonstrated good agreement. The investigation allowed improved understanding of the possible response of the dump material in consequence of a system disturbance caused by new excavation activity at the lignite open pit-mine site. The increased level of knowledge obtained through numerical modelling provides improved hazard assessment and data for mine planning purposes. The importance of performing sensitivity analyses with both Limit Equilibrium and Finite Elements approaches is highlighted within the analyses undertaken. Complementary use of both approaches is recommended for routine checks on model behaviour and associated results. The work highlights that sensitivity analyses should include both deterministic and probabilistic analyses, but an in situ monitoring system and site-specific analyses for the highlighted critical areas, with sample collections, are always fundamental to verify the results of the analyses in case of strongly heterogeneous materials with a high degree of uncertainty.



### **3 Conclusions**

#### **WP1 - Development and application of modern monitoring techniques for slope stability in open pit lignite mines**

WP1 included various activities aimed at acquiring photogrammetric and LiDAR data using UAVs and comparing results to survey data using terrestrial laser scanning, ground-based monitoring, and InSAR measurements. Results enabled the assessment of global and local slope stability features, which can be integrated into early warning systems. A comparative assessment of UAV cameras indicated that more cost-effective, lower resolution cameras could provide sufficiently accurate results (accuracy of less than 30 mm, ideally below 20 mm) if used with an appropriate layout (random placement) of ground control points.

A software application was developed that was able to process the UAV data and allowed identification of landslide scarp features. A methodology defined as Analytical Scarp Detection Model (ASDM) was developed and implemented through the software application.

New geotechnical data was obtained for the Belchatow mine and used within stability analyses. Data obtained from on-line inclinometer and pore pressure monitoring devices was made available for near real-time monitoring using the E-cenaris cloud-monitoring platform provided by INERIS.

A survey of the effectiveness of different monitoring systems, especially for large displacements and pore pressure evolution at rock faces and spoil heaps, was conducted. Dynamic inclinometers, total pressure cells and piezometers were employed to acquire data and to calibrate modelling processes and threshold definition, aiming to assist the geotechnical control of an open pit mine and its spoil dumps. Data from the Belchatow mine was analysed as well as from other sites such as CLC mine in Spain. The project enabled geomechanical characterization, providing an understanding of the problem and the triggering mechanism at the CLC mine through numerical modelling.

Laser scanning campaigns were undertaken at the Belchatow site in Poland, using a long-range Riegl VZ-4000 provided by 3D Laser Mapping (3DLM), enabling a comprehensive point cloud to be established. A similar scan at the CSA mine was also conducted using a shorter range Leica ScanStation C10. A document entitled "Feedback and recommendations of the use of laser scanning technology for open pit mine stability diagnostics" was produced, covering the development and application of technology, with focused discussion on deliverable outputs that can be generated from its deployment in open pit mining. Laser scanning using a FARO Focus3D X330 was used to characterise the stability of a small abandoned French coal mine. The laser scan results were integrated into a 3D numerical modelling process, demonstrated that terrestrial laser scanner technology can be a useful tool to characterize and analyse the stability of inaccessible slopes with very reasonable costs compared to classical displacement surveys.

#### **WP2 - Advanced modelling and risk analysis of open pit rock-face slopes**

WP2 aimed to develop reliability-based methods for assessing risk through probabilistic analyses, apply advanced numerical modelling to open pit mining applications and study how best to incorporate monitoring data from WP1 into the numerical modelling approach, and consider how the vulnerability of structures to open pit mining activities could be evaluated/improved.

A slope reliability model was developed that coupled the Monte Carlo simulation probabilistic method with the limit equilibrium method. Results demonstrated the probabilistic outcomes are primarily related to the cross-correlation between shear strength components, with the statistical distribution type that random variables follow also have a secondary role. Conservative results were shown to occur if the dependency between shear strength frictional and cohesive components was not considered. Lognormal distributions gave the lower calculated probability of failure values, whereas Normal truncated and Beta distribution yielded very similar probabilistic results. A slope reliability methodology was also developed using the point estimate probabilistic method with the finite element numerical method. Both local and global slope safety levels along critical slip surfaces were evaluated, with local and global safety factors matched with local and global probabilities of failure along certain critical slip surfaces. It was found that the probability of failure decreases from a slope's toe to the slope's crest. Areas within a slope presenting significant potential for local overstress and progressive failure occurrence were manifested.

A review was conducted in relation to probabilistic approaches for plane failure analysis and slope stability acceptance criteria, and application of Eurocode 7 requirements in a mining context. A report entitled "Probabilistic approaches to plane failure analysis" was written to complement the deliverables of the SLOPES project. The review was based on example plane failure analyses typically of a limited size (e.g. benches) using a probabilistic approach and different methods of solution. The review considered the geotechnical aspects of the probability of failure and consequences were considered mainly for the scale of the slope. The cases studied did not include consideration of singular features such as major faults.

A methodology was presented where UAV point cloud data (from WP1) and water table data were converted into geometrical surfaces and imported into numerical models. The free software *CloudCompare* was used. The UAV data was filtered and converted into subsampled surfaces. Mesh generation was achieved through a FISH code in FLAC3D, avoiding the use of additional (expensive) commercial software. A separate methodology was presented in a report entitle "Application of advanced numerical methods", suggesting a modelling approach for the different case studies highlighted within the SLOPES project, i.e. a framework for incorporation of remotely captured digital data in slope stability analysis.

Advanced numerical modelling was applied to several case studies, including work related to material characterization using in-situ and laboratory testing. Back-analyses were conducted to optimise material and water table characteristics, providing useful conclusions and recommendations for mine operators for future mining plans, and identifying pros and cons of the modelling processes. The distinct element method was used to assess the stability of open pit coal mines in Europe. The use of the distinct element allows one to take into account the natural features and faults and the induced discontinuities. The coupling between large scale and local scale numerical modelling with the observations help to explain the causes and the consequences of slope instabilities in active coal mines.

A global damage index (GDI) was proposed in the SLOPES project to quantify the vulnerability of structures to open pit mining activities. The developed methodology was applied using damage data recorded for the Mavropigi village in Greece, which is located near an active open pit lignite mine operated by the Public Power Corporation (PPC). The vulnerability analysis highlighted the main role of geological features to increase the influence of the mine excavations on surrounding buildings and infrastructure. Numerical modelling was used to evaluate the critical distance between the mine and the existing villages and infrastructure.

### **WP3 - Stability and long-term behaviour of lignite mine spoil heaps and reclaimed ground**

The aims of WP3 related to the collection of data and evaluation of stability and ground movements within lignite mine spoil heaps. The physical properties of spoil samples from Belchatów mine in Poland and Vrsany mine in the Czech Republic were evaluated and it was shown that there is significant variability in the reported physical characteristics of spoil soils; this is even true for samples obtained from a single spoil heap. As part of the SLOPES project, the variability of spoil properties from a single spoil heap was characterised to a degree not previously achieved using data from the Soulou spoil heap. The outcomes of this task are extremely valuable as they provide a unique quantitative assessment of the variability of spoil heap characteristics.

Physical and numerical modelling was conducted to evaluate issues related to the stability and movements of spoil heaps. The physical models included meso-scale experiments at 1-g and small-scale modelling within a geotechnical centrifuge. Experiments focused on the response of the spoil heaps to variation of water table levels as well as rainfall events. Results indicated that negative pore pressures (suctions) played a key role in maintaining slope stability. Different types of soils were tested; in pure sand, no failure mechanism was observed, whereas a silty sand exhibited failures under both low and high rainfall intensities. Failure was sudden for high intensity rainfall while a more progressive failure was observed for lower intensity rainfall. WP3 included ambitious aims related to physical modelling of spoil heap embankments incorporating unsaturated soil slopes, an area of significant challenge which has not been solved within the physical modelling community. Many lessons were learned and future research will endeavour to continue to find ways in which unsaturated soil slopes can be effectively modelled within the centrifuge.

Advanced numerical modelling focused on the case study from the Slatinice spoil dump at Vrsany mine, Czech Republic, using a variety of applications and considering different parameter effects. The Slatinice spoil dump represents a challenge considering that the spoil heap is currently registering movements and there is potential for future re-exploitation of the dump. Modelling indicated that there was a clear localised instability at the contact layer of the bottom part of the spoil, comprising water-saturated clay, and that the existence of pore pressure concentrations within this layer plays a leading role in the development of large scale failures of the dump. Numerous numerical modelling simulations using the Limit Equilibrium and Finite Element Methods demonstrated that the most critical condition of the slope is related to the superficial instability involving local benches. According to the results of the analyses (both LEM and FEM), instability occurs even in dry conditions, but a higher number of unstable benches are detected if the slope is considered fully saturated. A FLAC3D model of the spoil heap was developed to focus on the effects of hydrogeological conditions as well as excavation sequence. An advanced elasto-viscoplastic soil models was implemented in the commercial software PLAXIS and used to provide a comparative study between the EVP-SANICLAY, Mohr-Coulomb, and Modified Cam-Clay constitutive models. The results demonstrated some important differences between the models; the location of the predicted ground movements in the EVP-SANICLAY model was different than the Mohr-Coulomb model, but similar to the Modified Cam-Clay model (though magnitudes were considerably different).

Due to the observed variability of the spoil material, an additional numerical modelling exercise was conducted in which stability was assessed using multivariate random fields. The study considered four dependent random variables of void ratio, dry unit weight, cohesion, and friction angle which were cross-correlated using a multivariate Gaussian copula. The numerical model was a fully coupled transient hydro-elasto-plastic model constructed in Abaqus, where saturated permeability was related to the random field of void ratio. One thousand different random fields were generated and simulated using Abaqus. An analysis of the most likely failure surface and its safety factor was carried out. Results illustrated that a homogeneous spoil case gives a slip line smaller than most of the random field simulations, therefore showing the importance of considering heterogeneity. Results indicated that the factor of safety in a homogenous case is overestimated compared to the nonhomogeneous condition, while the sliding volume is underestimated. Moreover, the factor of safety decreases as the rainfall simulation continues and the probability of failure increases to nearly 100% after 10 days of rainfall.

The reliability methodology developed as part of WP2 was also applied for the case of spoil dumps, with benefits relating to its capability of disclosing both local and global slope reliability levels and in the possibility for considering a slope's construction method in the stability analysis. Limit Equilibrium and Finite Element analyses were used to assess the effects of data uncertainty on spoil heaps at a lignite operation in the Czech Republic. The case study provided valuable insight into the effects of geological parameters and model uncertainty. A sensitivity analysis was undertaken to understand the controlling influences of input parameters on model behaviour. The results highlighted, as expected, that water table level and material input parameters have the greatest influence on stability of the slope. The potential for both deep-seated instability and superficial land sliding were investigated.



## **4 Exploitation and impact of the research results**

### **WP1 - Development and application of modern monitoring techniques for slope stability in open pit lignite mines**

The use of modern monitoring techniques for slope stability (e.g. unmanned aerial vehicles) has a potential large impact on the safety and the security of the mine operations. They reduce the need to have people and equipment in areas that are potentially dangerous or have limited access. In addition, InSAR technologies, based on satellite data acquisition, has been integrated in this project as an extra-unmanned aerial technology. The results of the research present a real interest for the European open pit coal mines, during and after the abandonment of the mines. The analysis of the advantages and disadvantages of the different modern monitoring techniques is the basis of European recommendations for the applications of the modern monitoring in large open pit coal mines. UAV represents an important tool for the monitoring of potential unstable zones.

The on-line monitoring system implemented at the Belchatow mine is the first in a Polish opencast mine. The Belchatow mine is constantly receiving early warning monitoring data from this on-line system. The displacements up to the end of February 2019 reached 270 mm and pore pressure has dropped to 40 kPa. The continuous observation of the displacements is very important because of landslide risk. Due to the future closure of the Belchatow field the mine is conducting storage of spoil dump material on the west slope of this field which has caused additional loads. To predict the risk the mine is planning to use Riegl terrestrial laser scanner and UAV monitoring for future measurements. This should help to lower the risk for exploitation and environmental hazards. This represents a significant outcome of the project as it establishes a precedence for the implementation of these modern monitoring and risk evaluation techniques. Outcomes were presented in the IX International Lignite Mining Congress in Belchatow in 2016 and the XVIII Polish National Conference on Soil Mechanics and Geotechnical Engineering in Warsaw in 2018.

### **WP2 - Advanced modelling and risk analysis of open pit rock-face slopes**

The vulnerability study has a large impact on the mine design and planning process. The research results, mainly related to the damage scale developed in the project, will be helpful and can be used on European open pit coal mines and can be exported outside thanks to the international publications.

### **WP3 - Stability and long-term behaviour of lignite mine spoil heaps and reclaimed ground**

The developed framework for integrating monitoring data (e.g. point cloud data) into numerical modelling exercises will help to establish an appropriate protocol for adaptation of the modern monitoring methods and use within mine planning and risk assessment exercises. Several alternatives, using a variety of software and modelling approaches (incorporating both low-cost and higher-cost options) were developed and evaluated as part of the project. This information will prove invaluable to mine operators looking to undertake similar modelling exercises. The advanced numerical modelling conducted as part of this project demonstrate important features and differences between outcomes using models of varying level of sophistication. These outcomes will provide guidance to engineers and researchers in the future, through the project reports and associated journal publications.

#### **Papers published by project partners:**

#### **Publications, patents:**

- Al Heib M., Koukouzas N., Zevgolis I.E., Deliveris A., Coccia, S. 2018. Evaluation of building damages due to open pit mine activities. Application on Mavropigi open pit mine – Greece. Slope Stability 2018. Seville, Spain. April 10-13.
- Bednarczyk, Z. 2018. Emergency Warning of Landslide Natural Hazard Using Nearly Real-Time Monitoring Data, IAEG/AEG Annual Meeting Proceedings, San Francisco, California, 2018- Volume 5 Geologic Hazards, and Emergency Response, Part IV Emergency Response, editors Abdul Shakoor and Kerry Cato, Springer International, doi.org/10.1007/978-3-319-93136-4, pp. 103-113.
- Bednarczyk, Z. 2018. Geotechnical Investigations of Mine-Induced Ground Movements in Polish Opencast Mines, IAEG/AEG Annual Meeting Proceedings, San Francisco, California, 2018- Volume 3 Mining, Aggregates, Karst, Part I, Mining, editors Abdul Shakoor and Kerry Cato, Springer International, doi.org/10.1007/978-3-319-93130-2, pp. 3-13.
- Bednarczyk, Z. 2018. Implementation of on-line monitoring and numerical modelling at western slope of Belchatow mine (Poland). Proceedings of Slope Stability 2018 Symposium, Seville, Spain organized by Spanish Mining Council and Spanish Society of Mining Engineers South (Colegio Oficial De Ingenieros De Minas Sur) ISBN: 978-84-09-01295-4, paper No 69, pp. 1-12

- Bednarczyk, Z. 2017. Landslide Monitoring and Counteraction Technologies in Polish Lignite Opencast Mines, Advancing Culture of Living with Landslides, Vol 5, Landslides in Different Environments edited by Matjaz Mikoz, Vít Vilímek, Yueping Yin, Kyoji Sassa, Springer International, ISBN 978-3-319-53482-4, DOI10.1007/978-3-319-53483-1, pp. 33-43.
- Bednarczyk, Z. 2016. The methods of natural hazards predicting in opencast mining - a new international project from the EU Fund for Coal and Steel "Smarter Lignite Open-Pit Engineering Solutions "9th International Brown Coal Mining Congress" Belchatow - CD edition.
- Deliveris, A.V., Zevgolis, I.E., Koukouzas, N.C. (2016). Reliability assessment of slope stability on surface lignite mines as a complementary tool in the design process. Proceedings, 1st International Conference on Natural Hazards & Infrastructure (ICONHIC 2016), 28-30 June, 2016, Chania, Greece.
- Deliveris, A.V., Zevgolis, I.E., Koukouzas, N.C. (2018a). A coupled probabilistic-numerical model for the reliability-based design of slopes. Slope Stability 2018 - International Symposium on Slope Stability in Open Pit Mining and Civil Engineering, April 11-13, 2018, Seville, Spain.
- Deliveris, A.V., Zevgolis, I.E., Koukouzas, N.C. (2018b). Reliability evaluation during progressive failure of slopes. 14th International Symposium of Continuous Surface Mining (ISCSM), Thessaloniki, Greece, 23-26 September 2018.
- Fernández, A., Hurtado, J.M. 2018. Analytical Scarp Detection Model – Obtaining an Intuitive Indicator through Local Dispersion Analysis of Landslide Point Clouds. Slope Stability 2018. Seville, Spain. April 10-13.
- Masoudian, M.S., Zevgolis, I.E., Deliveris, A.V., Marshall, A.M., Heron, C.M., Koukouzas, N.C. (2019). Stability and characterisation of spoil heaps in European surface lignite mines: a state-of-the-art review in light of new data, Environmental Earth Sciences. In press.
- Masoudian M.S., Zanganeh H., Marshall A.M., and Heron C.M. 2018. Geotechnical characteristics of spoil materials in European open pit lignite mines. Slope Stability 2018. Seville, Spain. April 10-13.
- Masoudian, M. S., Hashemi, M. A., Tasalloti, A., & Marshall, A. M. (2019). A general framework for coupled hydro-mechanical modelling of rainfall- induced instability in unsaturated slopes with multivariate random fields. Computers and Geotechnics, 115(November), 103162.
- Matziaris, V., Masoudian, M. S., Marshall, A.M., and Heron, C.M. 2017. Centrifuge modelling of rainfall-induced slope instability in sand and silty sand. 19th International Conference on Soil Mechanics and Geotechnical Engineering. Seoul, Korea. 17-22 Sept. 2179-2182.
- Richard T., Al Heib M., Coccia, S. 2018. Applications of 3D laser scan data for slope characterization and stability analysis. International Symposium, Rock Slope Stability. France, 13-15 November
- Salas J., Pozo V., De Paz D., Galera J.M. Stability Analysis of the working face slope and inner dump in a lignite open pit mine. Slope Stability 2018. Seville, Spain. April 10-13.
- Vanneschi C., Burda J., Žižka L., Eyre M., Francioni M., Coggan J. 2018. Improved understanding of active slope instability mechanisms in lignite operations. Slope Stability 2018. Seville, Spain. April 10-13.
- Vanneschi C., Eyre M., Burda J., Žižka L., Francioni M., Coggan J. 2018. Investigation of landslide failure mechanisms adjacent to lignite mining operations in North Bohemia (Czech Republic) through a combined Limit Equilibrium/Finite Element modelling approach. Geomorphology. 320(1 November):142-153.
- Zevgolis, I.E., Deliveris, A.V., Koukouzas, N.C. (2018a). Probabilistic design optimization and simplified geotechnical risk analysis for large open pit excavations, Computers and Geotechnics, 103: 153-164.
- Zevgolis, I.E., Koukouzas N.C., Roumpos, C., Deliveris A.V., Marshall, A.M. (2018b). Evaluation of geotechnical property variability: the case of spoil material from surface lignite mines. Conference Proceedings, 5th International Conference on Civil Protection & New Technologies (Safe Kozani 2018), 31-3 November 2018, Kozani, Greece, pp. 236-245.
- Zevgolis, I.E., Deliveris, A.V., Koukouzas, N.C. (2019). Slope failure incidents and other stability concerns in surface lignite mines in Greece, Journal of Sustainable Mining. 18(4): 182-197.

## 5 List of Figures

Figure 2.1: Point density for the LiDAR to the left and for the manned aircraft photogrammetry to the right (note that the outline of the LiDAR extent is displayed as black polygon over the photogrammetry density) .....	15
Figure 2.2: Eight-colorized point cloud from the LiDAR acquisition. ....	15
Figure 2.3: Hillshade terrain of the point clouds from all 3 different sensors with the RGB imagery on the right. ....	16
Figure 2.4: Cloud to cloud comparison – reference is the LiDAR point cloud and the image shows the March 2017 photogrammetric point cloud colour coded by ground movement that occurred over 3 months. ....	16
Figure 2.5: Cloudcompare analysis of TL in comparison of the first photogrammetric survey using a Sony camera (West Slope at Belchatow open pit mine). ....	17
Figure 2.6: Cloudcompare analysis of TL in comparison to the YellowScan aerial LiDAR survey (West Slope at Belchatow open pit mine). ....	17
Figure 2.7: Cloudcompare analysis of TL in comparison to the MicMac aerial photogrammetric survey (West Slope at Belchatow open pit mine). ....	18
Figure 2.8: Neighbour search operation scheme (top) and example of 2D point cloud and main directions obtaining (right). Bottom figure modified after Peña (2002). ....	20
Figure 2.9: Structure of the obtaining of $\delta$ through local dispersion analysis of a point cloud.....	20
Figure 2.10: Local neighbourhood associated to points belonging to scarp edges (left) and example of the geometrical model used for the integration of $\lambda_1$ formula. ....	21
Figure 2.11: Example of obtained $\lambda_1$ eigenvalues for the geometrical model representing a 90° scarp (left) and folding angle results for the models of 60° and 90° (right).....	22
Figure 2.12: Proposed classification based on $\delta$ scalar field (left) and artificial scarps used for testing of the algorithms (right). ....	22
Figure 2.13: Combined analysis of ASDM classification and displacements calculation between August and October 2016, including scarps (green), dense vegetation (blue) and displacements (red-black coloured scale representing reduction-increase in Z coordinate) .....	23
Figure 2.14: Representation of the identified scarps (green), vegetation (blue) and slided/eroded areas (red-white scale shows reductions in Z coordinate). ....	24
Figure 2.15: Web-monitoring page of Belchatow web monitoring e.cenaris page overview.....	25
Figure 2.16: On-line monitoring station in Belchatow mine .....	26
Figure 2.17: (a) Displacement magnitude; (b) cumulative X, Y displacement at Belchatow mine ..	26
Figure 2.18: Comparison displacement and pore pressure values, Belchatow mine .....	27
Figure 2.19: Average displacement velocities: (a) coverage of the area processed by SPINUA; (b) zoomed-in view of the mining area .....	28
Figure 2.20: Labels of unstable areas identified through the analysis of the PS displacement maps. ....	28
Figure 2.21: Example of the computerised recording of B-bar parameter against time. ....	30
Figure 2.22: Top-left: view of the 3D colour point cloud realized by the Focus3D X330 and RealWorks software; Right: the position of one important landslide. ....	31
Figure 2.23: Location of Laser Scan Survey Stations in Belchatow Mine.....	32
Figure 2.24: Photo Textured Laser Scan Data .....	32
Figure 2.25: Application of Slope function using TL data acquired at (a) Belchatow test site in Poland, and (b) CSA test site in Czech Republic.....	33
Figure 2.26: 3D representation of Slope function output carried out using TL data acquired at CSA test site in Czech Republic. ....	34
Figure 2.27: Application of Aspect function using TL data acquired at Belchatow test site in Poland (a) and CSA test site in Czech Republic (b).....	34
Figure 2.28: (a) Probability of failure with varying residual friction angle of clay; (b) influence of RNG seed value on the probability of failure .....	35
Figure 2.29: (a) Relation between probability of failure and deterministic safety factor .....	36
Figure 2.30: Numerical modelling results (left) of the slope and in-situ observations (right).....	39

Figure 2.31: GEOCONTROL's approached scheme for integration of WP1 data into numerical modelling.....	39
Figure 2.32: Comparative between octree and extruded meshes from a topographical surface.....	40
Figure 2.33: Geometry of the geological model created by GEOCONTROL.....	40
Figure 2.34: Influence of fast water table rises in landslide activity. ATR monitoring line indicates cumulative displacements. Landslide events marked in red dashed line and preceding rises of JZ241 in red continuum segments (October 2012 – June 2017). .....	41
Figure 2.35: Observed influence of seasonal precipitation (week cumulated) in landslide displacement trend (October 2012 – June 2017). .....	41
Figure 2.36: (a) Local failure probability and reliability index along slope slip surface; (b) global probability of failure at the states of progressive failure .....	42
Figure 2.37: Location of slope stability analysis, risk zones and monitoring instrumentation .....	44
Figure 2.38: Results of slope stability analysis 20WE, FoS=1.14 .....	45
Figure 2.39: Flow chart .....	46
Figure 2.40: Modelling framework for continuum versus discontinuum modelling .....	46
Figure 2.41: 3DEC simulation showing displacement magnitudes using bench face geometry from terrestrial laser scanning point cloud data. Lower right inset map indicates bench face slope angle values (°) calculated in ArcGis .....	47
Figure 2.42: Comparison between results of 3DEC analysis and direct field observation .....	48
Figure 2.43: Increase in block size due to different persistence configurations in 3DEC .....	49
Figure 2.44: Schematic cross section of the materials involved in the Open Pit. .....	49
Figure 2.45. Cracks on the region northwards of Mavropigi.....	50
Figure 2.46: Pictures of the region north of Mavropigi taken in December 2011 .....	51
Figure 2.47: Observed damage in different buildings in Mavropigi village .....	52
Figure 2.48: Mavropigi plan view and building damage recordings and classification. Damage levels: green: slight damage, purple -medium to severe damage, red – very severe damage. ....	52
Figure 2.49: Red damaged building in Mavropigi village (CERTH) .....	52
Figure 2.50: Examples of damage can be observed after a landslide, (A) very slight damage, (B) moderate damage, (C) severe damage (Frattini et al. 2013).....	53
Figure 2.51: Numerical model (UDEC) of the Mavropigi open-pit mine. .....	55
Figure 2.52: Plastic points (red and green) due to mine excavation and the 14th January of 2014 landslide in the mine Mavropigi open-pit. .....	55
Figure 2.53: Vertical displacements along the faults in the area of the Mavropigi village.....	56
Figure 2.54: Soulou's spoil dump plan view operated by PPC .....	57
Figure 2.55: Spatial distribution of spoil material in Soulou's spoil heap .....	58
Figure 2.56: (a) Test box for large scale 1-g physical modelling, (b) HD webcams and Perspex windows, (c) standpipe. .....	60
Figure 2.57: Schematic representation of the instrumented soil slope and its geometry .....	61
Figure 2.58: (a) Surface settlements measured by LVDTs; (b) variations of pore water pressure in the slope model .....	62
Figure 2.59: The centrifuge climatic chamber: (a) exploded-view of the plane-strain container (b) spraying nozzles and components inside the box (under container lid) (c) components on top of container lid, including the water distribution system, solenoid valve and flowmeter. ....	63
Figure 2.60: Rainfall-induced displacement vectors at failure initiation in (a) test Sa90Si10-Low intensity at t= 1042 hr (b) test Sa90Si10-High intensity at t= 1.25 hr (t is prototype time).....	64
Figure 2.61: Pore water pressure measurement points for test SS-H .....	65
Figure 2.62: Geological profiles for the spoil dump analysis. ....	66
Figure 2.63: Localisation of displacements registered by inclinometers on section C-C'. Inclinometers and one of laboratory samples are marked in the figure. ....	66
Figure 2.64: Analysis of 1983 landslide: geometry of the spoil surface prior to the landslide and displaced mass (top-left), 3D view of the landslide (top-right) and profile for the back-analysis. ..	67

Figure 2.65: Cyclical changes of water content for the period between July 2016 and October 2017.	68
Figure 2.66: Shear strain plot for the shallow water table hypothesis.....	68
Figure 2.67: Potential sliding masses coloured based on their associated Factors of Safety, which represent the required strength reduction for the initiation of each instability mechanism (final state of Vrsany dump re-excavation under the pore-pressure concentration hypothesis). .....	69
Figure 2.68: Failure mechanism associated to FoS calculation.....	69
Figure 2.69: Calibration Model reaching a FOS of 0,962. ....	69
Figure 2.70: Detail of the phases for the excavation of the dump, and the selected area for FLAC3D analysis. ....	70
Figure 2.71: Meshing process employing Griddle-Rhinoceros .....	70
Figure 2.72: Multi-phase excavation for the analysis of the influence of the sequence in the slope stability.....	70
Figure 2.73: Left-side pictures show displacements during the phase excavations and final configuration, and right-side pictures shear strain contours in the same phases. Special attention must be paid to displacements in the toe of final benches for the accumulated volumetric shear strain increments. ....	71
Figure 2.74: Left-side picture shows shear strength increment along the contact layer when a Skempton B-bar coefficient reached 0.6. Right-side picture shows horizontal displacements. ....	71
Figure 2.75: Model profile of the numerical analysis.....	72
Figure 2.76: Total displacement field for (a) Mohr-coulomb, (b) Modified Cam-Clay, and (c) EVP-SANICLAY models.....	73
Figure 2.77: Marginal (one-dimensional) cumulative distribution functions of the dataset presented in Soenksen et al. (2003) .....	74
Figure 2.78: A typical set of random fields generated with multivariate copula and Gaussian auto-correlation function.....	75
Figure 2.79: Safety factor optimization with a circle then 5, 9 and 17 points splines .....	75
Figure 2.80: Heat map of slip line of all 1000 simulations, the homogeneous case is shown in blue .....	76
Figure 2.81: (a) Safety factors as a function of time with the homogeneous case shown in blue line; (b) volume of failure for all simulations, the red line shows the homogeneous case .....	76
Figure 2.82: Slide7.0 LEM deterministic stability analysis results with indication of mean FoS (above) and LEM sensitivity analysis results (below). Only failure surface with FoS lower 2 shown. ....	77
Figure 2.83: Spoil dumps incremental construction numerical simulation.....	79
Figure 2.84: Local slope's safety factor variation along slip surface.....	80
Figure 2.85: Local slope's safety factor probability of failure along slip surface .....	80
Figure 2.86: Results of Slide7.0 LEM probabilistic analyses performed for different water table locations (only failure surfaces with FoS < 2 are shown). .....	82
Figure 2.87: Scatter plot of FoS versus: (a) cohesion, water configuration (WC) 1; (b) friction angle, WC 1; (c) cohesion, WC 4, and (d) friction angle, WC 4. ....	83
Figure 2.88: Sensitivity analysis of possible pore pressure in the Contact layer. ....	84



## **6 List of Tables**

Table 2.1: Details of the 11 flights at the ČSA mine.....	18
Table 2.2: Comparison between the Phantom and S900 results.....	19
Table 2.3: Analytical eigenvalue equations obtained according to ASDM model .....	21
Table 2.4: Comparison of displacements recorded by automatic topographic control points and dynamic inclinometer.....	30
Table 2.5: Input data for Cases 1 to 3.....	37
Table 2.6: Input data for Cases 4 and 5 .....	37
Table 2.7: Summary of basic plane failure analyses and results. In Case 2 the output distribution of F has been taken as log-normal. In cases 4 and 5, triangular distributions were used for slope face and slope height; negative exponential distributions for water levels and seismic coefficient. MC is Monte Carlo simulation. .....	37
Table 2.8: Results of field strength penetrometer and vane tests. ....	42
Table 2.9: Results of index, direct shear and compression tests .....	43
Table 2.10: Results of triaxial tests.....	43
Table 2.11: The results of total and effective strength parameters for different types of tested soils .....	43
Table 2.12: The results of numerical modelling by SSR and LEM methods .....	45
Table 2.13: Orientation and Spacing of major discontinuity sets identified within test bench in Melbur Pit.....	47
Table 2.14: Model parameters related to the instability process at SAMCA Mine .....	50
Table 2.15: Geotechnical parameters of the rock layers and joints (faults) .....	54
Table 2.16: Uniform spoil material geotechnical parameter statistics .....	58
Table 2.17: Summary of triaxial test results on samples from Vrsany mine, Czech Republic .....	59
Table 2.18: Results of the B-bar evolution simulation when excavating the inner dump.....	71
Table 2.19: Model parameters for the contact layer and the coal seam .....	72
Table 2.20: Soil classification of the different layers.....	72
Table 2.21: Mohr Coulomb parameters for the dump material.....	72
Table 2.22: Cam-Clay parameters for the dump material .....	73
Table 2.23: EVP-SANICLAY parameters for the dump material .....	73
Table 2.24: Estimated multivariate copula correlation matrix for the dataset presented in Soenksen et al. (2003) .....	74
Table 2.25: Variables taken for the homogeneous case .....	76
Table 2.26: Sensitivity analysis: values for each geological formation (with indication of relative MINIMUM and MAXIMUM values for dump material).....	77
Table 2.27: Bedrock and spoil geotechnical parameters .....	79
Table 2.28: Shear strength parameters statistics.....	79
Table 2.29: Global slope safety factor statistics and probabilities of failure .....	80
Table 2.30: Statistical properties used in the probabilistic analysis for the dump material.....	81
Table 2.31: Statistical properties used in the probabilistic analysis for dump material. ....	83
Table 2.32: Statistical properties used in the probabilistic analysis for Contact layer. ....	85



## **7 List of Acronyms**

AOI - Area of Interest  
ASDM - Analytical Scarp Detection Model  
ASI - Italian Space Agency  
AUTH - Aristotle University of Thessaloniki  
CIU - Consolidated Isotropic Undrained (triaxial test)  
CID - Consolidated Isotropic Drained (triaxial test)  
CUPP - Consolidated Undrained Pore Pressure  
COV - Coefficient of Variation  
DEM - Digital Elevation Model  
EWS - early warning system  
FEM - Finite Element Method  
FS - Factor of Safety  
FoS - Factor of Safety  
FOSM - First Order Second Moment  
GCP - Ground Control Point  
GDI - Global Damage Index  
GIS - Geographic Information System  
GSD - Ground Sample Distance  
GSI - Geological strength index  
INS - Inertial Navigation System  
InSAR - Interferometric Synthetic Aperture Radar  
LEM - Limit Equilibrium Method  
LEA - Limit Equilibrium Analysis  
LiDAR - Light Interferometry Detection and Ranging  
LOS - line of sight  
MCS - miocene claystones  
MSFC - miocene stiff-fissured claystones  
MCC - Modified Cam-Clay  
OCR - over-consolidation ratio  
POP - pre-overburned pressure  
PPK - Post Processed Kinematic  
PPC - Public Power Corporation  
PS - Persistent scatterer  
PSI - Persistent Scatterer Interferometry  
RH - Rotational-Hardening  
RNG - random number generator  
SAR - Synthetic Aperture Radar  
SD - Standard Deviation  
SLC - Single-look complex  
SPINUA - Stable Points Identification in Non Urbanized Area  
SRF - Shear Reduction Factor  
SRT - Strength Reduction Technique  
SSR - shear strength reduction  
TL - terrestrial laser  
TLS - terrestrial laser scanning  
UAV - unmanned aerial vehicle  
Q - quaternary sediments  
QC - Quality Control  
USCS - Unified Soil Classification System



## **8 References**

- Aktualizacja ZTE Pola Szczercow wraz z biznesplanem. Wydobycie maksymalne. 2002, Część Ogólna Nr projektu - 1030.1325.002. Wrocław, POLTEGOR- PROJEKT (in Polish).
- Al-Rawabdeh, A., He, F., Mousaa, A., El-Sheimy, N., and Habib, A. 2016. Using an Unmanned Aerial Vehicle-Based Digital Imaging System to Derive a 3D Point Cloud for Landslide Scarp Recognition. *Remote Sensing*, vol. 8, no. 95.
- Alexander D. (1986) Landslide damage to buildings. *Environ Geol Water Sci* 8(3):147–150
- Antronico L. et al. (2015) Time evolution of landslide damages to buildings: the case study of Lungro (Calabria, southern of Italy). *Bull Eng Geol Environ* (2015) 74:47–59.
- Askarinejad, A., Beck, A., Springman, S.M., 2015. Scaling law of static liquefaction mechanism in geocentrifuge and corresponding hydromechanical characterization of an unsaturated silty sand having a viscous pore fluid. *Canadian Geotechnical Journal* 52, 708–720.
- Ayala F.J. et al (1978) Forecast Map for risk due to presence of expansive clays in Spain. CEDEX Manuals. 30-35.
- Bednarczyk J., A. Nowak A., 2010 Strategie i scenariusze perspektywicznego rozwoju produkcji energii elektrycznej z węgla brunatnego w świetle występujących uwarunkowań. 2010 Górnictwo i Geoinżynieria - Rok 34 - Zeszyt 4, 67-83. (in Polish).
- Bednarczyk, Z. 2017. Landslide Monitoring and Counteraction Technologies in Polish Lignite Opencast Mines, Advancing Culture of Living with Landslides, Vol 5, Landslides in Different Environments edited by Matjaz Mikoz, Vít Vilímek, Yueping Yin, Kyoji Sassa, Springer International, ISBN 978-3-319-53482-4, DOI10.1007/978-3-319-53483-1, pp. 33-43.
- Bovenga F., Refice A., Nutricato R., Guerriero L., Chiaradia M. T. 2004. "SPINUA ©: a flexible processing chain for ERS / ENVISAT long term interferometry", Proceedings of ESA-ENVISAT Symposium 2004, 6-10 September, 2004, Salzburg, Austria.
- Borecka, A., 2007. Dump soil – problems in evaluation of physical and mechanical parameters. *Geologos*, 11: 123-132.
- Brideau, M.A., Pedrazzini, A., Stead, D., Froese, C., Jaboyedoff, M., and Van Zeyl, D. (2011) Three-dimensional slope stability analysis of South Peak, Crownest Pass, Alberta, Canada. *Landslides*, 8, 139–158.
- Brideau MA, Stead D (2012) Evaluating kinematic controls on planar translational slope failure mechanisms using three-dimensional distinct element modelling. *Geotech Geol Eng* 30:991-1011
- Burda, J. 2011. Spatio-temporal activity of mass movements in the Krušné Hory Mountains (Czech Republic): dendrogeomorphological case study. *AUC Geographica*, vol. 46, no. 2 pp. 15-30.
- Burda, J., Hartvich, F., Valenta, J., Smítka, V., and Rybář, J. 2013. Climate-induced landslide reactivation at the edge of the Most Basin (Czech Republic) – progress towards better landslide prediction. *Natural Hazards and Earth System Sciences*, vol. 13, pp. 361-374.
- Burda, J., Žižka, L., and Dohnal, J. 2011. Monitoring of recent mass movement activity in anthropogenic slopes of the Krušné Hory Mountains (Czech Republic). *Natural Hazards and Earth System Sciences*, vol. 11, pp. 1463-1473.
- Carter L.C. (2015) Preliminary geotechnical assessment of the proposed life of mine excavation design for Melbur pit. Dissertation, University of Exeter, Camborne School of Mines
- Ciampalini A. et al. (2014) Analysis of building deformation in landslide area using multisensory PSInSAR TM technique. *International Journal of Applied Earth Observation and Geoinformation* 33 (2014) 166–180
- CloudCompare - 3D point cloud and mesh processing software, version 2.6.1, User Manual. 2017. Open Source Project under GNU General Public License.
- Coggan, J., and Eyre, M. (2013) Application of Rockfall Risk Assessment for Surface Mining Operations. In Proceedings of ICSMRI, 35th International Conference of Safety Mines Research Institutes2. p. 3-13.
- Diamantopoulos A, Dimitrakopoulos D and Fountoulis I (2004). Quaternary Deformation of the Mavropigi Lignite Field (Western Margin of Ptolemais - Kozani Graben, NW Macedonia, Greece). *Bulletin of the Geological Society of Greece*, 36(1): 310-319.
- Einstein HH, Veneziano D, Baecher GB, O'Reilly KJ (1983) The effect of discontinuity persistence on rock slope stability. *Int J Rock Mech Min Sci Geomech Abstr* 20:227-236
- Elmo D, Clayton C, Rogers S, Beddoes R, Greer S (2011) Numerical simulations of potential rock bridge failure within a naturally fractured rock mass. In: Eberhardt E, Stead D (ed) *Proceedings of the 2011 International Symposium on Slope Stability in Mining and Civil Engineering*, Vancouver, Canada, pp 13
- ESRI (2016) ArcGIS, Available at: <http://www.arcgis.com>
- Frattini P, Crosta GB and Allievi J (2013). Damage to buildings in large slope rock instabilities monitored with the PSInSAR™ technique. *Remote Sensing*, 5(10): 4753-4773.
- Geomorphological Services Ltd (1991) Coastal landslip potential assessment: Isle of Wight Undercliff, Ventnor. Technical report for the Department of the Environment. Research contract RECD 7/1/272.
- Girardeau-Montaut, D. (2017). CloudCompare - 3D point cloud and mesh processing software, version 2.6.1.
- Goodman RE (2003) A hierarchy of rock slope failure modes. *Felsbau* 21:8-12

- Gumhold, S., Wang, X., and MacLeod, R. 2001. Feature Extraction From Point Clouds. Proceedings of the 10th International Meshing Roundtable, Newport Beach, California, USA, 7-10 October 2001. pp. 293-305.
- Hawrysz, M., 2013, Metody oceny efektywnych parametrów wytrzymałości gruntów. Geoinżynieria – drogi mosty tunele 03/2013, 34-44. ( in Polish).
- Hochman A., 2000 Kopalnia Węgla Brunatnego Belchatow, od przedsiębiorstwa państwowego do spółki akcyjnej - in Polish.
- Itasca Consulting Group, Inc. (2012). FLAC3D - Fast Lagrangian Analysis of Continua in 3 Dimensions, Ver 5.0 User's Manual. Minneapolis.
- Jaky, J. 1944. The coefficient of earth pressure at rest. In Hungarian (A nyugalmi nyomas tenyezoje) Journal of the Society of Hungarian Architects and Engineering, 78 (22) (1944), pp. 355-358
- Jennings JE (1970) A mathematical theory for the calculation of the stability in open cast mines. In: Van rensburg P (ed) Planning of open pit mines: Proceedings of the Symposium on the Theoretical Background to the Planning of Open Pit Mines, with Special Reference to Slope Stability. Balkema, Johannesburg, pp 87-102
- Jonczyk W., Organisciak B. & Sedor A. 2013 – Ograniczanie zagrożeń osuwiskowych dla poprawy bezpieczeństwa robot gorniczych na przykładzie Kopalni Bełchatow. Mat. Konf. „Szkoła Górnictwa Odkrywkowego 2013”. AGH Kraków (in Polish).
- Kaltchev, I.S. and Germanov, T.S., 2005. Evaluation of the design parameters of overburden dump construction from an open pit mine in Bulgaria 16th International Conference on Soil Mechanics and Geotechnical Engineering, Osaka, Japan.
- Kasai, M., Ikeda, M., Asahina, T., and Fujisawa, K. 2009. LiDAR-derived DEM evaluation of deep-seated landslides in a steep and rocky region of Japan. *Geomorphology*, vol. 113, Issue 1, pp. 57-69.
- Kasmer, O., Ulusay, R. and Gokceoglu, C., 2006. Spoil pile instabilities with reference to a strip coal mine in Turkey: mechanisms and assessment of deformations. *Environmental Geology*, 49(4): 570-585.
- Kasztelewicz, Z. 2012 Węgiel brunatny na świecie i w Polsce. *Węgiel Brunatny* 2012/1/7
- Kavvadas M, Agioutantis Z, Schilizzi P and Steiakakis C. (2013). Stability and movements of open-pit lignite mines in Northern Greece. In: 18th International Conference on Soil Mechanics and Geotechnical Engineering, Paris, pp. 2193-2196.
- Keskin, T. and Makineci, E., 2008. Some soil properties on coal mine spoils reclaimed with black locust (*Robinia pseudoacacia* L.) and umbrella pine (*Pinus pinea* L.) in Agacli-Istanbul. *Environmental Monitoring and Assessment*, 159(1): 407-414.
- Keverne B, Howe JH, Pascoe DM, Eyre ML, Coggan JS (2015) Remediation of a hazardous legacy slope face using pre-split blasting. *Proceedings of the ISRM Regional Symposium Eurock2015 & 64th Geomechanics Colloquium*, pp 217-222
- Kulhawy, F. H. 1992 On the evaluation of static soil properties. In: Geotechnical Special Publication 31 ASCE. pp. 95-115. (1992).
- Lialiabis I and Dimoudi E (2011). Investigation for detection and recording of building damages due to surface fractures in the broader area of Mavropigi municipality of the Ptolemais town.In:Tsapanos T (ed.)Final report of the research of surface fissures phenomenon in the broader area of Mavropigi municipality of the Ptolemais town.Department of Geology, Aristotle University of Thessaloniki, Thessaloniki, Greece, pp. 137.
- Ling, H., Wu, M., Leshchinsky, D., Leshchinsky, B., 2009. Centrifuge Modeling of Slope Instability. *Journal of Geotechnical and Geoenvironmental Engineering* 135, 758-767.
- Marinos, VP., E Hoek, E., 2005 The Geological Strength Index: applications and limitations. *Bull. Eng. Geol. Environ* 2005 64, pp 55-65
- Masoudian, M. S., Hashemi, M. A., Tasalloti, A., & Marshall, A. M. (2019a). A general framework for coupled hydro-mechanical modelling of rainfall- induced instability in unsaturated slopes with multivariate random fields. *Computers and Geotechnics*, 115(November), 103162.
- Masoudian, M.S., Zevgolis, I.E., Deliveris, A.V., Marshall, A.M., Heron, C.M., Koukouzas, N.C. (2019b). Stability and characterisation of spoil heaps in European surface lignite mines: a state-of-the-art review in light of new data, *Environmental Earth Sciences*. In press.
- Masoudian M.S., Zanganeh H., Marshall A.M., and Heron C.M. 2018. Geotechnical characteristics of spoil materials in European open pit lignite mines. *Slope Stability* 2018. Seville, Spain. April 10-13.
- Matziaris, V., Marshall, A.M., Heron, C.M., Yu, H.S., 2015a. Centrifuge model study of thresholds for rainfall-induced landslides in sandy slopes. *IOP Conference Series: Earth and Environmental Science* 26, 012032.
- Meyerhof, G. G. (1970). Safety factors in soil mechanics. *Canadian Geotechnical Journal*, 7(4), 349-355.
- Mitra, N. J., and Nguyen, An. 2003. Estimating surface normals in noisy point cloud data. *Proceedings of the nineteenth annual symposium on Computational geometry*, San Diego, California, USA, 8-10 June, 2003. pp. 322-328.
- Monopolis D, Stiakakis E, AGIOUTANTIS E and Kavouridis C (1999). Geotechnical Investigation at Lignite Mines. *Mineral Resources Engineering*, 8(4): 405-418.
- Nitti, D.O, Nutricato, R., Lorusso, N., Lombardi, F. Bovenga, M. F., Bruno, M. Chiaradia, T. Milillo, G. "On the geo-location accuracy of COSMO-SkyMed products", SPIE Remote Sensing 2015,

Paper n. RS106-50, Tracking n. ERS15-RS106-50, Centre de Congrès Pierre Baudis, Toulouse, France, 21 - 24 September 2015

- Nichol SL, Hungr O, Evans SG (2002) Large-scale brittle and ductile toppling of rock slopes. *Can Geotech J* 39:773-788
- Papadaki E, Tripolitsiotis A, Steiakakis C, Agioutantis Z, Mertikas S, Partsinevelos P and Schilizzi P. (2013). Land movement monitoring at the Mavropigi lignite mine using spaceborne D-InSAR. In:First International Conference on Remote Sensing and Geoinformation of the Environment: International Society for Optics and Photonics, pp. 87951A.
- Pauly, M., Gross, M., and Kobbelt, L 2002. Efficient Simplification of Point-Sampled Surfaces. Proceedings of the conference on Visualization '02 Mining, Boston, Massachusetts, USA, 27 October-1 November 2002. IEEE Computer Society Washington DC, USA. pp. 163-170.
- Plaxis, b.v. (2018). Finite element geotechnical analysis software, Netherlands.
- PN EN 1997-1:2008 Eurokod 7. Projektowanie geotechniczne. Część 1: Zasady ogólne (in-Polish)
- Poulsen, B., Khanal, M., Rao, A.M., Adhikary, D. and Balusu, R., 2014. Mine Overburden Dump Failure: A Case Study. *Geotechnical and Geological Engineering*, 32(2): 297-309.
- Rajchl, M., Uličný, D., & Mach, K. (2008). Interplay between tectonics and compaction in a rift-margin, lacustrine delta system: Miocene of the Eger Graben, Czech Republic. *Sedimentology*(55), 1419-1447.
- Refice A., Bovenga F., Nutricato R , Chiaradia M.,t>, "Assessment of Multitemporal DInSAR Stepwise Processing", to appear in Proc. IGARSS 2004, Anchorage, Alaska, September 20-24 2004
- Riquelme, A. J., Abellán, A., and Tomás, R. 2015. Discontinuity spacing and analysis in rock masses using 3D point clouds. *Engineering Geology*, vol. 195, pp. 185-195.
- Riquelme, A. J., Abellán, A., and Tomás, R. 2016. Characterization of rock slopes through slope mass rating using 3D point clouds. *International Journal of Rock Mechanics and Mining Sciences*, vol. 84, pp. 165-176.
- Roumpos C and Papacosta E. (2013). Strategic mine planning of surface mining projects incorporating sustainability concepts. In:6th International Conference on Sustainable Development in the Minerals Industry, Milos Island, Greece, pp. 645-651.
- Rybicki S., (1996)- Zjawiska osuwiskowe w krajowych kopalniach węgla brunatnego, ich skala, charakter i uwarunkowania. Problemy Geotechniczne. Wydawnictwo Politechniki Krakowskiej: 157-164 ( in Polish).
- Salvini R, Mastrorocco G, Esposito G, Di Bartolo S, Coggan J, Vanneschi C (2017) Use of a remotely piloted aircraft system for hazard assessment in a rocky mining area (Lucca, Italy). *Nat Hazards Earth Syst Sci* 18:287-302. <https://doi.org/10.5194/nhess-2017-194>
- Soenksen, P.J., Turner, M.J., Dietsch, B.J., Simon, A., 2003. Stream bank stability in eastern Nebraska. U.S. Geological Survey, Lincoln, Nebraska. 156.
- Steiakakis, E., Kavouridis, K. and Monopolis, D., 2009. Large scale failure of the external waste dump at the "South Field" lignite mine, Northern Greece. *Engineering Geology*, 104(3-4): 269-279.
- Steiakakis C, Agioutantis Z, Apostolou E and Papavgeri G. (2017). Mining in a Landslide—Is It Possible? *Geotechnical Investigation and Analysis*. In: *Geotechnical Frontiers 2017 - GSP 278: ASCE*, pp. 264-274.
- Sturzenegger M, Stead D (2012) The Palliser Rockslide, Canadian Rocky Mountains: characterization and modeling of a stepped failure surface. *Geomorphology* 138:145-161
- Świtoniak;, M., Hulisz;, P., Różański;, S. and Kałucka, I., 2013. Soils of external dumping ground of the bełchatów open-cast lignite mine In: P. Charzyński;, P. Hulisz; and R. Bednarek; (Editors), Technogenic soils of poland. Polish Society of Soil Science, Toruń, pp. 358.
- Take, W.A., Bolton, M.D., Wong, P.C.P., Yeung, F.J., 2004. Evaluation of landslide triggering mechanisms in modell fill slopes. *Landslides* 1, 173-184.
- Taylor, R.N., 1994. *Geotechnical centrifuge technology*. CRC Press.
- Tripathi, N., Singh, R.S. and Chaulya, S.K., 2012. Dump Stability and Soil Fertility of a Coal Mine Spoil in Indian Dry Tropical Environment: A Long-Term Study. *Environmental Management*, 50(4): 695-706.
- Tsapanos T, Pavlides S, Voudouris K, Panagiotopoulos D, Karakostas V, Tsourlos P, Vargemezis G, Marinos V, Chatzopetros A, Stabolidis A, Fikos I, Mattas C, Lialiampis I, Dimoudi E, Koravos G, Delogkos E, Michailidou A, Karamanos C and Olasoglu E (2011). Final report of the research of surface fissures phenomenon in the broader area of Mavropigi, municipality of Ptolemaida. Thessaloniki, Greece: Department of Geology, Aristotle University of Thessaloniki.
- Tsige M. (1995) Regional Scale high-plasticity clay-bearing formation as controlling factor on landslides in Southeast Spain. Vol 120. 26-37.
- Ulusay, R., Arikan, F., Yoleri, M.F. and Çağlan, D., 1995. Engineering geological characterization of coal mine waste material and an evaluation in the context of back-analysis of spoil pile instabilities in a strip mine, SW Turkey. *Engineering Geology*, 40(1): 77-101.
- Vanneschi C, Eyre M, Francioni M, Coggan J (2017) The Use of Remote Sensing Techniques for Monitoring and Characterization of Slope Instability. *Procedia Engineering* 191:150-157
- Varela, C., Vazquez, C., Gonzalez-Sangregorio, M.V., Leiros, M.C. and Gil-Sotres, F., 1993. Chemical and physical properties of opencast lignite minesoils. *Soil Science*, 156(3): 193-204.
- Wyllie, Duncan C., and Mah, Christopher W, (2004). *Rock Slope Engineering* , Civil and Mining, 4th edition. Spon Press, London. 431 pp.

- Zevgolis, I.E., Deliveris, A.V., Koukouzas, N.C. (2018a). Probabilistic design optimization and simplified geotechnical risk analysis for large open pit excavations, *Computers and Geotechnics*, 103: 153-164.
- Zevgolis, I.E., Koukouzas N.C., Roumpos, C., Deliveris A.V., Marshall, A.M. (2018b). Evaluation of geotechnical property variability: the case of spoil material from surface lignite mines. Conference Proceedings, 5th International Conference on Civil Protection & New Technologies (Safe Kozani 2018), 31-3 November 2018, Kozani, Greece, pp. 236-245.
- Zevgolis, I.E., Deliveris, A.V., Koukouzas, N.C. (2019). Slope failure incidents and other stability concerns in surface lignite mines in Greece, *Journal of Sustainable Mining*. In press.
- Zhang, L.L., Zhang, J., Zhang, L.M., Tang, W.H., 2011. Stability analysis of rainfall-induced slope failure: a review. *Proceedings of the Institution of Civil Engineers - Geotechnical Engineering* 164, 299-316.

## Getting in touch with the EU

### In person

All over the European Union there are hundreds of Europe Direct information centres. You can find the address of the centre nearest you at:

[https://europa.eu/european-union/contact\\_en](https://europa.eu/european-union/contact_en)

### On the phone or by email

Europe Direct is a service that answers your questions about the European Union. You can contact this service:

- by freephone: 00 800 6 7 8 9 10 11 (certain operators may charge for these calls),
- at the following standard number: +32 22999696 or
- by email via: [https://europa.eu/european-union/contact\\_en](https://europa.eu/european-union/contact_en)

## Finding information about the EU

### Online

Information about the European Union in all the official languages of the EU is available on the Europa website at: [https://europa.eu/european-union/index\\_en](https://europa.eu/european-union/index_en)

### EU publications

You can download or order free and priced EU publications at: <https://publications.europa.eu/en/publications>. Multiple copies of free publications may be obtained by contacting Europe Direct or your local information centre (see [https://europa.eu/european-union/contact\\_en](https://europa.eu/european-union/contact_en)).

### EU law and related documents

For access to legal information from the EU, including all EU law since 1952 in all the official language versions, go to EUR-Lex at: <https://eur-lex.europa.eu>

### Open data from the EU

The EU Open Data Portal (<https://data.europa.eu/euodp/en/home>) provides access to datasets from the EU. Data can be downloaded and reused for free, for both commercial and non-commercial purposes.

The SLOPES project brought together experts from across Europe to advance the current technology and methodologies applied to understanding, analysing, and monitoring slopes within open pit lignite mines. The project targeted three main areas. Firstly, the research evaluated how modern monitoring techniques can be applied and integrated within automated systems that provide 'real-time' assessments of risk. A particular focus was the potential use of unmanned aerial vehicles because of their versatility and that they reduce the need to have people and equipment in hard to access and potentially dangerous areas. Secondly, the project conducted a variety of stability analyses of open-pit rock-face slopes. Advanced probabilistic analyses were developed, giving improved methods for evaluating the performance and potential risks associated with open-pit slope faces. Advanced numerical modelling techniques were applied to gain an in-depth understanding of the behaviour of the slope faces, as well as an assessment of the potential vulnerability of mining and other nearby infrastructure. Finally, the project studied the long-term behaviour of lignite mine spoil materials, with particular attention on stability and ground movements within spoil heaps and reclaimed ground. A rigorous approach involving laboratory testing of soils, small-scale physical modelling (including elevated gravity modelling using a geotechnical centrifuge), and numerical/probabilistic modelling was applied. The project outcomes will enable development of effective reliability-based methods for the evaluation of risks based on monitoring and modelling results which will provide significant benefits to design optimisation and decision support within open-pit lignite mines.

